Master Thesis

Numerical and Experimental Study on the Application of the SMFL-method for Monitoring Fatigue Cracks in Steel Structures

M. Abrahamse

13 July 2018

TU Delft

CRACK GUARD

royal roos

Master Thesis

Numerical and Experimental Study on the Application of the SMFL-method for Monitoring Fatigue Cracks in Steel Structures

by

M. Abrahamse

To obtain the Degree of Master of Science

Delft University of Technology
Faculty of Mechanical, Maritime & Materials Engineering
Department of Offshore & Dredging Engineering
Section of Ship Hydromechanics & Structures

&

Royal Roos B.V.

Student number:	4125494	
Supervisors:	Prof. dr. ir. M.L. Kaminski,	TU Delft, supervisor
	Ir. M.P. van der Horst,	TU Delft, supervisor
	Ir. F. Roos,	Royal Roos B.V., supervisor
Date of Defence:	16 July 2018	
Assessment Committee:	Prof. dr. ir. M.L. Kaminski,	TU Delft, Chair
	Ir. M.P. van der Horst,	TU Delft
	Dr. ir. L. Pahlavan,	TU Delft
	Dr. ir. P.Th.L.M. van Woerkom,	TU Delft
	Ir. F. Roos,	Royal Roos B.V.

Preface

This thesis is the final product of the research I conducted in order to obtain the Masters of Science degree in Offshore and Dredging Engineering at the Mechanical Maritime and Materials Engineering faculty of Delft University of Technology. At the start of this thesis, I was made aware by many people that a graduate thesis is not to be taken lightly. Therefore I cannot say that I was not informed. However, throughout the project, I found out that a graduate thesis is not to be taken lightly. A project that is entirely your responsibility and relies on your own efforts to progress, is able to confront you with your own vices and virtues. Looking back, it all looks to be so easy and obvious and I am sure that I could rewrite the thesis several times, while every time being able to improve the work. I guess that this shows that I have learned a lot from it.

This evaluation may sound disheartening so far. However, a lot of people made an effort to support me in the process. First of all, I would like to thank Fulko Roos and Veronica Breed for providing me the opportunity to graduate in cooperation with Royal Roos. During my thesis they have accommodated me in the office, arranged research opportunities for me and trying to make me part of their company team as much as possible. I would like to thank Fengfeng, Lennard and Henry for their advise, that sometimes made me painfully aware that theoretical researched is grounded in practical applications. And I would like to thank Einte and Salomon for keeping me company during the lonely lunch hours at SuGu Warehouse.

The TU Delft furthermore provided me with professional support, in the person of Menno van der Horst, my daily supervisor. Menno not only answered my questions to the best of his abilities, but was also my trusted companion in handling the handheld magnetometer on many research trips. I would like to thank Mirek Kaminski, who would always ask first how I was doing, before getting into business. My search for an interesting thesis subject started and ended in his office, when he told me of a 'fantastic graduation assignment' he had for me. I would like Pooria Pahlavan for his advise and ideas on the project. His late addition to the graduation comity made my work not easier, but better.

Finally I would like to thank Sylvia, who, at the start of my thesis, became my informal supervisor, by introducing me into the mysterious world of the CrackGuard. And Bart Scheeren, who gave me a crash course in LaTeXand who provided me with the template of this thesis report.

M. Abrahamse
Delft, Juli 2018

Abstract

Operating ship and offshore structures are continuously subjected to the action of waves, that, due to their cyclic nature, cause fatigue cracks to develop. Regular inspections, which are currently performed manually, are therefore required in order to guarantee the structural integrity of the structure. Fatigue crack monitoring is essential, since only cracks of critical length pose a problem for the structural integrity. The CrackGuard JIP has the goal of developing a system for reliable monitoring of fatigue cracks based on the characteristic magnetic pattern that occurs around a fatigue crack as a result of magnetization by the Earth magnetic field. This method, which is called the Self Magnetic Flux Leakage method, makes use of the disturbance caused by a fatigue crack on the magnetic flux inside the material and can be detected by a leakage pattern of this magnetic flux around the fatigue crack. In order to develop this system three knowledge gaps have been identified: The effect of the crack opening on magnetic flux leakage, the effect of complex geometries and welded joints and the application of this methods to full-scale structures.

The effect of crack opening on the magnetic flux leakage is investigated with the help of experimental and numerical research, where the crack opening in a plate is increased while the magnetic flux leakage is determined. The results of these experiments demonstrate that the opening of the crack has a linear relationship with the flux leakage around the crack, while the width of the signal is unaffected. This means that the magnetic flux leakage measured by the envisaged system will change during a loading cycle.

Earlier research indicated that welds cause a disturbance of the magnetic flux, which is similar to the magnetic flux leakage pattern as it appears around cracks. This is thought to be a result of a change in magnetic magnetic material property, namely the magnetic permeability, between the plate material and weld material. Experimental research on material from the weld filler material and heat affected zone demonstrates that magnetic material properties do not differ from that of regular structural steel, suggesting that other properties of the weld may induce the observed leakage pattern. Numerical simulations of a T-joint with a double-sided Fillet weld, in which a range of different magnetic permeabilities is assumed for the weld filler material and the heat affected zone, furthermore shows that the characteristic magnetic leakage pattern is still clearly detectable.

The application of the self magnetic flux leakage method for fatigue crack monitoring on a full-scale replica of a bridge deck demonstrates that the method, applied using a handheld magnetometer and a measurement grid, is very suitable for monitoring fatigue cracks in these type of structures. The amplitude of the flux leakage pattern is increased by the large amount of ferromagnetic materials in these structures, which improves crack monitoring and even allows for the tracking of a propagating fatigue crack on the bases of the obtained measurement results.

The testing of a prototype of the envisaged monitoring system on an operating trailing suction hopper dredger, in which fatigue cracks have been detected, in order to demonstrate whether the system produces measurements that can be used to monitor fatigue crack length. The results of this experiment show that the CrackGuard is able to detect the magnetic flux leakage around a crack and is able to detect changes in the signal strength due to unloading of the ship. However, the sensitivity and precision of the magnetic measurements will have to be improved, in order to monitor fatigue cracks effectively and reliably.

Finally it is demonstrated that post-processing of the results using interpolation and filtering of the measurement results can improve crack localization. Post-processing is furthermore shown to be able to separate the magnetic flux leakage from the permanent magnetization, which is a source of polution of the measurements.

List of Figures

List of Tables

List of Abbreviations

The following list contains the significance of all abbreviations used throughout this report. The page number refers to the first page where the abbreviation is used.

Abbreviation	Description	Page
AC	Alternating Current	13
CMOD	Crack Mouth Opening Displacement	14
CPU	Central Processing Unit	83
DC	Direct Current	84
FE	Finite Element	28
FEM	Finite Element Method	30
FPSO	Floating Production Storage and Offloading (unit)	86
HAZ	Heat Affected Zone	28
JIP	Joint Industry Project	1
MFL	Magnetic Flux Leakage	13
MMM	Metal Magnetic Memory (method)	14
MPI	Metal Particle Inspection	13
NDE	Non-Destructive Evaluation	1
NDI	Non-Destructive Inspection	7
NDT	Non-Destructive Testing	13
PCB	Printed Circuit Board	82
PSB	Persistent Slip Band	5
SMFL	Self-Magnetic Flux Leakage	14
SQUID	Superconducting Quantum Interference Device	88
TU Delft	Delft University of Technology	15
UART	Universal Asynchronous Receiver-Transmitter	86

List of Symbols

The following two lists contain the significance of all symbols used throughout this report.

Greek

Symbol	Usage
Δ	Range Difference
μ	Magnetic Permeability
ρ	Electrical Charge Density
σ	Stress
ξ	Magnetic Susceptibility

Latin

Symbol	Usage
a	Crack length
B	Magnetic Flux Density
C	Paris' Law Constant
D	Electrical Flux Density
E	Electric Field Intensity
H	Magnetic Field Strength
J	Current Density
K	Stress Intensity Factor
L	Plate Length
M	Magnetization
m	Paris' Law Constant
N	Demagnetizing Factor
T	Tesla (Unit)
t	Plate Thickness
W	Plate Width

Contents

1 Introduction

Most of today's marine structures operate under harsh environmental conditions, continuously subjected to the unceasing action of wind and waves. Due to the cyclical nature of these conditions, fatigue cracks are very common in these types of structures and various rules and codes have thus been developed to ensure safe operation with respect to people and environment. This requires operators to periodically inspect the structures on the presence of fatigue cracks, as the cracks initiate and grow. Cracks of critical length have to be repaired, while cracks of sub-critical length have to be monitored by inspection. Crack growth rates, however, are very uncertain due to their dependence on stochastic parameters, which causes operators to either increase inspection frequency or be conservative in the determination of critical crack length. This demonstrates the usefulness of a system designed to monitor crack lengths and growth rates, especially with the increasing economic value of offshore structures and the increased application of more fatigue sensitive high strength steels and the trend to operate with older ships in harsher environments. Such a system has the potential to increase safety, reduce inspection costs and allow for less conservative designs.

1.1. Problem statement

The CrackGuard Joint Industry Project has the goal of developing an affordable system for monitoring detected and allowable fatigue cracks in offshore structures based on the most recent achievements in crack propagation, sensing technology and wireless communication. In order to be competitive with conventional inspections, the system should have the following characteristics:

- Affordable
- Safe
- Wireless
- Robust
- Low energy consumption
- Easy to install
- Passive

According to earlier publications [4], a system based on the Self-Magnetic Flux Leakage (SMFL) principal fits this profile best. Although SMFL based monitoring techniques are very promising, there are still many challenges involved with this new NDE-technique. Uncertainties mainly exist on the subjects of material parameters, permanent magnetism, crack opening and closing, welded joints, complex geometries and the magnetomechanical effect (the coupling between magnetism and mechanical stress). In order to successfully develop the CrackGuard as a reliable system, able to replace current monitoring operations, more knowledge is needed on these topics. This thesis report does not encompass the full scope of the CrackGuard JIP, but instead focuses on the knowledge gaps that are most important, according to the author, in order to progress the CrackGuard JIP in this stage of the research. Therefore this report will focus on the following topics:

- The Crack Opening Effect
- SMFL in Welded T-joints
- Full-scale testing

1.2. Objective

This report aims to answer the posed research questions and thereby improve the understanding of crack monitoring using the CrackGuard as a SMFL-based evaluation method. The questions are formulated to advance the knowledge on the application of the SMFL for crack monitoring, with the aim of improving performance, safety and cost effectiveness of steel structures.

1.3. Problem approach

In order to establish a basis of knowledge and understand the current state of the art a literature study is first performed, giving a comprehensive overview on the topics of metal fatigue, magnetism and magnetic materials and magnetism-based non-destructive testing methods. The literature study is meant to provide a framework for the experimental and numerical studies performed by describing the context of the research and demonstrating the gaps in the current knowledge on the subject.

Following from the described knowledge gaps on fatigue crack monitoring using the SMFL, research questions have been formulated that address these knowledge gaps and aid as a guideline for the structure of the report. The research questions are formulated as follows:

1. What is the effect of crack mouth opening displacement (CMOD) on the SMFL measurements in a uniaxially loaded plate from the point of crack detection?
2. What is the magnetic permeability of weld filler material and HAZ material and how does it compare to the magnetic permeability of a s235 structural steel plate?
3. How does the magnetic permeability of a double sided fillet weld influence the magnetic flux leakage around a through thickness crack located at the weld toe?
4. Is it possible to monitor crack length of a fatigue crack in the cross beam of a full-scale replica of a bridge deck using the SMFL method?
5. Is it possible to monitor crack length of a fatigue crack in the torsion box of an operating trailing suction hopper dredger using the CrackGuard LT?
6. How can post-processing of SMFL measurement data improve fatigue crack monitoring?

The first research question addresses the effect of opening and closing of the crack on the SMFL around this crack. Due to the cyclical nature of the loading, fatigue cracks in operating offshore structures will open and close following a cyclical pattern as well, which in turn influence the local magnetism in the material. Precisely how the SMFL is affected by the opening and closing of the crack is currently unknown, however it is expected that this effect has a significant impact on the magnetic measurements. This research question is answered using a dual approach. Firstly, a numerical simulation is performed where the SMFL around a crack is simulated while the CMOD is varied. Secondly an experiment is performed where the SMFL is measured using a magnetometer while the CMOD is controlled using a universal testing machine. This dual approach allows for a comparison between experiments and a more profound insight into the mechanism that influences the coupling between CMOD and SMFL.

The second and third research question work in synergy with one another to advancing the knowledge on SMFL around cracks in the vicinity of welded joints. It is known that fatigue cracks most often occur in the vicinity of material or geometric changes. In marine and offshore structures this situation is frequently encountered in welded joints, such as a T-joint, where a change in geometry is paired with a change in material properties. Previous research on SMFL induced by fatigue cracks (see 2.2.3) has, until now, been focused on fatigue cracks in center cracked plates. It is however unlikely that the CrackGuard will be applied under these simplified conditions and the influence of the welded T-joint structure on the monitoring of fatigue cracks will therefore have to be researched. This gap in the knowledge will be approached with the help of a FE

model and an experimental study. The second research question is intended to find the right material input for the FE model in order to obtain reliable results from the numerical study. The FE model will subsequently be used to answer the third research question with the help of a numerical simulation that addresses the influence of the magnetic permeability on the SMFL.

The fourth research question explicitly addresses the validity and application of the SMFL method as a way of monitoring fatigue cracks in full-scale steel structures by directly testing the method on a full-scale replica of a bridge deck. As mentioned before, the SMFL method has not been tested on a full-scale steel structure, while this is where the SMFL method is envisaged to find its application. Therefore, a experimental test will be performed on a fatigue crack in the crossbeam of a structural steel bridge deck replica. The SMFL method will be used in this test to see how the flux leakage is affected by a propagating fatigue crack. The experiment closely simulates the conditions on an operating offshore structure and thereby provides an opportunity to function as a experiment to test the concept of crack monitoring using SMFL in full-scale structures.

The sixth research question directly addresses the subject of this thesis in an uncomplicated way. A prototype of a SMFL-based fatigue crack monitoring system, which is called the CrackGuard LT, will be installed over a fatigue crack that was detected in the torsion box of a trailing suction hopper dredger. The SMFL measurement results will be examined in order to determine if the prototype is capable of detecting and monitoring the fatigue crack during operation of the ship.
Lastly, the seventh research question will study the interpretation of the SMFL measurement data and explore how it can be improved to better understand the measurements. This will be done by a numerical study of previously obtained SMFL measurement data.

1.4. Report outline

The posed research questions will be answered using three different approaches: literature study, experimental measurements and numerical simulations. The outline of the report follows this approach in the same order.

Chapter number two describes the theory and literature concerned with the monitoring of fatigue cracks using the SMFL principal. The chapter gives a brief introduction into the basics of metal fatigue, metallurgy of welds and magnetism in ferromagnets as well as a summary of the research on SMFL until the now. This should make the reader aware of the current state of art and the existing knowledge gaps.

Chapter number three describes the experimental methods used to answer the earlier posed questions and the results that can be derived from it. Three experiments will be described: the crack opening experiment, the T-joint experiment and the bridge deck experiment.

Chapter number four gives a description of the models used to conduct numerical simulations and presents the subsequent numerical results. Furthermore, the assumptions, simplifications and limitations of the numerical models is described and discussed

Chapter number five will report on a numerical study of the exploration of post-processing techniques on the SMFL measurement data with the aim of a better understanding of the SMFL measurements.

Chapter number six will provide a summarizing conclusion of the earlier presented findings, combining results of experimental measurements and numerical simulations to answer the overarching research questions. Finally a recommendation on further research will be made.

2

Theory and Literature Study

This chapter contains an introduction into the theory behind the concept of fatigue crack monitoring using SMFL and the underlying working principals.

2.1. Fatigue and fracture in metallic materials

According to Craeger [6] metal fatigue is defined as: ''Failure of a metal under a repeated or otherwise varying load which never reaches a level sufficient to cause failure in a single application". Although a rigorous definition of metal fatigue is difficult, this definition includes two important characteristics that define fatigue of metals: the necessity of cyclic loading and the presence of a stress level that is below the yield strength of the material. The accumulation of damage and finally failure of the structure due to metal fatigue is divided into three stages: crack initiation, crack growth and final failure.

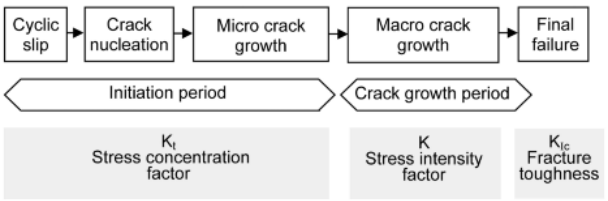

Figure 2.1: Different phases of the fatigue life time with relevant factors [1]

2.1.1. Fatigue Crack Initiation

The stage of crack initiation is characterized by the development of microscopic stress concentrations in the material. Microscopic stress concentrations may originate from different sources that may already exist in the material or develop in the process of fatigue damage accumulation. These microscopic stress concentration sources are:

- Persistent slip bands (PSBs)
- Grain boundaries
- Corrosion pits
- Manufacturing defects
- (Welding induced) inclusions, voids and pores.

Persistent Slip Bands develop due to movement of dislocations under cyclic loading and occur as a consequence of shear stresses at a level below the yield stress and is often referred to as micro-plasticity. This micro-plasticity is a consequence of oxidation of external layers and strain hardening, which are both irreversible processes. The result of the formation of Persistant Slip Bands (PSBs) 2.1.1 is a surface roughness of exclusions and inclusions [1], as is depicted in figure 2.2.

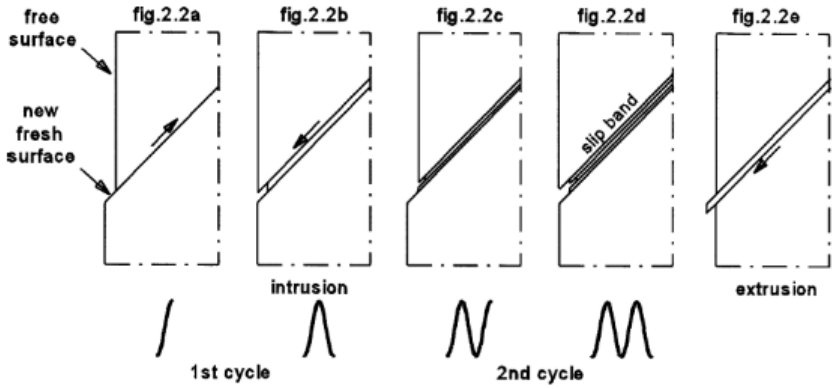

Figure 2.2: The development of a Persistent Slip Band [1]

The process of crack initiation is considered a surface phenomenon, because of a multitude of surface qualities that reinforce the development of these microscopic stress concentrations, such as corrosion, surface damage and the plane stress condition on the surface of the material. Fatigue resistance in this stage is therefore best improved by reducing the microscopic stress concentration sources. This is often done by treatment of the surface of the material.

In offshore structures micro-cracks often originate from inclusions, voids and pores that are introduced to the material as a consequence of the welding process. The resulting defects cause the added weld material and the heat affected zone to have a lower fatigue initiation resistance. The result is that fatigue cracks are often found around welded connections, at locations where a combination of low fatigue initiation resistance and geometrical stress concentrations is present.

A definition of the transition between the stage of crack initiation and further crack growth is described in a qualitative way as the point at which micro crack growth is no longer depending on material surface conditions.

2.1.2. Fatigue Crack Growth

At this point, the microscopic stress concentration has turned into a macroscopic stress concentration that is depending on bulk properties of the material. The crack growth resistance of the material is now controlling the crack growth rate. The crack growth rate depends on the grain structure, far field stress amplitude and the material strength, which is characterized by the Young's modulus. The direction of crack growth is in this stage perpendicular to the main principal stress.

Fatigue growth rate

In marine and offshore structures, the fatigue life time is dominated by fatigue crack growth. The initiation life time is relatively short, due to the aforementioned voids, inclusions and pores induced by the welding process. Knowledge on the fatigue crack growth is therefore essential to predict the fatigue behavior of these structures. The main question with regards to fatigue crack growth therefore becomes: how long does it take for a crack to grow from a certain initial size to the maximum permissible size? Three aspects need to be addressed to answer this question [2]:

- What is the initial crack size a_d?
- What is the maximal permissible crack size a_{cr}?
- What is the period of crack growth between a_d and a_{cr}?

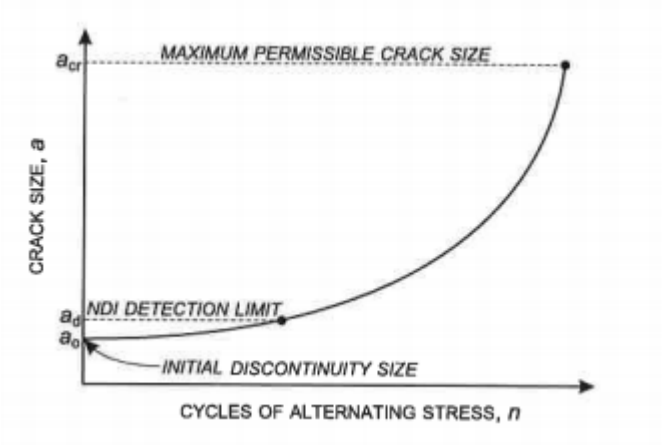

Figure 2.3: Schematic fatigue crack growth curve [2]

The initial crack size ad with regards to crack monitoring corresponds to the minimum crack size that can be detected using NDI methods, that is, assuming that the minimum detectable crack size is equal to the minimum monitorable crack size. When the latter aspect is of main concern, which is the case when we focus on the monitoring of cracks using the CrackGuard, the initial crack size ad corresponds to the minimum monitorable crack size using the CrackGuard. Although this crack size is dependent on several factors related to Self-Magnetic Flux leakage (see. 2.2.3), this crack size may be assumed to be well above the size of the microscopic stress concentrations that are concerned with crack initiation.

An indication of the concept behind the maximum permissible crack size or critical crack size can be derived from figure 2.1, where fatigue growth is followed by fracture of the material. The critical crack size therefore corresponds to the crack length from which unstable crack extensions results. The mechanism behind unstable crack extension is related to the fracture toughness of the material more so than the fatigue resistance of the material and can be derived from classification rules in the case of marine and offshore structures.

The period between a_d and a_{cr} can be characterized using the fatigue crack growth rate. The fatigue crack propagation rate da/dn is defined as the crack extension da, during a small number of cycles dn [2]. The fatigue crack growth rate curve can be described using one of the crack growth laws of which the most widely known is the Paris' equation (equation 2.1). This crack growth law makes use of the stress intensity concept (see equation 2.2), which uses the correlation between dK and da/dn to describe the crack growth rate. The notion that da/dn is fully determined by ΔK is known as the similitude approach, with ΔK as a similitude parameter [2]. The approach can defined as: ''similar conditions applied to the same system will have similar consequences" [7]. This means that a similar K cycle applied to a crack in one construction will induce the same crack length extensions as a crack in another structure with another geometry, as long as the material qualities are the same.

$$\frac{da}{dn} = C(\Delta K)^m \tag{2.1}$$

$$K_I = C\sigma\sqrt{\pi a} * f(\frac{a}{W}) \quad \text{with:} \quad f(\frac{a}{W}) \quad \text{being a function of geometry} \tag{2.2}$$

The fatigue crack growth rate curve in figure 2.4 shows the characteristic sigmoidal shape of the fatigue crack growth rate. In this figure, three stages can be distinguished. The first stage is known as the threshold stress intensity range, in which cracks do not propagate or very slow. The second stage the crack growth rate increases relatively rapidly. This region is the region which is approximated using the aforementioned Paris' law. In the third stage the stress intensity approaches the critical stress intensity factor and crack extension is followed by final failure.

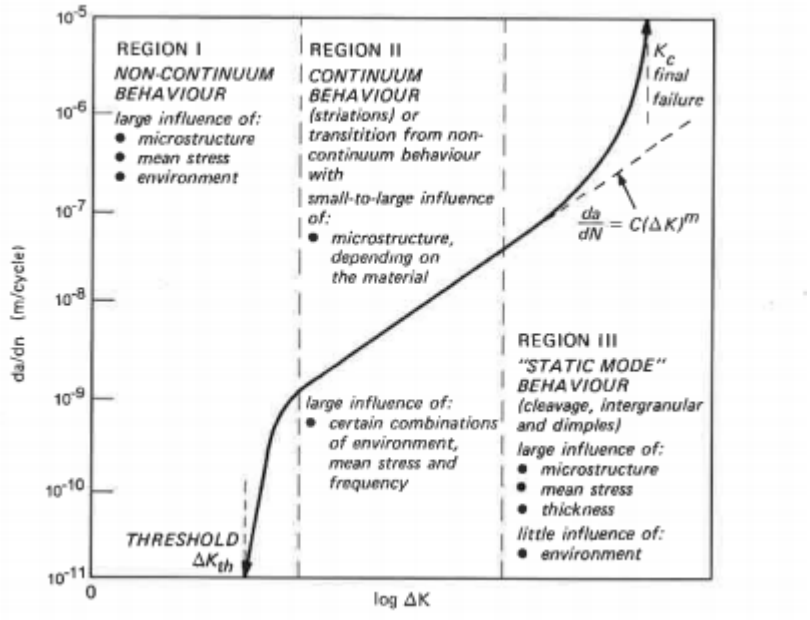

Figure 2.4: Characteristic crack growth rate curve [2]

Although a extensive amount of literature has been published on the prediction of crack growth rates, there is in practice still a lot of uncertainty around fatigue crack propagation because of the complex loading involved and stochastic distribution of material properties. However, a reliable crack monitoring system can simply track fatigue crack propagation and compare it to a predetermined critical crack length, in order to determine the safety of the structure. This show that there is merit to the development of a reliable crack monitoring device, such as the CrackGuard, despite the ongoing development of knowledge on the propagation of fatigue cracks.

2.1.3. The Crack closure phenomenon

The crack closure phenomenon was discovered by Elber [8] in the early 1970s. He found that the fatigue cracks are closed for a significant portion of a tensile load cycle, due to residual plastic deformation along the crack front. This plastic zone occurs as a result of the difference between the plastically deformed areas that result from loading (monotonic zone) and subsequent unloading (cyclic zone) of the crack (see figure 2.5). As a result, the residual plastic deformation around the crack flanks consists of elongated material. This causes the crack to close before the crack has returned to its unloaded state. The stress level at which this premature crack closure occurs will be marked as the effective stress σ_{eff}. The resulting effective stress intensity range ΔK_{eff} will therefore differ from the nominal stress intensity range ΔK. The latter has some important implications with regards to the stress ratio, which is outside the scope of the report.

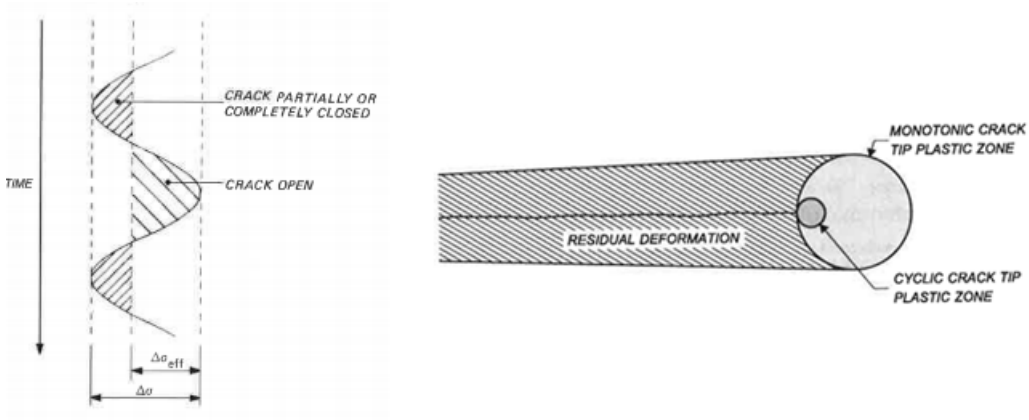

Figure 2.5: The crack closure phenomenon [2]. Left: crack opening and closing over a loading cycle. Right: zones of plastic deformation in the vicinity of a fatigue crack.

An important conclusion with regards to crack monitoring can be drawn from this as well. Although fatigue cracks in marine and offshore structures are not always fully unloaded during a fatigue cycles, depending on the situation, the crack closure phenomenon may still cause the fatigue crack to be closed for a significant portion of the loading cycle. Since the magnetic stray field around fatigue cracks are most pronounced when there is opening of the crack (see 3.1), this means that the crack closure effect may make it the fatigue crack less 'visible' for SMFL-based crack monitoring systems. However, Elber [8] further suggested that full crack opening is required for fatigue crack growth, which implies that, as long as fatigue crack growth is present, there will be a period in the loading cycle where crack opening is inevitable in the case of tensile loading.

2.2. Magnetism and magnetic materials

This section is intended to give a comprehensive overview of the magnetic properties of ferromagnetic materials, more specifically structural steel. The material properties of base material and weld material are described as well as their influence on magnetic properties.

2.2.1. Hysteresis in magnetic materials

The phenomenon of magnetic hysteresis in ferromagnetic materials is caused by the alignment of magnetic domains inside the material. A magnetic domain is a small region (1-100 microns) within a magnetic material in which the magnetization has a uniform direction, meaning that the magnetic moments of the atoms are aligned with one another within this magnetic domain. The full ferromagnetic structure comprises a large number of these magnetic domains, with each a different orientations of their magnetization direction. The total Magnetization M of the material can be considered as the vector sum of these magnetic moments per unit of volume.

When the ferromagnet is not magnetized, the sum of the magnetic moments of the domains throughout the material is zero, minimizing its internal energy. When an external magnetic field is applied, the orientations of the magnetic domains start to align.

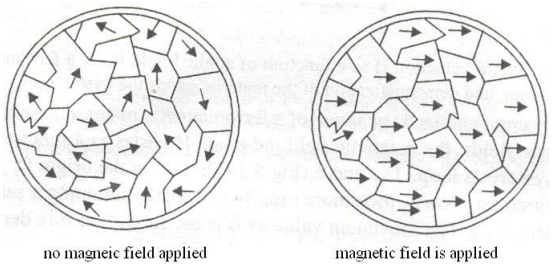

Figure 2.6: Domain structure in a ferromagnetic material [3]

In the case that all the magnetic domains are aligned in the direction of the applied magnetic field, the magnet is magnetically saturated. When the external magnetic field is removed, some magnetic domains tend to retain their orientation and thereby cause hysteresis. The main mechanisms causing the hysteresis property of ferromagnetic materials are domain wall bulging, which is a reversible process, and domain wall displacement, which is an irreversible process. Impedance to these mechanisms is caused by pinning sites, which can be caused by small defects or precipitates (see 2.2.2). This causes a hysteresis loop (figure 2.7) to develop [9]. The magnetization that remains after the external magnetic field is removed, is called the retentivity. In order to reduce the magnetic moment in the plate to zero again, a magnetic field with an opposing direction has to be applied. This point on the hysteresis loop is called the coercivity. Figure 2.7 gives a graphical representation of this hysteresis loop.

It can be seen from figure 2.7 that the relation between the magnetizing force M and the flux density B is non-linear. There is however no general shape of the hysteresis loop that applies to every ferromagnetic material. Since most magnetic materials are inhomogeneous and anisotropic this hysteresis curve may vary for different directions and locations within the material.

The fact that the ferromagnetic material retains some of its magnetization after the external magnetic field is applied, causes the material to 'memorize' its previous state. It is this property in combination with the fact that some magnetic properties and mechanical properties of the material are related, that enable the detection of mechanical changes in the material with the help of magnetic measurements and form the basis of some nondestructive testing methods based on magnetism.

Within ferromagnetic materials, distinction is made between magnetically hard and soft materials, indications that can be linked to their mechanical hardness and softness as well. Magnetically soft materials are easily magnetized and display a narrow hysteresis loop, whereas magnetically hard materials are hard to magnetize and display a wider hysteresis loop. The conjunction between magnetic and mechanical prop-

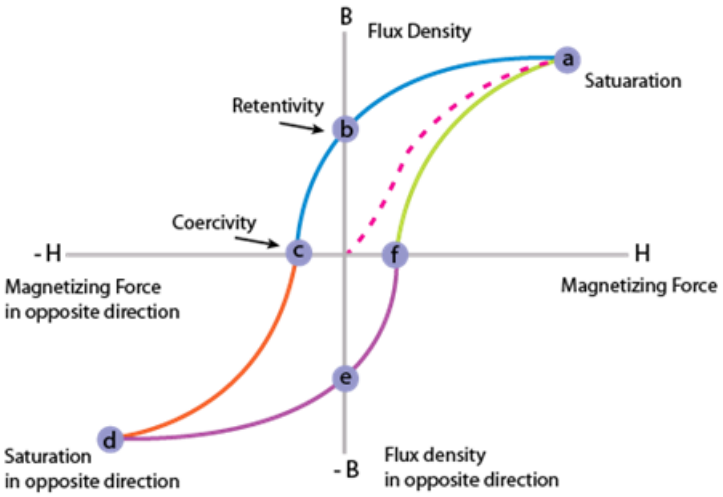

Figure 2.7: Graphic representation of a hysteresis loop in ferromagnetic materials

erties can be explained by the interaction between the micro-structural properties of the material and the magnetic domains. It is known that dislocations in the material have an associated local stress field which gives rise to highly inhomogeneous micro-strains within the material [3]. Through magnetoelastic coupling the dislocations pin domains walls. Therefore, the higher the dislocation density within a ferromagnet, the greater the impedance to domain wall motion. Further, magnetic inclusions with different magnetic properties, such as insoluble second-phase material, oxides, carbides or even pores, voids and cracks, may impede domain wall motions as well and cause changes in the hysteresis properties [3]. Introducing more pinning sites that impede domain wall motion lead to an increased coercivity and a decrease in magnetic permeability. The same is also true of dislocations when their number density is increased by plastic deformation, either in tension or compression. So for example, the addition of carbon in the form of iron carbide particles increases coercivity and hysteresis loss. Cold-working of the material has a similar effect, when compared to the same steel in a well-annealed state.

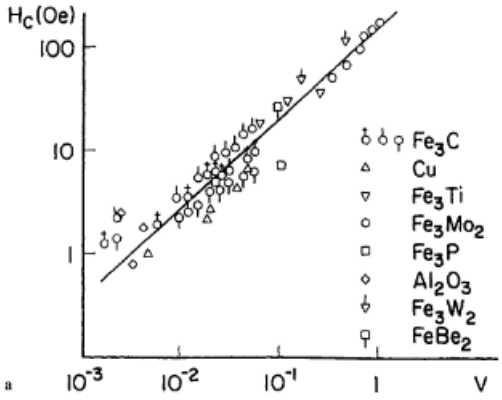

Figure 2.8: Coercivity of various steels as a function of the total volume fraction of inclusions [3]

2.2.2. Permeability

The permeability of a material represents the ability of the material to support the formation of a magnetic field within itself. It is expressed in Henries per meter (H/m) or equivalently in Newtons per Ampere squared (N/A^2). The permeability of the material is typically denoted with a μ and is the product of the relative permeability μ_r and the permeability in a classical vacuum μ_0, where $\mu_0 = 4\pi * 10^{-7}$. The permeability of the material relates the magnetic flux density B to the magnetization M and magnetic field strength H through equation 2.3.

$$B = \mu * (H + M) = \mu_r * \mu_0 * (H + M) \tag{2.3}$$

Equation 2.3 shows that the magnetic flux density B is linearly dependant on the magnetic field strength H and the magnetization M. Applied to a case that is more specific to the CrackGuard, this means that the magnetic field strength H represents the Earth magnetic field and the magnetization M represents the possible retentive magnetization of the plate (see figure 2.7). The latter term is also known as permanent magnetization, as opposed to the induced magnetization. The permanent magnetization of a steel structure is influenced by remanence, stresses and temperature fluctuations, is non-uniform and varies slowly in time, while the induced magnetization is influenced by geometry of the structure, the applied background field and the magnetic permeability. The permanent magnetism in a steel plate is hard to predict due to the unknown history of the different influence factors [10].
Equation 2.4 describes the relation of the magnetization M and the magnetic field strength H by the magnetic susceptibility χ_m, a dimensionless proportionality constant that indicates the degree of magnetization of a material in response to an applied magnetic field.

$$M = \chi_m * H \tag{2.4}$$

Where the magnetic susceptibility χ_m can be related to the permeability through the relation in equation 2.5.

$$\mu_r = (1 + \chi_m) \tag{2.5}$$

The value of the relative permeability μ_r and magnetic susceptibility χ_m characterize the magnetic properties of the material. A high value means that the material is easily magnetized. Ferromagnetic materials typically have a magnetic susceptibility χ_m of χ_m= 10^3-10^5. Diamagnetic materials are characterized by a negative value of the magnetic susceptibility χ_m, which means that they develop an induced magnetic field in the direction opposed to that of the applied magnetic field. The value of the magnetic susceptibility χ_m, changes along the hysteresis curve, until it reaches a value of 1, where the magnetization is equal to the magnetic field.

Magnetic permeability of weld material

In marine and offshore structures, fatigue cracks in steel plates often occur in the vicinity of welds. Although some research has been done on the permeability of steel plates[11], there is currently no published research on the magnetic permeability of weld material. One paper [12] found a reduction in the permeability of the weld material compared to the base material, but was not able to accurately predict the permeability using existing literature. This reduction in permeability compared to the base material was largely attributed to a difference in grain size between the weld and base material. It is however known that magnetic properties of ferromagnets depend greatly on other microstructural properties such as pearlite fraction, carbon content and manganese content [13],[14]. Another factor that influences magnetic properties, specifically magnetic permeability, can be found in defects that cause domain wall pining such as dislocations, internal stresses, vacancies and impurities [15].

2.2.3. Magnetism-based Nondestructive testing methods

Self-Magnetic Flux Leakage testing is a relatively new method of non-destructive testing. Some of the principals used in Self-Magnetic Flux Leakage are used in other, more researched methods of non-destructive testing as well. In order to improve the understanding of the self-magnetic flux leakage phenomenon, it is helpful to have an understanding of NDT methods using physically related principals.

Magnetic Particle Inspection

Magnetic Particle Inspection is a very popular, low-cost method to perform non-destructive testing in ferromagnetic materials. In order to perform MPI, the test specimen is first magnetized by applying an external magnetic field. This magnetic field is best applied in the direction perpendicular to the crack plane. In places of reduced magnetic permeability, the magnetic flux density is reduced, which creates magnetic flux leakage at the location of the defect. When a suspension of ferromagnetic particles is applied to the location, the ferromagnetic particles are attracted to the locations where flux leakage occurs, whereas the particles run of in other locations (see figure 2.9). The suspension of ferromagnetic particles is usually pigmented, for example by making use of fluorescent powders, in order to reveal sites of accumulated ferromagnetic particles. MPI is an economical, fast and reliable method for the detection of surface and even shallow subsurface defects. The MPI method is most suited to revealing defects and give a visual indication of the length and width of the defect, still requiring human observation. Furthermore MPI cannot be used to measure the depth of the revealed defect and does not allow for quantitative measurements of the leakage field [16].

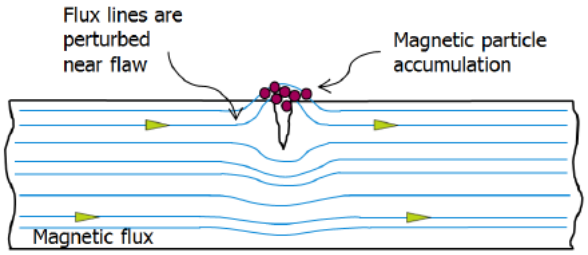

Figure 2.9: Principle of Magnetic Particle Inspection [4]

Magnetic Flux Leakage Testing

Magnetic flux leakage techniques are widely used for pipe and tank floor inspection. This technique requires magnetization of the specimen under test. The magnetization generates magnetic flux flowing in the specimen in a certain direction, which is ideally perpendicular to the axis of the crack to be detected. The presence of flaws will manifest as an abrupt change of magnetic permeability to the flux in the specimen. Since the permeability of the flawed part is generally lower than flawless parts, this provides high resistance to the flux and forcing it to take a different route. In cases where the other routes are magnetically saturated, some flux leaves the specimen to the surrounding space temporarily causing flux leakage (see figure 2.10). This leakage is readily detectable by a magnetic sensor located in the proximity of the specimen surface. The defect parameters that affect the distribution of the leakage flux are the ratio of depth of the defect to the thickness of the pipe wall, length, width, sharpness at the edges and sharpness at the maximum depth. In practice the magnetization device is usually a permanent magnet or an electromagnet. For AC inspection , Hall devices, magnetoresistives and SQUIDs can be used to measure the leakage field. The advantage of MFL techniques is its simplicity and low cost. The technique is more robust to the variation of magnetic properties in magnetic materials compared to for example eddy current techniques, which belong to electromagnetic NDT techniques as well. Like many electromagnetic techniques, MFL is also non-contact, which is a very useful feature for online dynamic inspection. Unlike eddy currents techniques, however, MFL only works with magnetic materials [17].

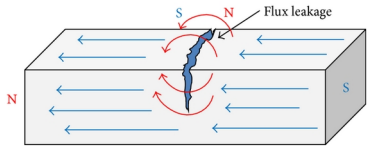

Figure 2.10: Principle of Magnetic Flux Leakage [5]

This methods differs from SMFL testing in the fact that MFL makes use of an externally applied magnetic field other than the earth magnetic field, to induce a magnetic field in the test specimen. This applied magnetic field is much stronger than the earth magnetic field, making the flux leakage effect more pronounced compared to the permanent magnetism in the plate. This promotes the detection and monitoring of cracks in the plate and makes quantitative measurements possible. MFL testing however requires active magnetization, which is not required in SMLF testing.

Metal Magnetic Memory method

The Metal Magnetic Memory method is a passive NDT technique applied to locate stress concentrations and detect defects in ferromagnetic materials, based on the residual magnetic field of the specimen. The technique was firstly introduced by A.A. Dubov in 1995 [18]). The technique makes use of magnetodislocation hysteresis to detect internal stresses in the material and by doing so, is able to detect the onset of material damage, such as stress concentration, micro-crack and fatigue damage of ferromagnetic components, early in the process [19].

the MMM method differs from MFL mainly due to the fact that it uses the earth magnetic field instead of an external magnetic field to magnetize the material, making it a passive NDT technique. Under the combined operation of external loads and ambient geomagnetic field, abnormal magnetic signals are generated in the stress concentration zones where the tangential component of magnetic flux leakage $H_p(x)$ as well as the normal component H_p(y) appear with a maximum value [20]. This magnetic state is still retained even if the load is removed. Therefore, the stress concentration zones of ferromagnetic materials can be detected by analyzing the surface magnetic signal characteristics, and even the residual lifetime of the components made of ferromagnetic materials could be predicted. However, as a comparatively new and weak magnetic test method, this technique is still limited in its mechanism research and quantitative detection due to its short history and various disturbance factors in testing [21].

Review of self-Magnetic Flux Leakage Testing

The technique of using SMFL as a method to monitor cracks is relatively new. Although research shows that it is possible to measure a crack using only the earth magnetic field to create a leakage field, there are still gaps in the knowledge on this technique that have to be overcome before it can be reliably used to replace human inspections. This section summarizes the recent research that has been performed to investigate the properties of this method and to improve its performance.

In 2008 Chinese researchers showed, in a tension-tension fatigue test of a centre cracked plate, that spontaneous stray fields induced by the earth-magnetic field on the surface of a plate where influenced by the pre-notched crack in the plate. They measured the $H_p(y)$ distribution on the surface of the plate at different numbers of constant amplitude fatigue cycles. The paper discussed the feasibility of predicting fatigue crack propagation life with crack-induced abnormal magnetic signals. The paper showed an increase of the peak-to-peak value with the amount of fatigue cycles. The measurements of ΔH_p(y) even seemed to predict the onset of fatigue crack growth, by appearance of a reversal of the out-of plane flux density even when no clear crack in the material could be detected. In the same paper a linear relation between the crack length 2a and the peak-to-peak value $\Delta\ H_p$(y) was found. This finding could indicate that for ferromagnetic structures bearing fatigue load, the state of fatigue crack propagation can be easily determined by monitoring $\Delta H(y)$ value on the positions where fatigue cracks are prone to be initiated in ferromagnetic materials. However, it has to be seen whether this relation can be verified in other cases as well. Earlier research from the same author demonstrated that the measurements of $\Delta\ H_p$(y) were not effected by paint or grease on the specimen.

Research by van der Horst [22] observed a similar leakage field and detected a sign change in H_p(y) at the location of a crack in a plate using a linear array of Hall sensors. The same paper proved that it is possible to determine the location of the crack tip using a matrix of Hall sensors placed over the a crack. Further numerical simulations showed that the signal strength generated only by the induced magnetic field was larger then the detection threshold of modern Hall sensors.

Research on the effect of butt welds and cracks on the magnetic field in a S235JR steel plate has been performed by Bachelor students of the TU Delft[12]. The experiment was design to investigate the effect of a weld on the magnetic field and determine weather a crack can be distinguished from a weld, when both defects are placed in the vicinity of one another. In order to numerically model the magnetic properties of the weld, an estimation of the magnetic permeability was made based on research of [23] and [23]. The reduction in permeability was solely attributed to a difference in grain size between the weld and the base material. A difference in permeability between base material and weld of a factor 7 (resulting in a relative permeability of μ_r=17) was found. The experiments however showed that this resulted in an underestimation of the permeability of the weld. From experiments a drop in flux density in both a crack and a weld was observed. The results further showed a peak-to-peak value in both the crack and the weld that can be detected with a Hall probe that is precise within micro Tesla. The experiments where performed with heat treated and non-heat treated plates, to show the effect of demagnetization on the measurements. The effect of the residual stress and permanent magnetism where found to be of the magnitude of the earth-induced magnetic field.
The most recent research on SMFL was performed by Van der Horst [11], in which the role of permanent magnetism on the leakage field around a crack was researched. In an experiment in which the SMFL in a square plate with a pre-machined slit was measured, they showed that the leakage field was strong enough to be detected, even when the plate was not demagnetized beforehand. Comparing the results to a numerical investigation, in which only the induced magnetic field was taken into account, and contributing the difference between results to the permanent magnetism, they concluded that the contribution of the permanent magnetic part to the SMFL was much larger than the contribution of the induced magnetic part. Again a linear increase of the peak-to-peak value over the length of the crack was found, similar to the findings of [24]. The numerical investigation however did not show this behavior, showing that this linear increase can be attributed to the permanent magnetism in the plate. This means that SMFL measurements on a crack are not sensitive to variations in the earth magnetic field. The same paper investigated two important magnetic material parameters, the relative permeability μ_r and the permanent magnetization M_p. Using a Quantum Design MPMS-5S SQUID magnetometer, the relative permeability μ_r was determined to be 115, while the permanent magnetization was approximated to be zero in the entire volume of the steel plate.
The role of stress induced magnetization on magnetic flux leakage was described by van der Horst [25]. A tensile test in a 5 mm thick steel plate with an elliptical hole, showed that stress induced magnetization influenced the SMFL-field to a significant degree, demonstrating that the stress induced magnetization should be taken into account for the interpretation of the measured signal. It was furthermore demonstrated that the distribution of the stress induced magnetization was non-symmetrical and fully reversible.

Further research by van der Horst [10] that analyzed the magnetic permeability of two FeE225 steel plates for use in FEM simulations found relative permeabilities of 350 and 225 for the two plates. Moreover, the magnetic permeability of the plates was found to be reasonably uniform throughout the plate. In the same paper the distribution of the permanent magnetization was inspected. The permanent magnetization in the plate was found to be non-uniform. It was furthermore concluded that modeling of the permanent magnetization will be extremely challenging due to the unknown history of the factors that influence it.

Another paper [26] focused on the numerical simulation and analysis of several influence factors of the Earth-induced MFL. The paper showed the effect of the altitude, Earth field orientation, crack opening, crack length and geometries of welded joints near a through thickness crack in a center cracked plate. The first simulation demonstrated that an increase in the altitude results in a decrease of he signal strength as a power function, while the a linear increase of the signal width was found. The second simulation showed the effect of the Earth field orientation on the MFL. It was found that the signal strength is proportional to the induced magnetization component perpendicular to the crack. The signal width was shown to be unaffected by Earth field orientation. The Third simulation demonstrated the effect of the CMOD on the MFL signal, which showed a monotonically increasing signal strength with an increase in crack opening. The fourth simulation analyzed the crack length effect and demonstrated a gradual increase in the middle of the crack as a result of an in-

crease in crack length. The last simulation was performed on a double-sided and unpenetrated fillet welded T-joint with a through thickness weld toe crack. This simulation showed that a crack is clearly detectable despite a decrease in MFL as a result of geometry.

2.3. Conclusion of Literature Study

The foregoing literature study yields some important conclusions that provide a basis and functions as a starting point for further research on fatigue crack monitoring using the SMFL method.

2.3.1. Metal fatigue

Metal fatigue is a phenomenon that occurs as a result of cyclic loading of a metallic material. The conditions under which metal fatigue occurs are optimal at the surface, generally causing fatigue cracks to initiate from the surface of the material, where they arise from small defects. Fatigue cracks are therefore usually found at stress concentrations near welds. After initiation and potential detection, an important part of the fatigue life time is spent in the crack growth phase. Although several theories exist on the subject of crack growth rates, in practise a lot of uncertainty still exist due to complex loading schemes and scatter in material bulk properties. After the growth growth period, the crack reaches a critical crack length at which point crack growth becomes unstable and eventually fracture occurs.

During the stable crack growth stage, propagation occurs as a consequence of opening and closing of the crack and subsequent plasticity at the crack tip. However, as a result of residual plastic deformation along the crack front, opening of the crack may only occur for a relatively small portion of the loading cycle.

2.3.2. Magnetism and Magnetic materials

Ferromagnetic materials can be magnetized as a result of an externally applied magnetic field. The extend to which a material is magnetized by a given background field is dependent on the magnetic permeability, which is a material property. In some cases a relation exists between magnetic material properties and mechanical material properties: The hardness of a material can be related to the shape of the hysteresis loop and other microstructural properties of welds can be related to the permeability of the material. Although no direct research has been done on the permeability of welds or weld material, the aforementioned relationships may result in a difference between the amount of magnetization of the material around welds and welded joints. Extrapolating from the assumed relations, we can expect the magnetization around welds to be negatively impacted.

2.3.3. Magnetism based Non-destructive testing methods

Existing magnetism based NDT methods have showed that magnetism can be used reliably to inspect and detect defects in ferromagnetic materials. Although the methods differ, inspection and detection of flaws is based on the disturbance of the local magnetic field. Flaws are characterized by a decrease in magnetic permeability, which causes a magnetic stray field to arise.

The SMFL method uses the earth magnetic field as a source to induce a magnetic field in the research material. This enables passive crack monitoring, but simultaneously results in a relatively low magnetization of the material.

2.3.4. State of the Art

The current state of the art shows a need for more research in several areas, when concerned with the application of the SMFL-method for monitoring cracks in steel structures. This report will address some of these topics.

One important topic towards the application of the SMFL-method for crack monitoring in ships consists of the effect of the opening of the fatigue crack on the MFL-signal. It is known that fatigue cracks will open and close during the fatigue crack growth stage (see 2.1.2). However, it is currently unknown how the MFL is affected by the opening and closing of the crack. Besides the opening and closing of the crack, stress magnetization and the crack closure phenomenon may play a role in the resulting flux leakage field.

Furthermore, a lack of knowledge on the magnetic permeability of weld material exists. This inhibits the development of reliable numerical models of structures that involve welded joints. Determination of this permeability is of importance, since fatigue cracks tend to initiate in the vicinity of these welded joints (see 2.1.1).

Another important topic that will have to be addressed when applying the SMFL-method on steel structures is the role of complex geometries on the MFL field. Earlier research has focused on simplified geometries, while fatigue cracks often develop in areas of stress concentrations that are often caused by changes in geometry (see 2.1.1). This accentuates the need for research in this area.

Finally it can be concluded from a study on the current body of literature that no practical research on the application of the SMFL-method towards the monitoring of cracks in full-scale steel structures has been performed. Instead, most research has focuses on small-scale experiments. Although some research demonstrates the effectiveness of the SMFL-method in detecting fatigue cracks [22] in ship sections, there is currently no research on the capability of the SMFL-method to monitor the length of these fatigue cracks.

3

Experimental results

3.1. Crack Opening Experiment

The crack opening experiment is designed to provide an answer to the first research question and therefore should answer the question:

What is the effect of crack mouth opening displacement (CMOD) on the SMFL measurements in a uni-axially loaded plate from the point of crack detection?

This section describes the experimental equipment, the experimental method and the corresponding experimental results.

3.1.1. Experimental Setup

The experiment was performed by securing a center cracked specimen inside universal tensile testing machine (see figure 3.4), using a magneto meter to take measurements of the magnetic field. A Koshava-USB magnetometer was used to perform measurements on the magnetic field [27]. The magnetometer was calibrated before every measurement with help of a zero Gauss chamber. Using this magnetometer the background field at the test location was recorded to be B_{BG}(x,y,z) = (-0.011,0.001,-0.017) μT at a temperature of 23.5°C.

The test specimen used in the experiment consist of a center cracked plate with tapered ends. The dimensions of the test specimen can be found in figure 3.1. The crack in the center of the plate originates from a 1 mm diameter hole with a machined defect on both sides of the hole. The defects are fabricated using electrical discharge machining. A fatigue crack was induced in the plate through use in a previous experiment and has a length of 20 mm, originating from both defects on the edge of the hole. The specimen is fabricated from s235 structural grade steel and has a predicted maximum tensile load of 82.5 kN (with a 95% change of underestimation) and an expected maximum tensile load of 100 kN (with a 50% of underestimation).

A measurement grid, consisting of 13 parallel measurement paths of 20 mm length (see figure 3.2), perpendicularly crossing the fatigue crack has been attached to the plate. A spacing between the measurements paths of 5 mm is used (see figure 3.1).

3.1.2. Experimental method

During the experiment the specimen was gradually loaded for a relaxed situation (0 kN) up to its prescribed yield limit of 80 kN, with load increments of 10 kN. The magnetic field surrounding the crack was measured during every loading step. Measurements where manually taken, along the predefined linear paths depicted in figure 3.2. During a 4 second period the magnetometer was moved along this measurement path, while measurements were taken with a frequency of 5 Hz. The measurements where performed while a lift-off distance of 1 mm between the sensor and the specimen was maintained. Prior to the experiment the specimen was loaded up to 50% of the expected yield limit, to avoid disturbance of the measurements caused by a

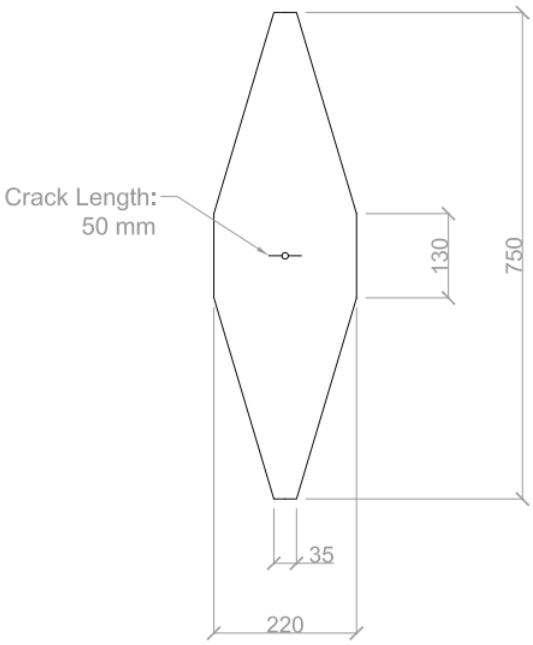

Figure 3.1: Global measurements of the test specimen

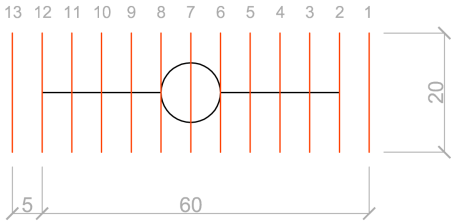

Figure 3.2: Measurement grid around the crack

'shake-down' like effect. This phenomenon was namely encountered in previous test, where the first loading step seemed to cause a slight change in the permanent magnetic field around the crack, resulting in a proportionally big change in the magnetic field. After reaching the recommended yield limit of the specimen, the tensile loading on the plate was in two steps increased to the expected yield limit of 100 kN, in order to increase the CMOD even further. While approaching the expected yield limit, signs of yielding of the plate began to occur and the maximum tensile load was found to be 96 kN. After this procedure the specimen was unloaded again and a second experiment was performed.

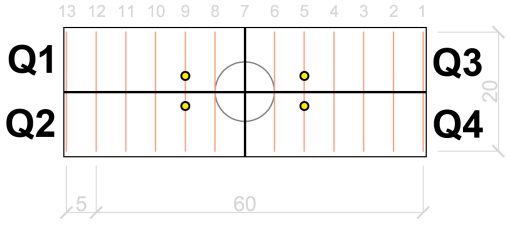

Figure 3.3: Drawing of the location of measurement points Q1, Q2, Q3 and Q4

In this second experiment the development of the out-of-plane magnetic flux density B_z at consecutively Q1, Q2, Q3 and Q4 (depicted in figure 3.3) was tracked, while the load was manually increased from the relaxed conditions (0 kN) up to the recommended yield limit of 80 kN. The location of measurement points Q1 to Q4 coincide with the location of the local maxima and minima on measurement paths 5 and 9.Again a lift-off

distance of 1 mm was maintained during the measurements at all four locations. Subsequently the plate was unloaded to conclude the experiment.

Figure 3.4: Test specimen clamped in the universal tensile testing machine

3.1.3. Results and Analysis

The results of both experiments described in 3.1.2 are presented in figure 3.5 and 3.6. In order to analyze the SMFL with the purpose of finding a relationship between the CMOD and the SMFL, it is most practical to evaluate the peak-to-peak amplitude generated by the crack in the plate. The following analyses of the results will therefore focus on the peak-to-peak value as the defining parameter to describe the amount of SMFL. In this report the peak-to-peak value is defined by equation 3.1.

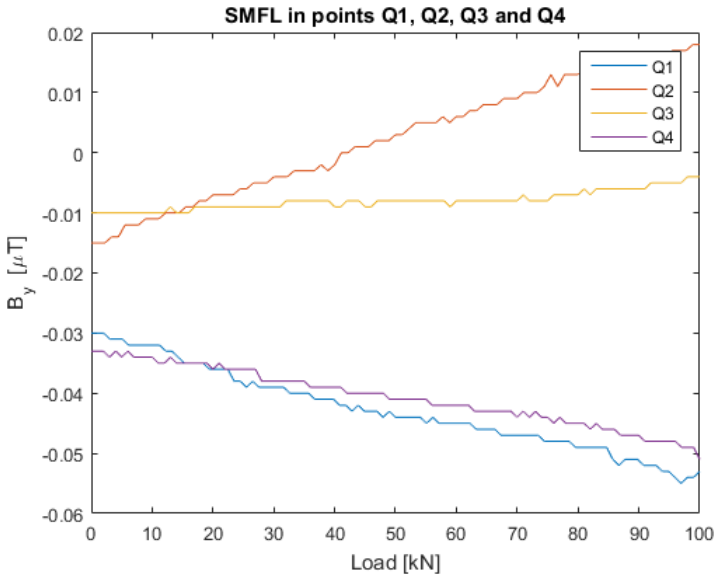

Figure 3.5: Results of the second experiment. The graphs describe the SMFL recorded at for locations (Q1 to Q4) while the tensile load was increased.

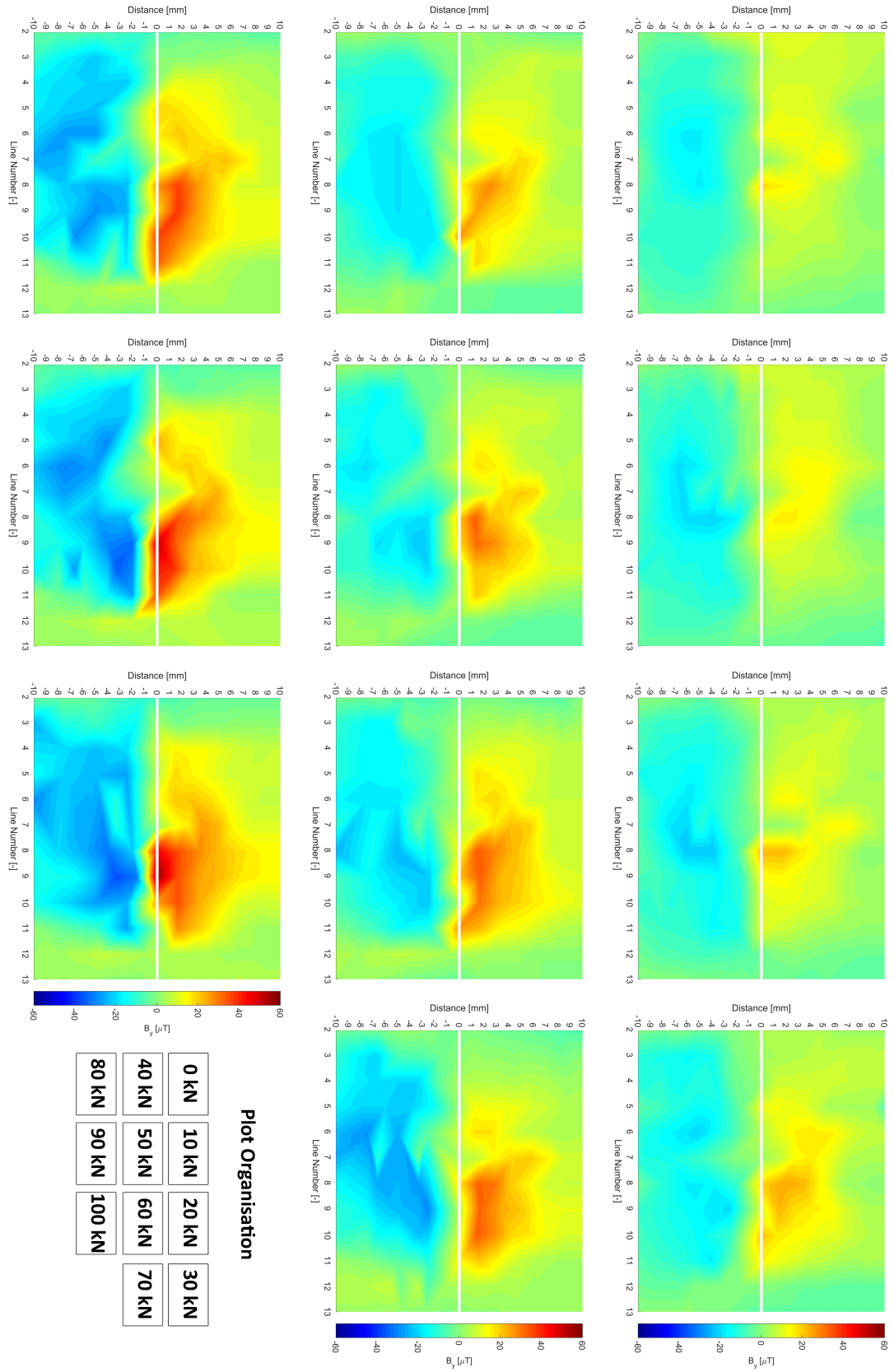

Figure 3.6: SMFL measurement results around a 50 mm crack in a plate, plotted at different tensile loads

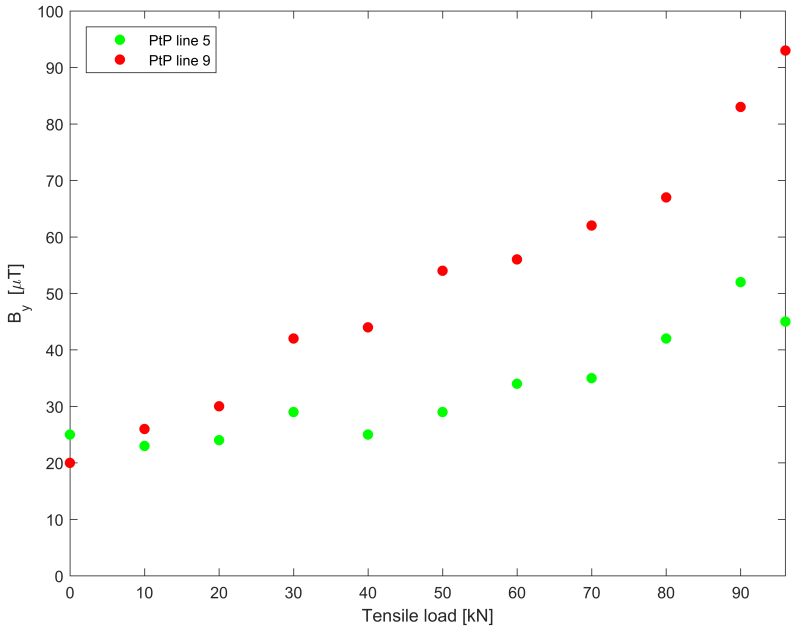

Figure 3.7: Peak-to-peak value at measurement lines 5 and 9 for different tensile loads

Analysis of the data will proceed using this definition of the SMFL signal strength. Although no data on the development of the CMOD during the test was collected, the relationship between the applied tensile force and the corresponding peak-to-peak value over the crack will be analyzed. The development of the peak-to-peak value of measurement lines 5 and 9 with increasing load obtained in experiment 1 is shown in figure 3.7. Measurement lines 5 and 9 are most suited for this analysis, since they are located outside of the influence sphere of the circular defect in the center of the plate while being positioned near the center of the crack.

$$\Delta B_y = max(B_y) - min(B_y); \tag{3.1}$$

The results of figure 3.7 can now be compared to the results of the second experiment described in 3.1.2. Using the data in figure 3.5 and the same definition of equation 3.1 a second peak-to-peak value over measurement line 5 and line 9 can be established. Figure 3.8 combines the results of both experiments and shows a increase of the peak-to-peak value with an increase in the applied tensile force.
The data from experiment 1 can further be used to shed light on the development of the SMFL along the length of the crack. Figure 3.9 shows the peak-to-peak value along the length of the crack at every load step.

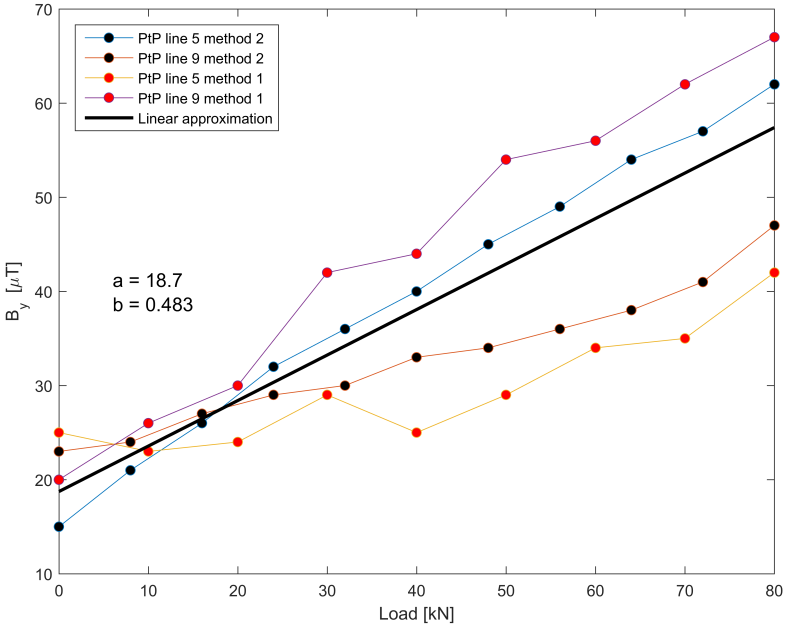

Figure 3.8: Peak-to-peak value of measurement line 5 and 9 for different tensile loads. In this figure the results of two measurement methods are combined

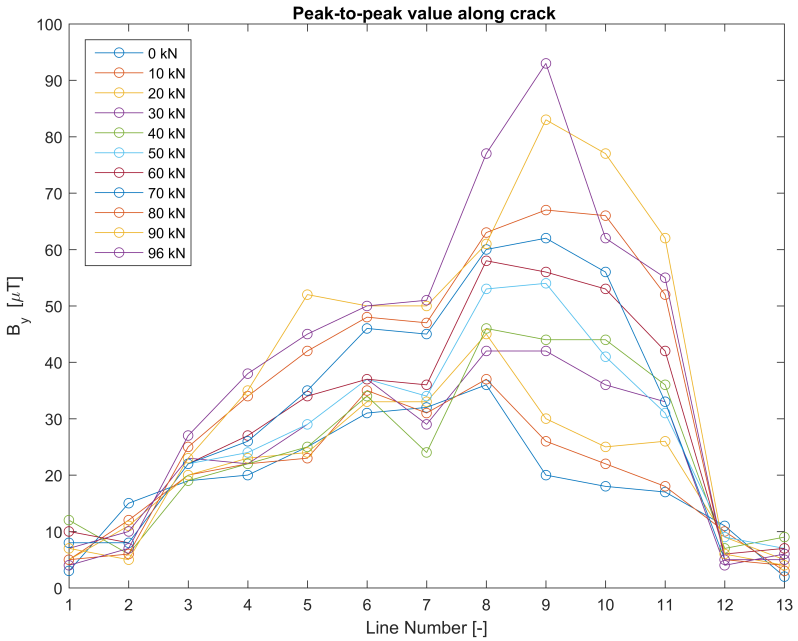

Figure 3.9: peak-to-peak value along the length of the crack at every load step

Finally, the SMFL signal width is analyzed, which is represented by the distance between the maximal and minimal value of the SMFL along the measurement path. Although the signal width cannot be used to estimate the fatigue length or depth, it may give some insight into the grid spacing of SMFL method based monitoring tools. The results from the signal width analysis can be viewed in figure 3.10. The signal width of the measurement path crossing the circular hole (line 7) are again omitted from the analysis. Figure 3.10 shows a signal width ranging from 1.5 to 11.6 mm with an average of 5.1 mm.

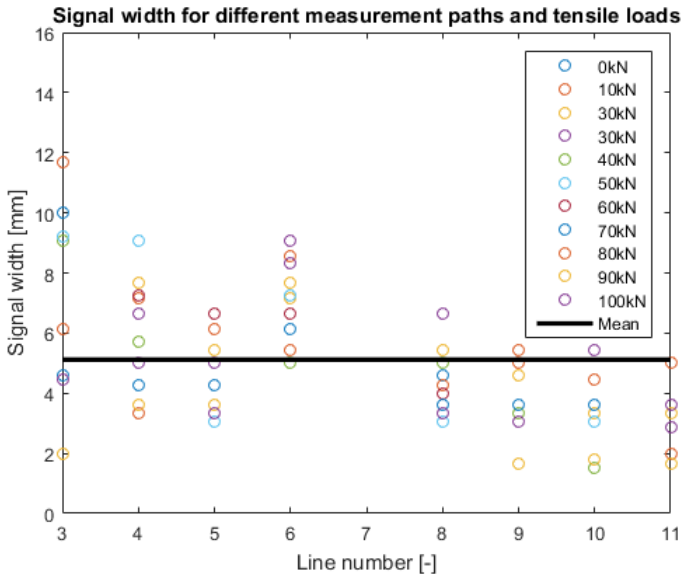

Figure 3.10: Signal width along the fatigue crack plotted at every tensile load step.

3.1.4. Discussion

The analysis of the results of this experiment rely on two important assumptions. The first assumption is is that CMOD increases with tensile load. The second assumption is that the formulated peak-to-peak value is indicative of SMFL strength. The first assumption is probable if a linear elastic material is assumed. Since the applied tensile loads generate nominal stresses below the yield stress of the material, it is reasonable to assume that linear elastic mechanics apply. At the crack tip, where a stress concentration can be found, plasticity may however occur, which should be taken into account in the analysis of the results. Secondly, the crack closure phenomenon (see section 2.1.3) is not accounted for in this experiment. This phenomenon may manifest itself by a discrepancy between tensile load and CMOD.

Looking at figure 3.6, it can be concluded that the second assumption is reasonable. From this figure it can be observed that an increase in SMFL is accompanied by an increase in the highest and lowest values of the out-of-plane magnetic flux density. With these assumptions in mind, it will be concluded that an increase in peak-to-peak value with tensile force (see 3.8) is equal to an increase in SMFL signal strength with CMOD. The result in figure 3.8 furthermore show that some SMFL occurs, even when no tensile force is applied to the specimen.

Analyzing the peak-to-peak value along the crack length, which is shown in figure 3.9, it can be concluded that the peak-to-peak value increases from crack tip to crack center. This observation was observed in earlier research as well[24]. It can be observed from the same figure that an increase in peak-to-peak value is more apparent on the right side of the crack, compared to the left side. This observation may be explained by unsymmetrical clamping of the plate in the testing machine, which in turn causes a difference in crack opening between the right and left side of the crack.
The analysis of the signal width is based on the assumption that the magnetometer was manually moved over the measurement path with a constant speed. Judging from the results in figure 3.6, this is a reasonable assumption, since it can be observed that the real crack position correlates reasonably well with the crack location as predicted by the SMFL measurements.

Now, looking at the results of the signal width analysis in figure 3.10, it can be concluded that the signal width does not seem to depend on the applied tensile load. The signal width furthermore does not seem to change from crack tip to crack center to any significant degree. It is however unclear whether the determined signal width is applicable to full-scale structures as well.
Finally it should be mentioned that stress magnetization may have influenced the measurement results. The measured data does however not provide any indication on the magnitude of this effect.

3.1.5. Conclusion

Fatigue cracks develop in steel structures as a result of cyclic opening and closing. This cyclic opening and closing is therefore inherent to the development of fatigue cracks and its effect on SMFL should therefore be taken into account when designing a system aimed at monitoring fatigue cracks. In the described experiment the CMOD of a fatigue crack is increased by means of applying a tensile load on a center cracked plate, while the SMFL around the crack is monitored. This is action is performed to replicate the opening portion of a fatigue cycle and discover how the SMFL is influenced.

Based on the results of the experiment it can be concluded that the SMFL signal increases with an increase in CMOD. The results furthermore show that some SMFL can even be detected, when the fatigue crack is fully relaxed. The measured SMFL is however more apparent when the CMOD is increased. Additionally, it is concluded that the SMFL increases towards the center of the crack. Towards the application of the SMFL method for monitoring fatigue cracks, this means that the measured SMFL signal strength may change significantly over time, as a result of cyclic opening of the fatigue crack. In order to use the SMFL method to monitor crack length, measurements should be taken during the entire load cycle.

The obtained data of the measurements in the experiment is furthermore used to analyze the SMFL signal width. Regarding the signal width it is concluded that the signal width does not depend on CMOD or location along the crack length. More research is however needed in order to say something quantitatively about the signal width in full-scale structures.

3.2. Magnetic permeability experiment

The Finite Element Method (FEM) can be used to model MFL around fatigue cracks and can be especially advantageous to analyze the influence of isolated parameters. In order to obtain useful information from these models it is important to provide the model with the right material parameters. This experiment focuses on one such parameter, used in the numerical simulation of a T-joint 4.4, where the influence of the magnetic permeability on the MFL around a crack at the weld toe of a double sided fillet weld is investigated. Based on one paper [12] that looked into the MFL around a butt joint it is expected that weld material has a lower magnetic permeability than a structural steel plate. The paper predicts a lower magnetic permeability based on a literature study on the difference in magnetic material properties between base material and weld material and subsequently measured MFL around a butt weld using a magnetometer. However, based on the analysis of a numerical simulation of the same butt weld it is concluded that the predicted magnetic permeability does not correspond to the permeability of the tested weld. The following test is devised to experimentally determine the magnetic permeabilities of base material, weld filler material and material from the HAZ, in order to provide input for use in FE models. The described experiment should answer the following research question:

What is the magnetic permeability of weld filler material and HAZ material and how does it compare to the magnetic permeability of a s235 structural steel plate?

This section describes the experimental equipment, the experimental method and the corresponding experimental results. Background information on the determination of magnetic permeability can be found in appendix B.

3.2.1. Method

The permeability determination was performed in accordance with test method 5 from the ASTM standard test methods for permeability of weakly magnetic materials [28]. The test was performed using a vibrating sample magnetometer. The test was performed on a total of 9 specimens of 2x2x2 mm, originating from three different locations in around the weld (see figure 3.11). The weight of the specimens can be found in table 3.1. The specimens were taken from a double-sided fully penetrated T-joint from plates of s235 structural steel that was produced by MIG-welding. The specimens were obtained from this T-joint by electrical discharge machining. During the test the magnetic field strength was raised up to 0.3 T in order to simulate a weak magnetic field. The specimen were numbered 1.1 to 3.3, where the first digit refers to the location in the material (see figure 3.2). The magnetometric demagnetizing factor N_m used to calculate the demagnetizing field was chosen to be 0.276, which is in accordance with [29].

3.2.2. Results

The results show no significant difference between the magnetic permeabilities of the three designated locations within the T-joint specimen, as can be observed from table 3.1. Furthermore, it can be seen from the standard deviation in table 3.1 and an example of one of the measurement series in figure 3.12 that the results have a narrow scatter band.

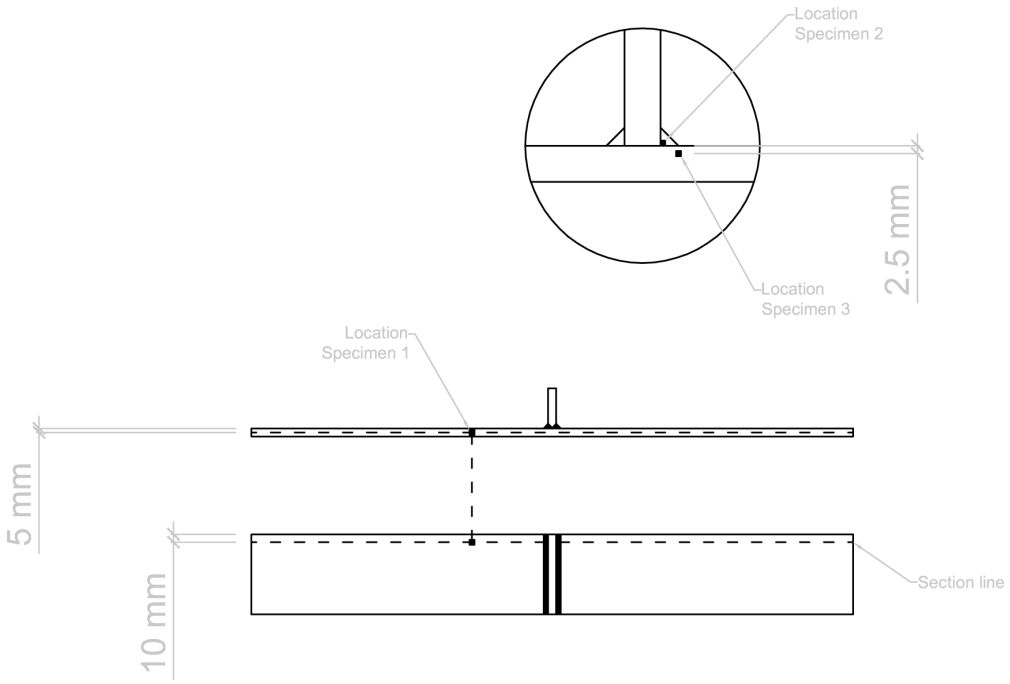

Figure 3.11: Location of the Specimens. 3 Specimens were taken from each location.

Specimen number	Relative permeability [-]	Standard deviation [-]	Weight [mg]
1.1	171.23	4.61	59.48
1.2	175.80	4.71	59.59
1.3	173.21	4.72	59.64
2.1	178.27	3.18	59.77
2.2	169.54	4.97	59.86
2.3	177.45	5.70	59.97
3.1	173.28	4.02	59.93
3.2	170.65	3.99	59.54
3.3	171.59	4.45	59.72

Table 3.1: Description of material type and weight of all specimens

3.2.3. Discussion

From the experimental results it can be concluded that no statistically significant difference between the magnetic permeability of base material, weld filler material and HAZ can be found. The resulting magnetic permeabilities fall in a range of magnetic permeabilities found in earlier research [10][11].

Based on earlier research that found MFL around a butt weld [12] and differences in material properties between weld and base material that are known to influence magnetic permeability [14][13] a difference in magnetic permeability was anticipated. This notion could lead one to one of two conclusions: either the MFL around a butt weld found in [12] is caused by other factors than a difference in permeability between base material and weld material or the results found in the permeability experiment are not valid.

The first conclusion would point to other factors involved with welding process to be responsible for the measured MFL around the butt weld. One could speculate that the MFL could in this case be induced by factors related to residual stresses and permanent magnetization, since it is known that residual stresses can impact magnetization[30] and that permanent magnetism can be influenced by electric current, such as the electrical currents involved in the welding process. Currently no knowledge exists on the influence of residual

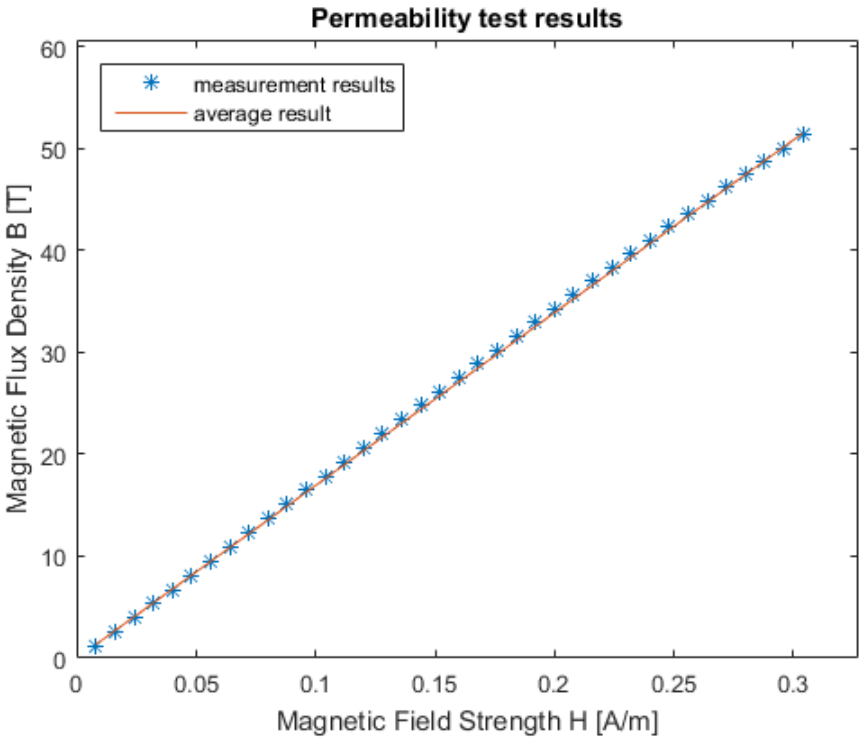

Figure 3.12: Permeability measurements of the described test on specimen 1.1.

stresses on the stress induced magnetization. In addition it should be noted that the influence of mechanical stress on magnetism is complex and it is therefore hard to extrapolate from the current body of literature. It is however known that electrical currents can influence the permanent magnetization of the plate.

The alternative conclusion can be supported by arguments that question the validity of the performed permeability experiment. In this case the machining used to obtain the specimens could be responsible for the converging of the resulting magnetic permeabilities. The electrical discharge machining used in the fabrication of the specimens is a thermal process that may impact the material locally. The impact of this manufacturing process on the magnetic permeability is currently unknown, but it could be hypothesized that the thermal stressing of the material could affect have an annealing effect. This would impact the grain size of the material of the specimen and subsequently change the permeability, causing the magnetic permeabilities to converge to a similar value.

It should furthermore be noted that the cubical shape of the specimens does not allow homogeneous magnetization throughout. This causes the demagnetizing field, which is calculated as the product of the magnetization M of the specimen and the magnetometric demagnetizing factor N_m, to be inhomogeneous as well. The permeabilities are however calculated based on the assumption of a homogeneous magnetization inside the specimen. It is however impossible to investigate this effect, since the orientation of the specimens inside the Vibrating Sample Magnetometer cannot be controlled. The way in which this unknown orientation impacts the results should however be relatively modest, since the specimens have a small aspect ratio. This presupposition is supported by the low scatter in the experimental results. Concerning the inhomogeneous magnetization of the specimens, it is difficult to quantitatively describe the size of its effect.

3.2.4. Conclusion

The Finite Element Method (FEM) is a useful tool to analyze magnetic leakage field around cracks to help interpret SMFL measurements. Numerical models require reliable material models to produce reliable results. Based on previous experiments and differences in material properties, that may impact the magnetic permeability, between base material and weld material it is expected that a difference between the magnetic permeabilities of base material and weld material may exist. In order to construct numerical models that

involve welded joints it is essential to know the magnetic permeability of weld material. The permeability experiment described in this section is designed to determine the magnetic permeabilities of s235 structural steel and weld filler material and HAZ of a fully penetrated weld manufactured using MIG welding.

The results of the experiments show a relative magnetic permeability of 173.41 for base material, 175.09 for weld filler material and 171.84 for the HAZ. The difference between the magnetic permeabilities is however not statistically significant.

3.3. Bridge Deck Experiment

The CrackGuard JIP intents to develop the a reliable system for the monitoring fatigue cracks in ship and offshore structures using the SMFL method. Earlier research [11][22] has proven the concept of the SMFL method for monitoring fatigue cracks in small-scale specimens. However, full-scale steel structures are expected to differ from these small-scale specimens by a higher magnetization among other things and may even present challenges that are currently unknown. The Bridge deck experiment is designed to assess the application of the SMFL on a full-scale steel structure. The experiment is aimed at demonstrating whether it is possible to monitor fatigue crack length in the cross beam of a full-scale replica of a bridge deck using the SMFL method. This replica of a bridge deck, which is set-up in the structures laboratory of the TU Delft, is a partial copy of an existing bridge in the Netherlands and provides the opportunity to test the SMFL method in conditions similar to conditions on operating full-scale structures.

3.3.1. Experimental Setup

The described bridge deck replica is part of an experiment to test the response of the structure to fatigue loading with a frequency of 3 Hz. As a result of this fatigue loading, fatigue cracks have appeared in the crossbeam of the structure, where they originate from the welds of box girders that run along the deck of the structure and propagate into the transverse crossbeams (see figures 3.13 and 3.14). Cracks 1 and 2, as depicted in figure 3.13 are located in a different crossbeam than crack 3. The plate thickness of the cross beams is 16 mm and the box girders are 6 mm thick, both are made of FeE355 steel. One of the fatigue cracks, on which measurements were performed for this experiment, propagated during the experiment as a result of a transverse load that was applied cyclically on the deck between the box girders as seen in figure 3.15.

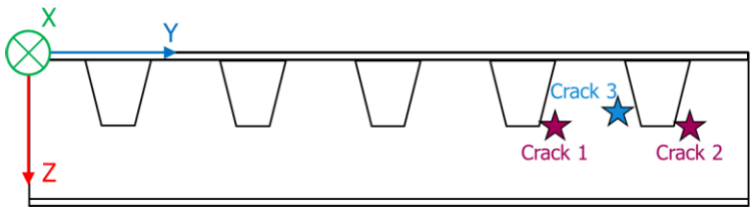

Figure 3.13: Schematic cross-section of the bridge deck with location of the fatigue crack

Figure 3.14: Fatigue crack (25 mm) propagating into the crossbeam of the bridge deck

Figure 3.15: Loading on the bridge deck responsible for propagation of the fatigue crack

3.3.2. Experimental Method

During the experiment measurements of the MFL around three fatigue cracks (see figure 3.13) were taken using a hand-held magnetometer [27] and the CrackGuard (see A). These measurements recorded the out-of-plane component of the magnetic flux density with a lift-off of respectively 1 mm and 2 mm. A measurement grid with a grid spacing of 5 mm was placed on top of the cracks and used to perform the measurements of the hand-held sensor, which is shown true to size in figure 3.18.

Figure 3.16: Fatigue crack propagating into the crossbeam of the bridge deck

Two situation are discussed in this experiment: the measurement of cracks 1 and 2 (see figure 3.16) and separately the measurements of crack 3 (see figure 3.14). In the first situation measurements of the out-of-plane magnetic flux density around the crack were taken using the hand-held sensor only.

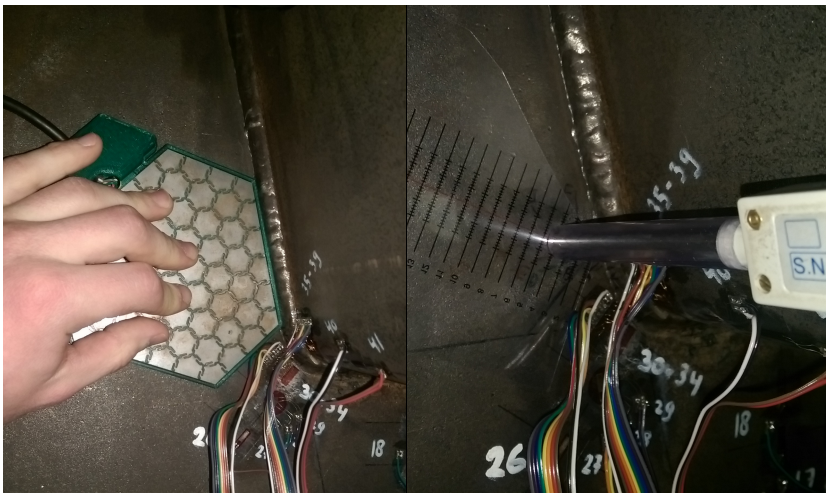

Figure 3.17: Measurement methods using the CrackGuard (Left) and the Koshava USB Magnetometer (Right)

In situation 2, measurements were taken with the hand-held sensor at each grid point from column 3 to 21 and row 1 to 5 during every set of measurements. At the start of the experiment the fatigue crack in figure 3.14 had a length of 25 mm, meaning that the crack tip was located under column 4. Fatigue crack 3 propagated thereafter from right to left relative to the measurement grid during the experiment. Measurements with the CrackGuard were taken simultaneously with measurements of the hand-held sensor. A set of measurements (using both the hand-held sensor and the CrackGuard) of fatigue crack 3 was taken at crack lengths of 25, 30, 35, 41, 44, 48 and 50 mm. The length of the propagating fatigue crack was measured manually with the help of a magnifying glass. The Earth magnetic background field at the time of the measurement on the specific location was measured to be B_{BG}(x,y,z) = (7, -8, 31) μT with the axis corresponding to the coordinate system in figure 3.13

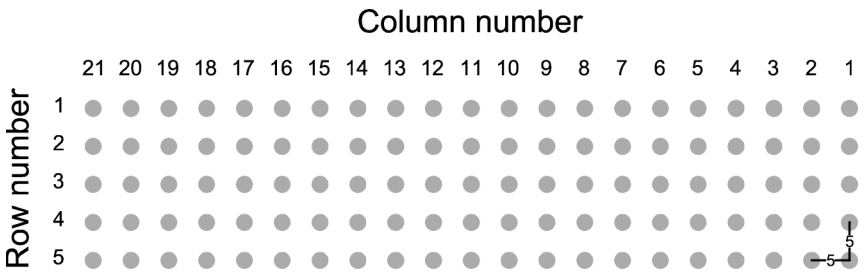

Figure 3.18: Measurement grid used to perform the the measurements of the hand-held sensor

3.3.3. Results and Analysis

The presented measurement results of the hand-held magnetometer show the measured magnetic flux density in out-of-plane direction at an altitude of 1 mm above the plate surface. Results of the SMFL measurements recorded with the CrackGuard show the same component of the magnetic flux density. It should be noted however that the altitude of the hall effect sensors in the CrackGuard is 2 mm and involve the effect of a backplane (see section A.4) behind the sensors.

The experimental measurements were initiated by a preliminary investigation on the magnitude of the expected SMFL signal. This was done by measurements on fatigue cracks 1 and 2, that were already present in the structure. The results of the preliminary SMFL measurements performed with the hand-held magnetometer on fatigue crack 1 and 2 can be found in figures 3.19. The crack tips of fatigue cracks 1 and 2 were in these measurements located under column 14 and 6 respectively. Furthermore, preliminary measurements of the SMFL around fatigue cracks 1 and 2 were taken with the CrackGuard as well, in order to explore the effect of different orientations of the CrackGuard on the subsequent measurements. The results of these measurements are presented in figure 3.20.

After the preliminary measurements on fatigue cracks 1 and 2, which showed hopeful results, another series of measurements was performed on fatigue crack 3. These measurements consisted of SMFL measurements using the hand-held magnetometer as well as the CrackGuard in different stage of fatigue crack propagation. The results of the SMFL measurements performed with the hand-held magnetometer of fatigue crack 3 can be found in figure 3.21, whereas the results of the SMFL measurements performed with the CrackGuard on fatigue crack 3 can be found in figure 3.22.

The post-processing of the data of the SMFL measurements performed with the hand-held magnetometer on fatigue crack 3 was later performed, in order to improve the understanding of the measured results and apply newly gained insights to the obtained data. Post-processing was performed in accordance with the conclusions in chapter 5 by interpolation of the data using a spline function and presenting the data in the integrated form with an average per row compensation.

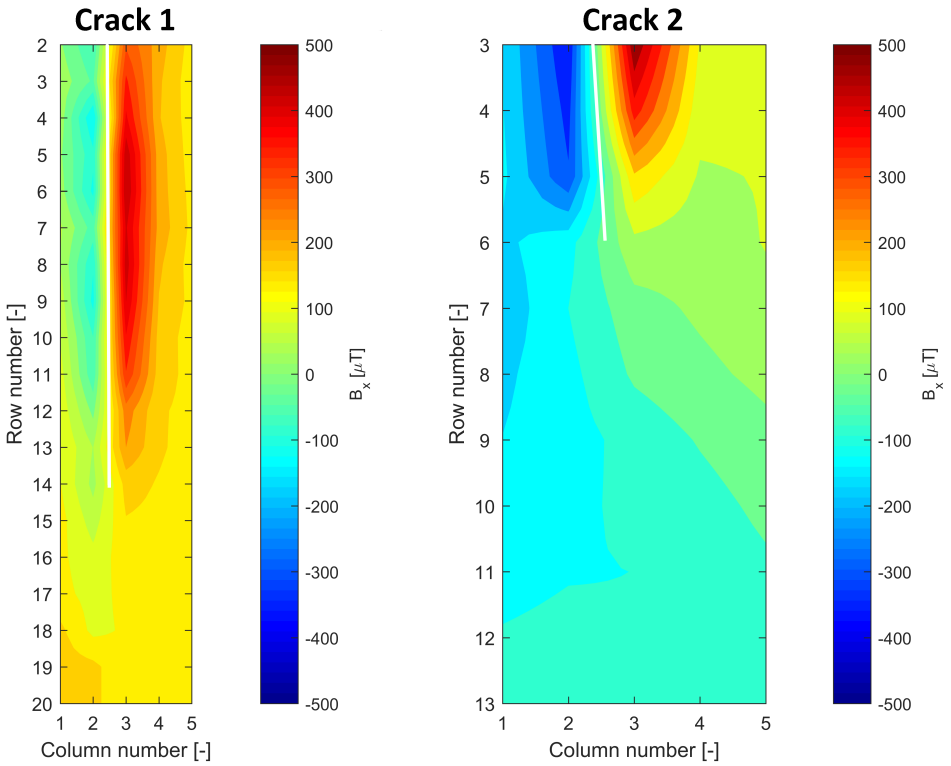

Figure 3.19: Preliminary SMFL measurement results using the hand-held magnetometer for fatigue cracks 1 (Left) and 2 (Right). The location of the fatigue crack is approximated by the white line. The results are presented in the linearly interpolated form

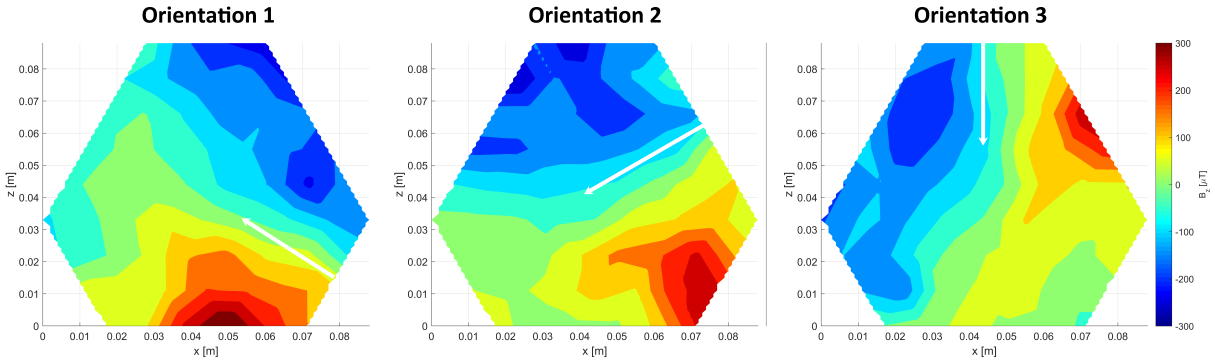

Figure 3.20: Preliminary SMFL measurement results using the CrackGuard for fatigue crack 1 at different orientations of the CrackGuard relative to the fatigue crack. The fatigue crack direction is indicated by the white arrow. The results are plotted using linear interpolation

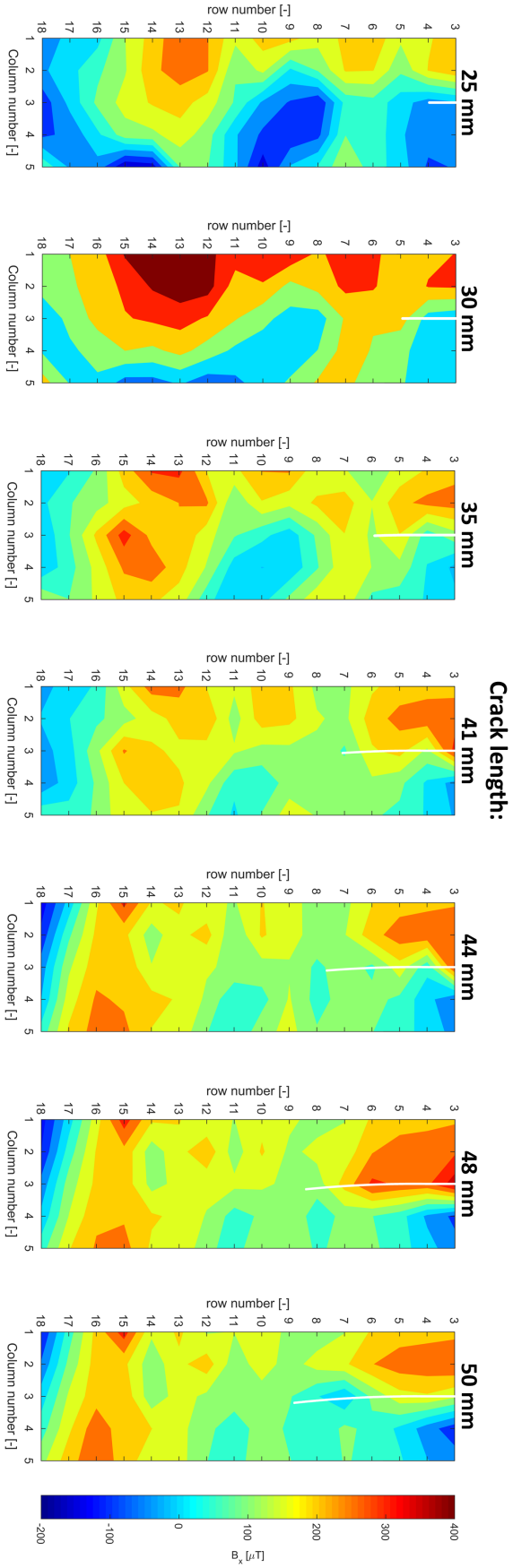

Figure 3.21: SMFL measurement results of fatigue crack 3 at different stages of crack propagation. The fatigue crack is indicated in white. The results are presented in the linearly interpolated form

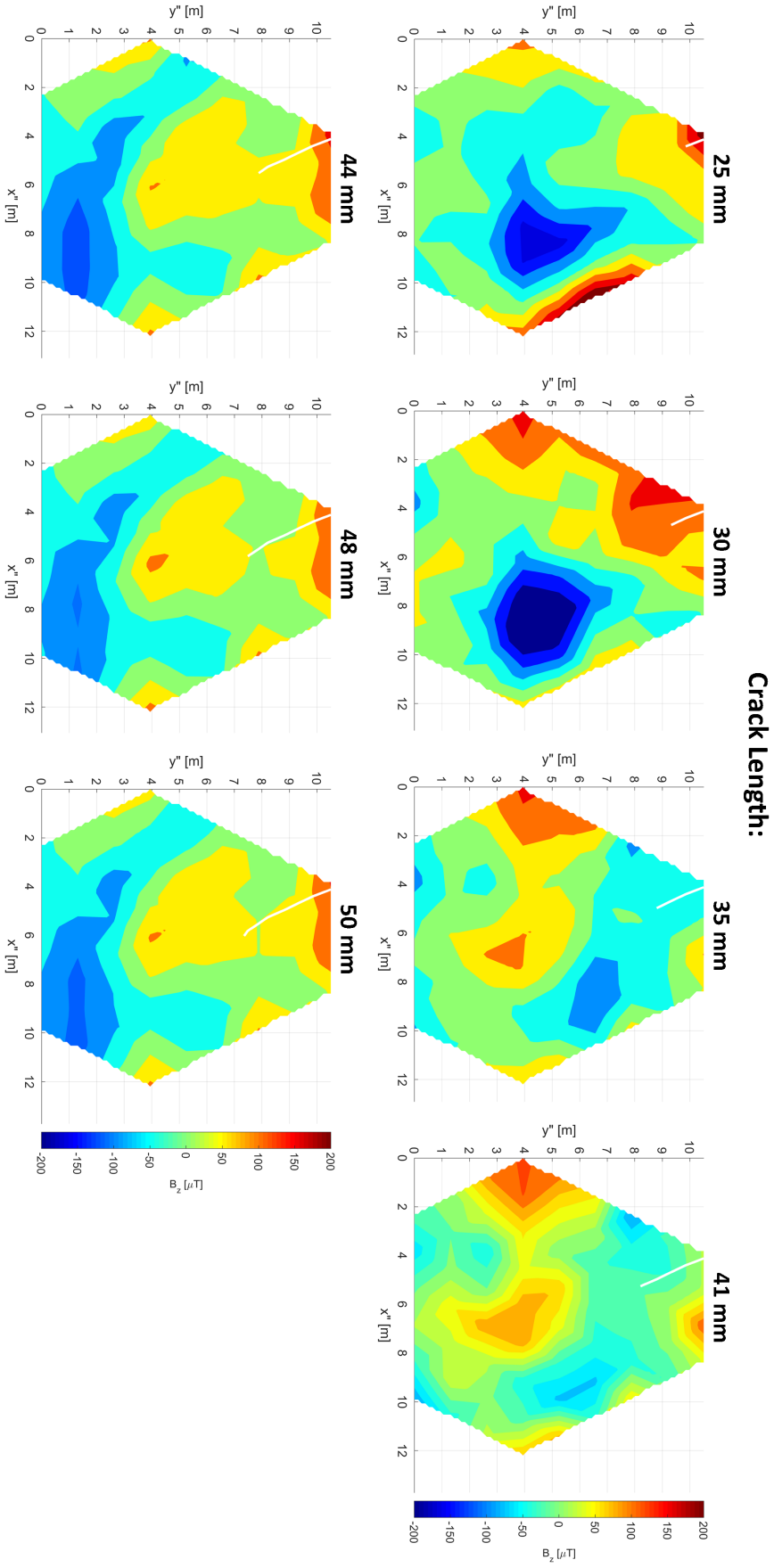

Figure 3.22: Spline interpolated and integrated SMFL measurement around the fatigue crack.

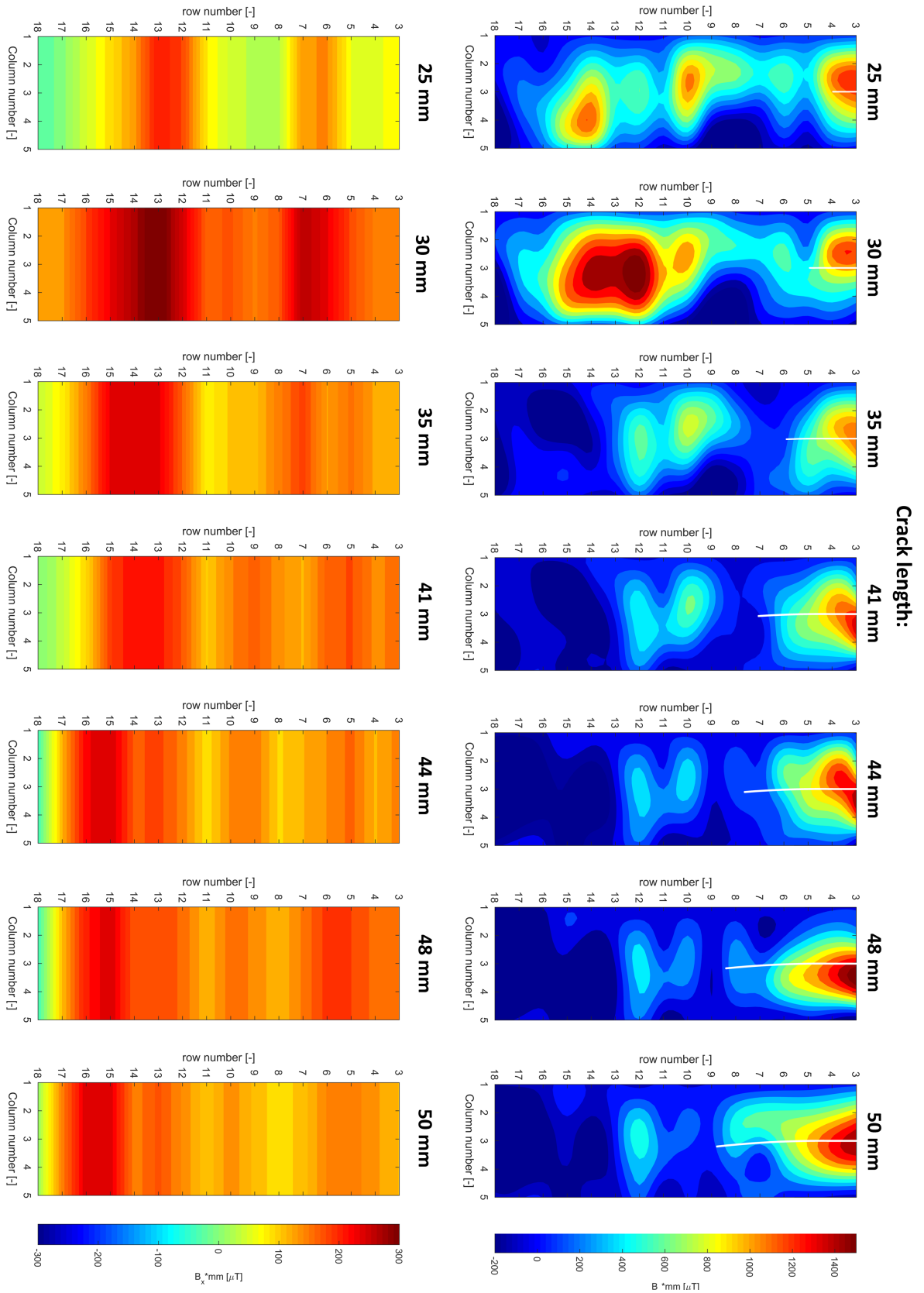

Figure 3.23: Post-processed SMFL measurement results per crack length. The fatigue crack is marked by the white line. Left: Average rest magnetization per column. Right: results presented in the integrated presentation form (average per row compensation) with spline interpolation.

3.3.4. Discussion

Evaluation of the preliminary measurements (figures 3.19 and 3.20) demonstrates that the characteristic SMFL pattern can be observed using a hand-held magnetometer with a 5 mm grid spacing. The magnitude of the measured SMFL is significantly greater than the measured SMFL in small-scale specimens. This difference can be attributed to a higher magnetization of the full-scale replica, compared to the small-scale specimens, due to a larger amount of ferromagnetic material. Measurement results of the CrackGuard show that it is possible to recognize the fatigue crack in the measured SMFL, as is demonstrated by the change is SMFL when the orientation of the CrackGuard is changed. The CrackGuard measurements show furthermore that the leakage pattern is dispersed over a larger area, as compared to the measurements of obtained with the hand-held magnetometer. This might be caused by the combined influence of the backplane and the greater sensor altitude of the CrackGuard.

Looking at the SMFL measurements of the hand-held magnetometer of fatigue crack 3 (figure 3.21), it can be observed that the characteristic SMFL pattern increases with an increase in crack length. This observation supports and strengthens the hypothesis that the SMFL method might in the future be applied as a valuable tool for fatigue cracks monitoring. The measurements show that the characteristic SMFL pattern develops as the fatigue crack propagates. The results show however that the SMFL pattern diminishes and finally vanishes towards the crack tip. The crack tip seemingly does not disturb the magnetic flux enough to cause a notable flux leakage, which can be attributed to the fact that the fatigue crack is not fully developed (as a through thickness crack) at the crack tip.

Inspection of the SMFL measurements of the CrackGuard in figure 3.22 shows that the CrackGuard is less capable of detecting the characteristic SMFL pattern around fatigue crack 3. Although the measurements show that some SMFL generated by the fatigue crack can be observed, the signal of a lower magnitude, less pronounced and more dispersed over the area. The causal factors for this difference are most probably the effect of the backplane, the increased sensor altitude, the larger grid size and the lower precision of the hall effect sensors in the CrackGuard.

The post-processed results in figure 3.23 show that post-processing improves the interpretation of the measurement data and thereby supports the conclusions in Chapter 5. Looking at the results of the integrated and interpolated results, it can be observed that the applied compensation to the rest magnetization is reasonably successful, especially in filtering the rest magnetization with a relatively constant distribution. The compensation is however less capable of filtering more local and abrupt changes in the rest magnetization. The derived rest magnetization field is 3.23 shows that the rest magnetization is changing over time, which is in accordance with earlier research [10]. Furthermore, the derived rest magnetization is of a magnitude similar to the characteristic SMFL pattern, emphasizing the importance of filtering techniques in order to be able to monitor fatigue cracks reliably. It should be said that this rest magnetization is primarily caused by the influence of permanent magnetization and that nothing can be said about the influence of stress magnetization on the SMFL measurements based on the presented results.

The same measurements show a notable disturbance of the crack site at the second stage of crack propagation (30 mm). At this stage of crack propagation the crack length and depth profile had was measured periodically using alternating current potential drop equipment, which involved placement of electrical probes using permanent magnets on the steel surface around the crack. The permanent magnets were not always placed at the exact same location so the disturbance they induced cannot be calibrated for. This disturbance is clearly visible in all measurements of fatigue crack 3 as well, including the measurements obtained with the CrackGuard. It is important to note that this disturbance disappears with time and normalizes over subsequent stages of crack propagation. This effect has been observed in the Crack Opening experiment (section 3.1) as well and might be attributed to a shake-down effect caused by mechanical loading around the fatigue crack.

3.3.5. Conclusion

The CrackGuard JIP is created with the goal of developing a reliable system for monitoring fatigue cracks in ship and offshore structures using the SMFL method. This method has proved to be an effective technique for monitor fatigue cracks in test specimens under laboratory conditions. In order to apply the SMFL method reliably to operating ship and offshore structures, the method has to be tested on full-scale structures. The described experiment consists of a series of measurements on 3 different fatigue cracks in a full-scale replica of a bridge deck that has been subjected to fatigue loading.

The results of the measurements show that it is possible to detect and monitor fatigue cracks in the described structure using a hand-held magnetometer by taking measurements on a 20x100 mm grid with 5 mm grid spacing. The measurements furthermore show that it is even possible to follow the development of a propagating fatigue crack to some extend. The measured SMFL pattern is of a significantly greater magnitude than the SMFL pattern observed in small-scale experiments. Additionally, it can be observed that the influence of the permanent magnetization in the structure is of a similar scale as the crack induced SMFL. This permanent magnetization can be seen to change slowly over time and to normalize partially after disturbance.

Post-processing of the obtained results by separating the permanent magnetization and the induced magnetization is demonstrated to be reasonably effective and to improve interpretation of the data. The applied technique is however not sufficient to filter out the influence of the permanent magnetization entirely. Therefore, more research in this area of post-processing and the distribution of the permanent magnetization will be necessary to improve filtering techniques and thereby improve crack localization using the SMFL measurements.

Measurements performed using the latest prototype of the CrackGuard demonstrate that the CrackGuard can be succesfully applied to detect fully developed fatigue cracks in full-scale structures. However, the prototype needs to be improved in order to use its measurement data effectively to monitor the development of propagating fatigue cracks. This improvement should be aimed at increasing the sensitivity of the involved Hall effect sensors and increasing the precision of the obtained measurements.

3.4. Dredger Experiment

The CrackGuard LT is one of the latest developments in the application of SMFL-based systems for monitoring fatigue cracks. A previously performed experiment on a full-scale replica of a bridge deck has demonstrated that it is indeed possible to recognize the characteristic SMFL pattern around a fatigue crack from the collected data. However, this pattern is only detected when the associated magnetization is relatively high and the fatigue crack is in the later stages of its development. The application of the CrackGuard on even bigger steel structures could help to improve the measured signal, since it is known that bigger structures have a higher induced magnetization. The dredger experiment is designed to demonstrate how the CrackGuard performs on an operating ship, the type of structure for which the CrackGuard has been designed. The associated research question, which should be answered by this experiment is:

Is it possible to monitor crack length of a fatigue crack in the torsion box of an operating trailing suction hopper dredger using the CrackGuard LT?

This section describes the experimental equipment, the experimental method and the corresponding experimental results.

3.4.1. Experimental Setup

The experiment is performed on board of a trailing suction hopper dredger. Inspections on this hopper dredger have revealed the existence of multiple fatigue cracks in the torsion box of the dredger. These fatigue cracks originate from slot welds (80x25 mm) in connecting the plating (15 mm thickness) with transverse plates (20 mm thickness) inside the torsion box. Drawings of this construction can be found in figures 3.24 and 3.25. A schematic overview of the ship including axis system can be found in figure 3.26.

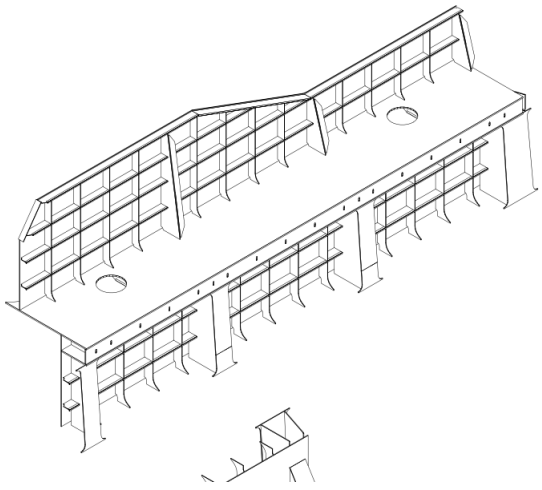

Figure 3.24: Global drawing of the torsion box

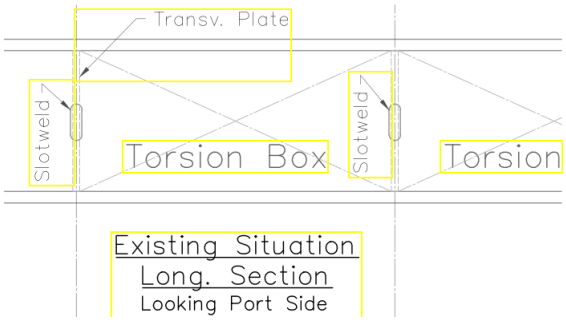

Figure 3.25: Detailed drawing of the torsion box

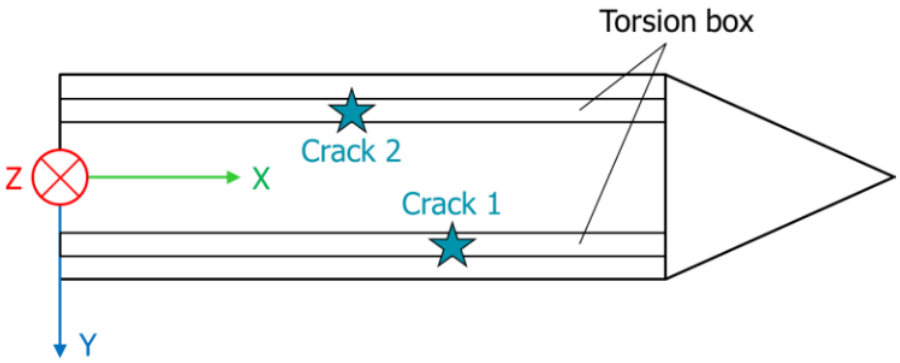

Figure 3.26: Situation sketch of the dredger including axis system

3.4.2. Experimental Method

The experimental method will consist of two visits to the dredger: A first visit aimed at crack inspection and a second visit to conduct the experiment.
On the first visit the magnetic leakage field around the fatigue cracks will be investigated using a KOSHAVA USB magnetometer [27]. This will be done by placing a measurement grid around the fatigue crack, which consists of parallel measurement paths with a spacing of 5 mm. With help of the magnetometer the maximum and minimum out of plane magnetic flux density B_z will be determined along these measurement paths. These measurements will take place while the dredger is moored alongside a quay, in a location where a calm sea state is present. Based on these measurements a signal range can be determined. Based on these preliminary measurements it will be concluded whether the signal strength is sufficiently strong to be able to use the CrackGuard LT (see Chapter A) for monitoring the crack length. Two of the cracks on which preliminary measurements were performed can be found in figure 3.27. The first cracks is located in a spot where significant corrosion occurred as a result of paint removal for inspection purposes. The second crack is located at the small corrosion spots and is still covered by a layer of paint.

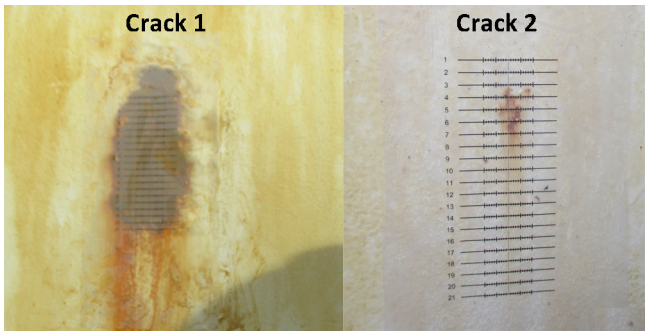

Figure 3.27: Situation sketch of the dredger including axis system

During the second visit the experiment will be conducted. First, the Earth's magnetic background field at the location of the crack is determined with help of a hand-held magnetometer [27]. Secondly, the MFL around the fatigue crack is determined using the hand-held magnetometer, to establish a reference measurement. This is done by the measurement of the out-of-plane magnetic flux density at every grid point on the measurement grid. For this experiment the same measurement grid was used as the grid used in the bridge deck experiment (figure 3.18). Finally, the CrackGuard is installed over the fatigue crack, using double sided tape to keep the sensor in place (see figure 3.29). A protective case is placed over the CrackGuard, in order to shield it from sea spray. Following the installation of the equipment on the ship, the sailing course of the dredger has be recorded using the compass on board, while the dredger is simultaneously collecting sediments.

In the second part of the experiment, the MFL around the fatigue crack is recorded with help of the CrackGuard during the unloading of the hopper, which is performed at the end of a dredging cycle. During this

operation, the dredger goes from fully loaded to fully unloaded condition in 5 to 10 minutes by dumping the content of the 26 ton hopper while maintaining heading.

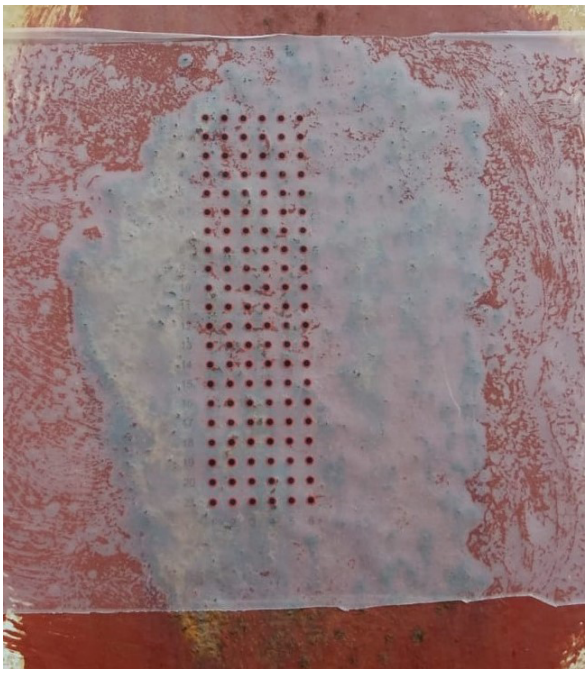

Figure 3.28: Fatigue crack 1 as encountered on measurement day 2, including measurement grid used for measurements with the handheld sensor

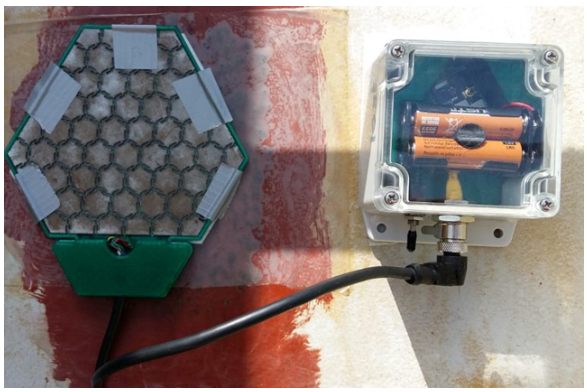

Figure 3.29: The CrackGuard installed over fatigue crack 1

3.4.3. Results and Analysis

The presented measurement results of the hand-held magnetometer show the measured magnetic flux density in out-of-plane direction at an altitude of 1 mm above the plate surface. Results of the SMFL measurements recorded with the CrackGuard show the same component of the magnetic flux density. It should be noted however that the altitude of the sensors in the CrackGuard is 2 mm and involve the effect of a backplane (see section A.4) behind the sensors. The results of the preliminary measurements of measurement day 1 are presented in figure 3.30. During these measurements the Background field was recorded to be $B_{Background}$(x,y,z) = (-29, 71, 35)μT. A maximum signal amplitude of 1656 μT was recorded on crack 1, while a maximum signal amplitude of 269 μT was recorded on fatigue crack 2.

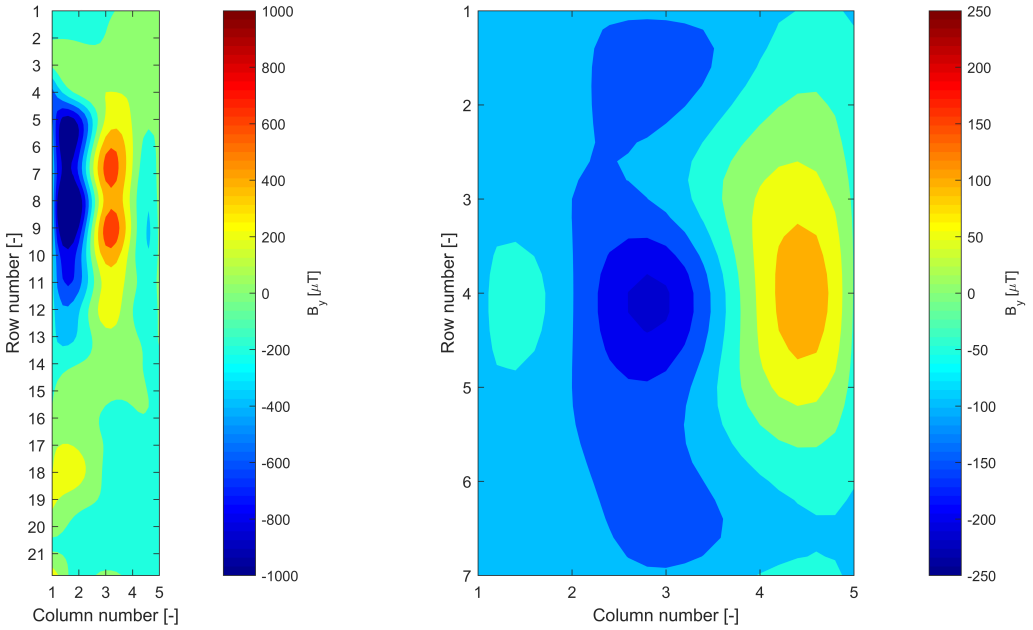

Figure 3.30: Results of measurements performed on day 1 of cracks 1 and 2. The plot shows the SMFL around cracks 1 and 2 measured by the handheld magnetometer on the grid points of the measurement grid and are interpolated using a spline function.

Based on the results of the preliminary measurements of measurement day 1 it was decided to apply the CrackGuard on fatigue crack 1 for the second measurement day. The signal amplitude around this crack is comparable to the signal amplitude of crack 1 in the bridge deck experiment, where it was possible to recognize the fatigue crack location from the obtained SMFL measurement data. A second measurement day was therefore scheduled 4 months after measurement day 1. The results of the reference measurements obtained with the handheld magnetometer are presented in figure 3.31. A maximum signal amplitude of 220 μT was recorded during these measurements.

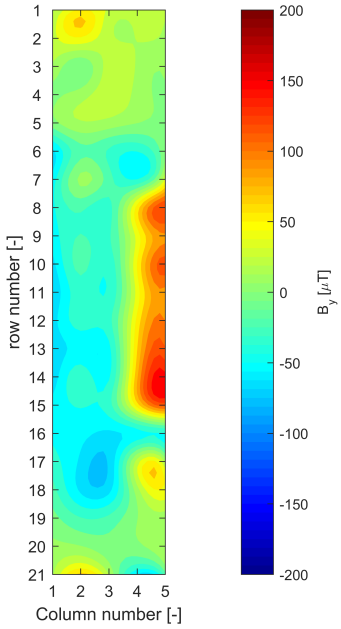

Figure 3.31: Results of measurements performed on day 2 of cracks 1. The plot shows the SMFL around cracks 1 and 2 measured by the handheld magnetometer on the grid points of the measurement grid and are interpolated using a spline function.

Results of the measurements of measurements day 2 recorded with the CrackGuard are presented in figures 3.32 and 3.33. The first figure shows the results of the SMFL measurements by the CrackGuard, while dredging. The heading of the ship was recorded simultaneously and is presented as well. The second figure shows the results of the SMFL measurements by the CrackGuard, while the dredger was unloading its hopper. During the unloading the hopper kept a constant heading of 105 degrees.

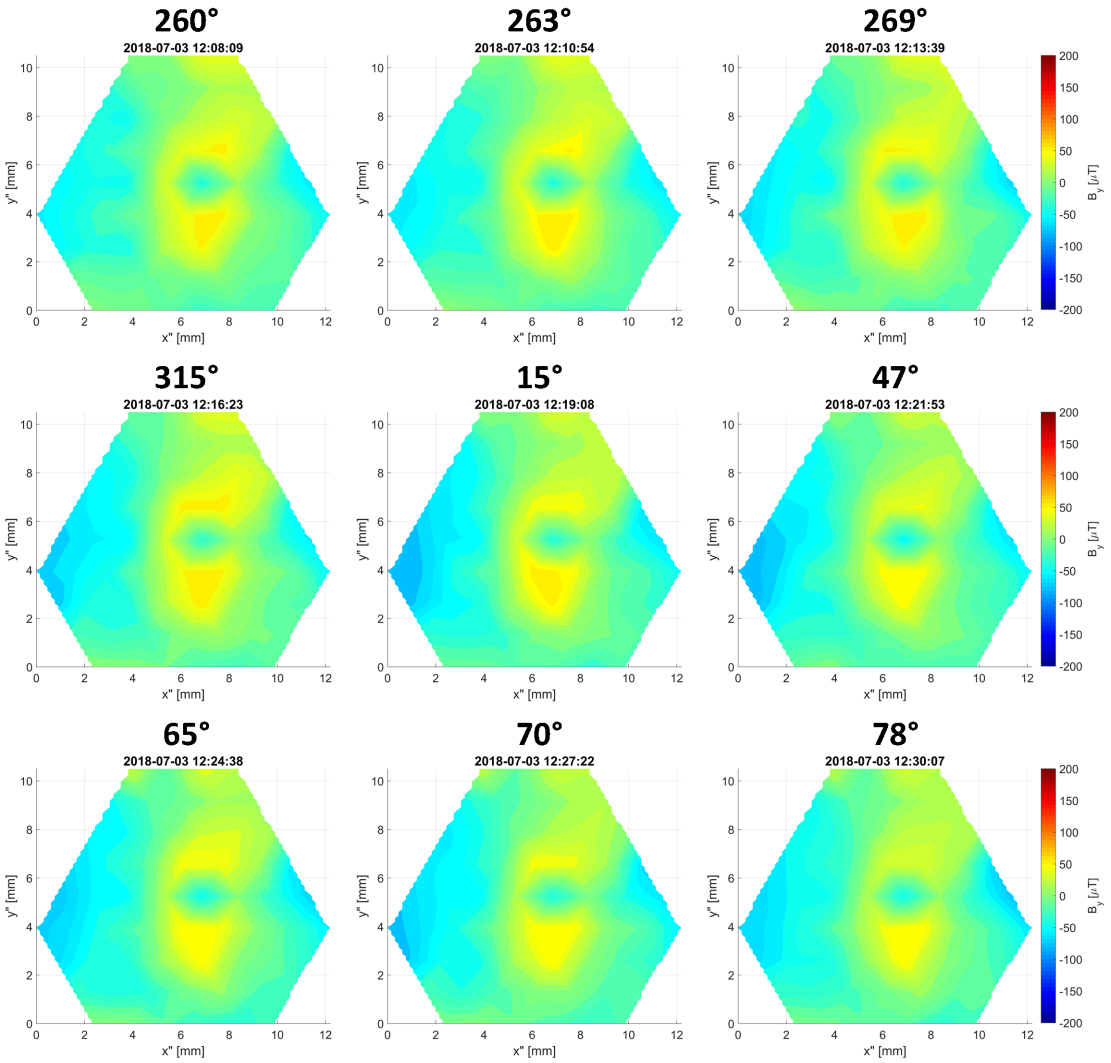

Figure 3.32: Results of SMFL measurements recorded with the CrackGuard on measurement day 2 while the dredger was collecting sediments. The heading of the ship is presented together with the SMFL measurements. The measurements are presented using linear interpolation.

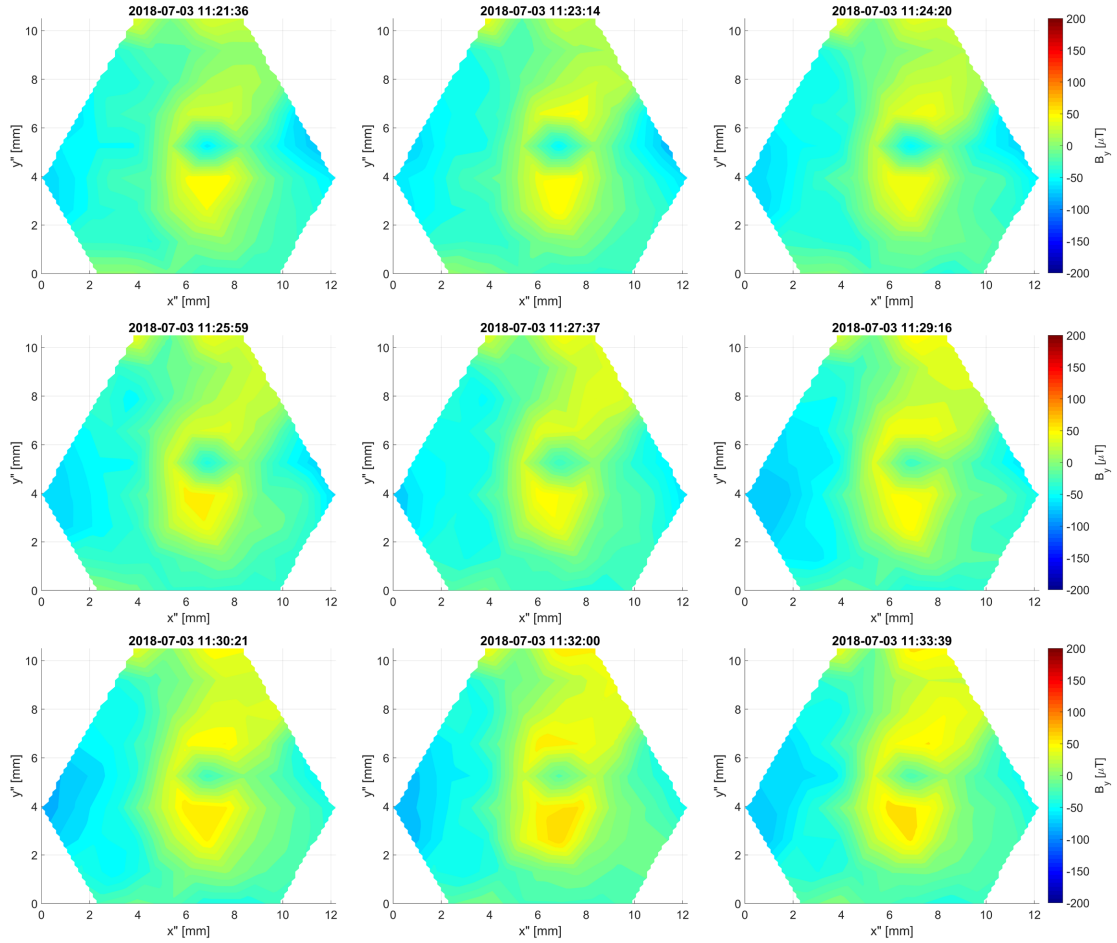

Figure 3.33: Results of SMFL measurements recorded with the CrackGuard on measurement day 2 while the dredger was unloading its hopper. In a period of 12 minutes the dredger went from fully loaded to fully unloaded condition by gradually dumping its 26 tonne load. The measurements are presented using linear interpolation.

3.4.4. Discussion

When comparing the results of measurement day 1 and 2 the first evident difference is the signal amplitude in the SMFL measurements between the preliminary measurements and the reference measurements (figure 3.30 and figure 3.31). During the period between measurement day 1 and measurement day 2 maintenance work was performed on the dredger. During this maintenance the crack was likely repaired, although the captain was unaware of any reparations on this crack. It can be seen from figure 3.28 that the crack has been treated with a red paint.

The results of the preliminary measurements furthermore show that the SMFL method is very suitable for crack monitoring on ship structures. The recorded signal amplitude is significantly greater than the signal amplitudes recorded on test specimens under laboratory conditions and is even greater than the signal amplitudes recorded during the bridge deck experiment. This observation demonstrates that the SMFL method is more effective when the monitored structures are bigger.
Analyzing the reference measurements in figure 3.31, it becomes clear that some SMFL still occurs, albeit significantly reduced. This may indicate that the crack has reappeared or was not repaired completely. The recorded SMFL around fatigue crack 1 can be recognized in the measurements obtained with the CrackGuard as well. The SMFL of crack 1 recorded with the CrackGuard is however more dispersed, likely as a result of the backplane, the hall sensor altitude and the grid spacing.

The results of the first part of the experiment in figure 3.32 show that the heading of the ship and thereby its orientation in the Earths magnetic field does not seem to influence the measurements of the CrackGuard to a significant degree. Earlier research on the influence of magnetic field direction on the MFL around a crack as a result of induced magnetization only showed a direct proportionality between the magnitude of the component perpendicular to the crack direction and the occurring MFL [26]. This relationship is not supported by the measurement results of the CrackGuard, which supports the conclusion that SMFL is caused largely by the permanent magnetization component [11]. It should be noted that the measurements were recorded while dredging. The loading of the hopper may therefore have impacted the recorded results to some degree.

The results of the second part of the experiment in figure 3.33 show that the unloading of the ship induces a change in the recorded SMFL amplitude. The location of the torsion box on the deck of the ship, causes the fatigue cracks to go from compression into tension during unloading of the ship, as the ship goes from sagging to hogging. This in turn causes relaxation of the cracks in the torsion box, increasing the crack opening, and possibly causing an increase in SMFL amplitude.

Furthermore, it should be noted that the measurement results of the CrackGuard are changing noticeably over relatively short amount of time, when compared to the envisaged measurement frequency of the CrackGuard. It is unlikely that this change is caused by any crack propagation. It is therefore recommended research is performed to the consistency of the measurements, since short term changes in SMFL measurements may not be noticed at low measurement frequencies and interfere with reliable fatigue crack monitoring.

3.4.5. Conclusion

The CrackGuard LT is one of the first steps towards the application of the SMFL method for crack monitoring of steel structures. The prototype has already shown to produce measurement results that enable the detection of fatigue cracks in the later stages of crack propagation in full-scale replica of a bridge deck. The application of the CrackGuard on bigger steel structures could improve the SMFL measurement results, since these structures have a higher associated magnetization. In the described experiment, preliminary measurements were performed on fatigue cracks in the torsion box of a dredger. In the second part of the experiment the SMFL around one of the fatigue cracks was tracked during sailing and unloading of the ship, while the heading was recorded.

The results of the preliminary measurements show that the SMFL method is very suitable for the monitoring of fatigue cracks in ship structures. The recorded SMFL amplitude around a fatigue crack of high compared to small-scale specimens and even the SMFL results of the bridge deck experiment. The preliminary measurements furthermore show that heavy corrosion or a layer of paint do not disturb the magnetic measurements significantly.

The results of the second part of the experiment show that the CrackGuard is able to detect SMFL with an amplitude of 220 μT, although the sensitivity should be improved in order to obtain measurements suitable for reliable crack monitoring. This could be done by decreasing hall sensor altitude, decreasing the effect of the backplane or increasing hall sensor sensitivity.

Results of the second part of the experiment furthermore show that the orientation of the ship inside the Earth magnetic field does not affect the measurements of the CrackGuard to a significant degree. The stress situation in the ship does however influence the measurements of the CrackGuard. This is likely caused by the opening of the crack due to the transition of sagging to hogging during the unloading of the hopper.

It is recommended that further research on the application of the CrackGuard on steel structures focuses on long duration fatigue crack monitoring. The described experiment demonstrates that measurements are influenced by external factors, which may interfere with precise crack length prediction.

4

Numerical Simulations

4.1. Model assumptions and restrictions

Numerical models are always a simplification of reality, capturing the most important elements in order to simulate the behavior of the system. The numerical models used in this research are no different. Restrictions on computational power and gaps in the knowledge about magnetic behavior lead to some important simplifications and restrictions for these models.

The numerical models used in this research are created using the AC/DC module in COMSOL multiphysics 5.2. This research focuses on magnetostatic problems in the absence of electromagnetic currents. In COMSOL multiphyisics these problems are best analyzed using the 'Magnetic fields, no current' interface. This physics interface solves Gauss' Law for magnetic fields using the scalar magnetic potential as the dependent variable and is the primary choice for modeling permanent magnets. Subsequently the stationary solver was used to create a solution (see [31]).

In the models the magnetic hysteresis curve is approximation by a linear curve. This approximation is reasonable when the applied magnetic field is low, which is the case for the earth magnetic field. Furthermore the permanent magnetic field is neglected in these models ($\vec{M} = 0$, see equation 4.3). This is an important assumption, since the permanent magnetic field and the magnetic field induced by the earth magnetic field are of the same order. We are however forced to make this assumption because of the fact that the permanent magnetic field is hard to model, due to its dependence on the magnetic and mechanical history of the material, which is unknown and varies slowly with time. Another component to the magnetic field neglected in these numerical simulations is the magnetomechanical effect. Currently there are no physics packages available able to simulate the coupling between mechanical stresses and the magnetization of materials. It is however known that this coupling can have a significant contribution to the magnetization inside the material, with it even being the working principal behind the first applications of the Metal Magnetic Memory method (see 2.2.3). These assumptions are the cause of an importance difference between the numerical simulations and the experimental results.

The material models inside the numerical models make use of another important approximation, namely the approximation of a homogeneous an isotropic material. Although it is known that the material properties may vary depending on location and direction, the best approximation is to represent the material properties by a single value for each direction and location within the same material.

In the models, the steel plate is surrounded by an air box, which makes sure that the solution is not influenced by the boundaries of the model. This is accomplished when the air box is of infinite size, but is impossible to model. An air box that is sufficiently large in order not to influence the solution should therefore be chosen. The featured models include an air box of 3x3 meter, to minimize the influence on the solution. Furthermore the applied magnetic field is homogeneous throughout this air box.

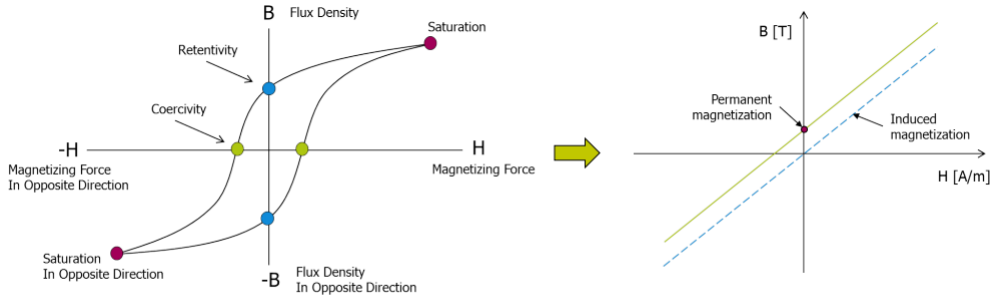

Figure 3: Hysteresis curve of ferromagnetic steel and its linear approximation

Figure 4.1: Assumption of the linear approximated curve in ferromagnetic materials

The assumptions and approximations discussed in this section place some important restrictions on the numerical results and applications and should be kept in mind when comparing the numerical results to the experimental results.

4.1.1. Finite Element Method

The physics interface solves Maxwell's equations formulated using a combination of magnetic vector potential and magnetic scalar potential as the dependent variable. Maxwell's equations are a set of equations stating the relationships between the fundamental electromagnetic quantities. These quantities are:

- Electric field intensity E
- Electric flux density D
- Magnetic field intensity H
- Magnetic flux density B
- Current density J
- Electric charge density ρ

The equations are presented in the differential form because it leads to differential equations that the finite element method can handle.

$$\Delta \times \vec{H} = \vec{J} \tag{4.1}$$

$$\Delta \times \vec{B} = 0 \tag{4.2}$$

$$\vec{B} = \mu_0(\vec{H} + \vec{M}) = \mu_0\mu_R\vec{H} + \mu_0\vec{M} \tag{4.3}$$

The first and second relation are referred to as Ampere's Law and Gauss' Law, respectively. The third equation is a constitutive relation that describes the macroscopic properties of the medium. In magnetostatic problems where no electric currents are present, it is possible to formulate and solve the problem using a scalar magnetic potential. In a current-free region you have $\Delta \times \vec{H} = 0$. This implies that the magnetic scalar potential V_m can be defined from the relation $\vec{H} = -\Delta V$, which is analogous to the definition of the electric potential for static electric fields. Using the constitutive relation $B = \mu_0(\vec{H}+\vec{M})$, the equation $\Delta\vec{B} = 0$ becomes:

$$-\Delta * (\mu\Delta V_m - \mu_0\vec{M}) = 0 \tag{4.4}$$

The Magnetic Fields, No Currents Interface uses this equation for modeling of magnetostatics in the absence of electric currents (see [31]).

Boundary Conditions

The problem of electromagnetic analysis on a macroscopic level is that of solving Maxwell's equations subject to certain boundary conditions. In the AC/DC module of COMSOL multiphysics 5.2 [31] several boundary conditions are defined to be applied to nodes in the numerical model. The boundary conditions used in the formulated models are listed below, including a physical explanation of there function. In the preceding text the applied boundary conditions will be referred to with the names listed below:

- Magnetic Flux Conservation: the Magnetic Flux Conservation node adds equation 4.4 for the magnetic potential and provides an interface for defining the material properties and the constitutive relation for the magnetic flux density. It is used when there are no currents and all the magnetic fields are originated by permanent magnets and/or external systems not included in the model.

$$-\Delta * (\mu \Delta V_m - \mu_0 \vec{M}) = 0 \tag{4.5}$$

- Magnetic Insulation: the Magnetic Insulation node for the Magnetic Fields, No Currents interface provides magnetic insulation using the relation in equation 4.6 and sets the tangential components of the magnetic flux density to zero. Insulation is the default boundary condition. This condition is useful at boundaries confining a surrounding region of air or to model symmetry cuts.

$$\vec{n} \times \vec{A} = 0 \tag{4.6}$$

- External Magnetic Flux Density:The External Magnetic Flux Density boundary condition forces the reduced magnetic flux density to be zero on the boundary, or equivalently, forces the total field to be equal to the background field. This boundary condition is applied to external boundaries that are at a distance far enough from the system so that its effect on the background field is negligible.
- Zero Magnetic Scalar Potential: The Zero Magnetic Scalar Potential node provides a boundary condition that specifies a zero magnetic potential on the boundary $V_m = 0$. This will make sure that the field intensity H at this point is perpendicular to this boundary (parallel to the normal vector). This boundary condition can be used to simulate anti-symmetry.

4.2. Model Validation

This section describes the validation of the numerical simulation method by comparing the model to the analytical solution of a thin steel plate.

4.2.1. Analytical Solution

There exists an analytical solution for a rectangular plate inside a homogeneous background field. This analytical solution can only be found when the following assumptions are valid:

- The plate can be considered a thin plate. This means that its sides are long in comparison to its thickness (t « L and t « W)
- The material in the plate responds magnetically linear with relative permeability μ_r
- The magnetization in the plate due to the background field is homogeneous

These assumptions are in accordance with the assumptions made in the numerical simulation. In order to formulate this analytical solution a plate with width W, length L and thickness t in respectively x, y and z-direction in a Cartesian coordinate system is considered with its origin in the center of the plate. The magnetic flux density in the middle of the plate is given by:

$$\vec{B}(\vec{r} = \vec{0}) = \mu_0(\vec{H} + \vec{M}) = \mu_0 \mu_r \vec{H} = \frac{\mu_0 \mu_r}{1 + (\mu_r - 1)K} H_e \vec{u}_x \tag{4.7}$$

with K described by:

$$K = \frac{2tL}{\pi W \sqrt{W^2 + L^2}} \tag{4.8}$$

A derivation of this expression can be found in [22]. The plate is rotated parallel to the direction of the earth magnetic field and a background field with the strength of the local earth magnetic field is applied. Presently the World Magnetic Model 2015 [32] predicts a earth magnetic field strength of (BX, BY, BZ) = (19163,351,45130). This results in a background field H of 39 A/m.

$$\vec{H} = H_e \vec{u}_x = \frac{|\vec{B}|}{\mu_0} = \frac{\sqrt{19163^2 + 351^2 + 45090^2} * 10^{-9}}{4\pi * 10^{-7}} = 39\vec{u}_x \quad [A/m] \tag{4.9}$$

Consequently, the magnetic flux density in the middle of a structural steel plate (1 m x 1 m x 2.5 mm) is:

$$\vec{B}(\vec{r} = \vec{0}) = \frac{\mu_0 \mu_r}{1 + (\mu_r - 1)K} = \frac{4\pi * 10^{-7} * 100}{1 + (100 - 1)0.0056} 39\vec{u}_x = 4.41 * 10^{-3}\vec{u}_x \quad [T] \tag{4.10}$$

4.2.2. Numerical Solution

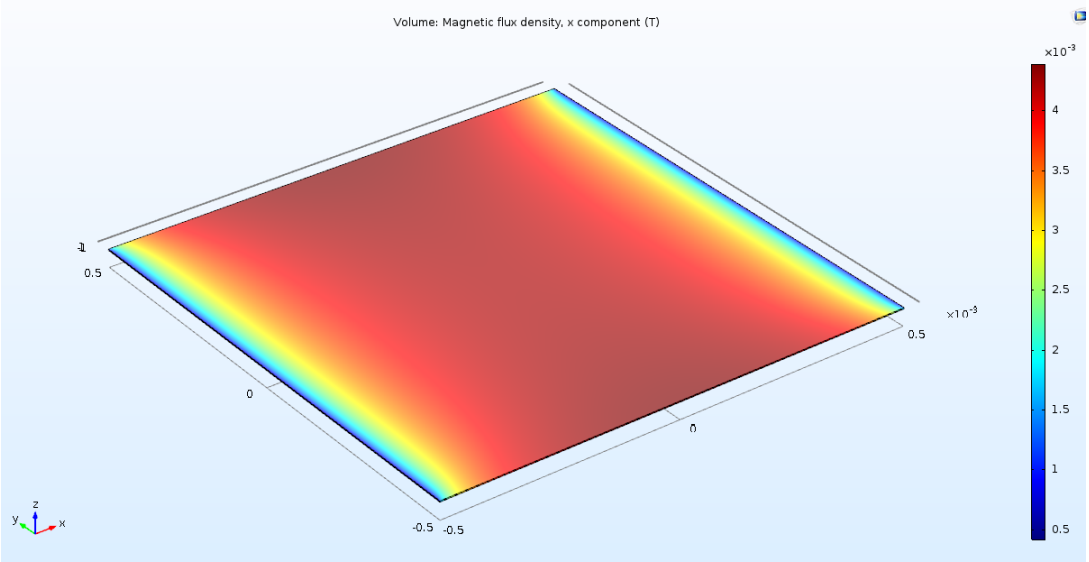

Figure 4.2: Numerical solution of a 1 m x 1 m x 2.5 mm structural steel plate

In the numerical model a structural steel plate (permeability of $\mu_r = 100$) of 1m x 1m x 2.5 mm was simulated using the previously described COMSOL multiphysics 5.2 software package. The plate was modeled inside an (6 m x 6 m x 1.5 m) air box, in order to make sure that the numerical solution is influenced by the model boundaries. Several test showed that the chosen dimensions made sure that the boundaries had no significant impact on the solution. The permeability of the air inside the air box was set to $\mu_r = 1$. Furthermore, a grid convergence test made sure that the solution was independent of the chosen element size (see 4.3). The numerical solution can be seen in figure 4.2.

Evaluation of the x-component of the magnetic flux density in the middle of the plate (x,y,z) = (0,0,0) resulted in a value of $4.23 * 10^{-3}$ A/m and a subsequent relative error of 4.1%. This error is acceptable since the analytical solution is based on the assumption of homogeneous magnetization, which is not exact and the assumption that the plate is thin. The latter was found to have a significant effect on the results over several iterations, with the numerical results converging to the analytical solutions when increasing the length of the sides of the plate compared to the thickness of the plate. The dimensions of the plate were not increased further than the mentioned values, because of constraints on the computational power.

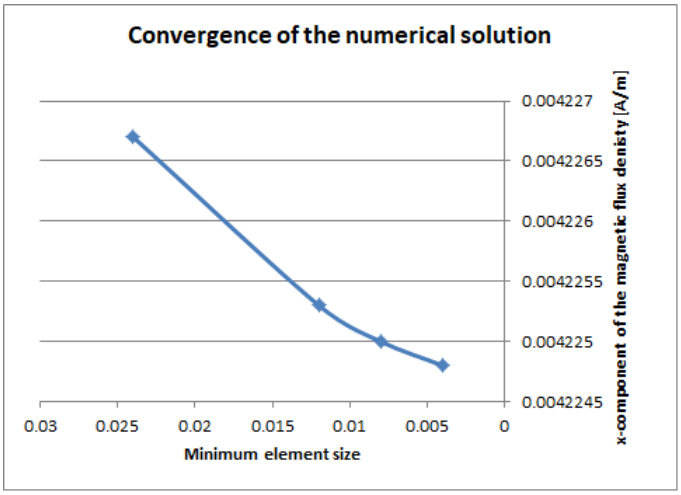

Figure 4.3: Convergence of the numerical solution of a thin structural steel plate

4.3. Crack Opening model

Following the experiment on crack opening experiment, a numerical model of a comparable situation is constructed. The numerical results of this simulation provide a some insight to better interpret the experimental results and a allow for a comparison between the results, which can be used to improve numerical simulations. For this reason the numerical model assumes a similar shape and background field to the experimental specimen. Moreover, the CMOD applied in the numerical model is of the same order as the estimated CMOD in the experiment, in order to increase the similarity between the model and the experiment. The center hole in the experimental specimen was however excluded from the numerical model to make an analysis of the relation between the SMFL in the middle of the crack and the CMOD possible. The latter is essential in answering the first research question.

4.3.1. Geometry

The dimensions of the plate modeled in the numerical simulation are equal to the dimensions of the experimental specimen, as was mentioned before. The air box was chosen sufficiently large (dimensions (x,y,z) = (2m, 2.5m, 3m)) in order to not influence the solution and in accordance with the dimensions of the air box used in the validating numerical model. The crack in the specimen was modeled as a through thickness rectangular air gap. Although a crack modeled by an elliptical air gap is probably a more realistic representation of the situation, it comes at computational cost as well. This simplification will specifically influence the solution around the crack tip, which is not the main interest in this research. Furthermore, numerical models by [33] have made use of the same rectangular crack geometry and encountered no problems in the comparison between numerical and experimental results as a consequence of this simplification.

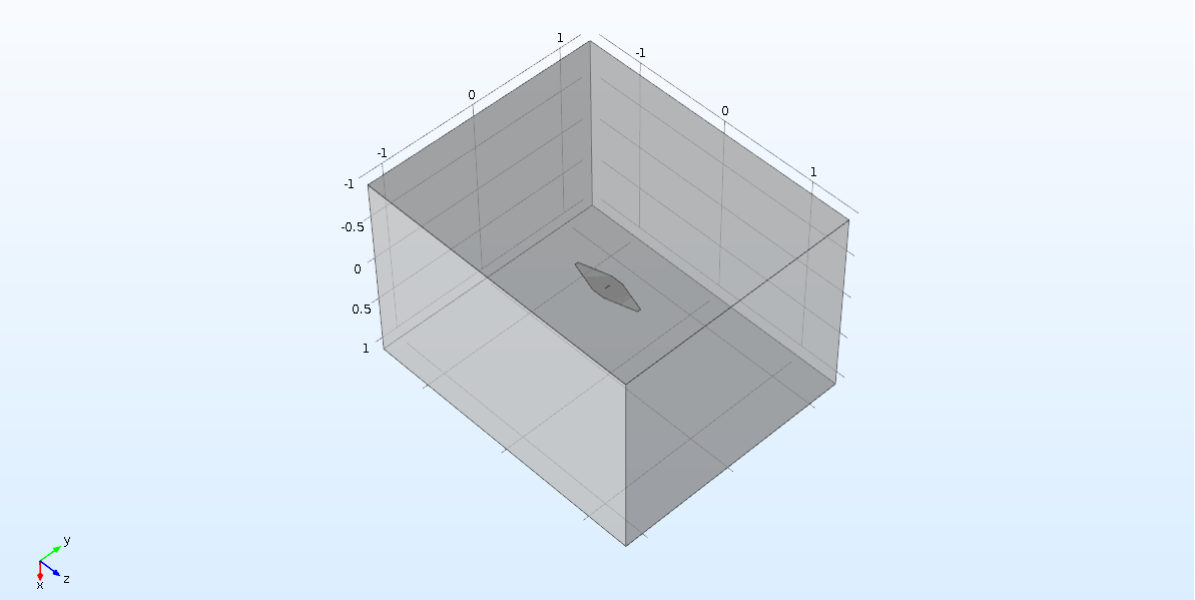

Figure 4.4: Overview of the geometry modeled in the numerical simulation

4.3.2. Material

The material modeling of the specimen requires only two parameters to be defined: The relative permeability of S235 structural steel and the relative permeability of the air. The permeability of s235 structural steel was experimentally determined by [10] to be 225, while the permeability of of air was assumed to be equal to the permeability of free space (mu_r = 1)[34].

4.3.3. Magnetic field and Boundary Conditions

The magnetic background field applied to the numerical simulation is equal to the background field measured by the Koshava-USB magnetometer during the experiment ($B_{background}$ (x,y,z) = (-20, -2, -30) mT). In the formulation of the numerical model two boundary conditions were applied: the magnetic flux conservation condition and the external magnetic flux density condition. The magnetic flux conservation condition

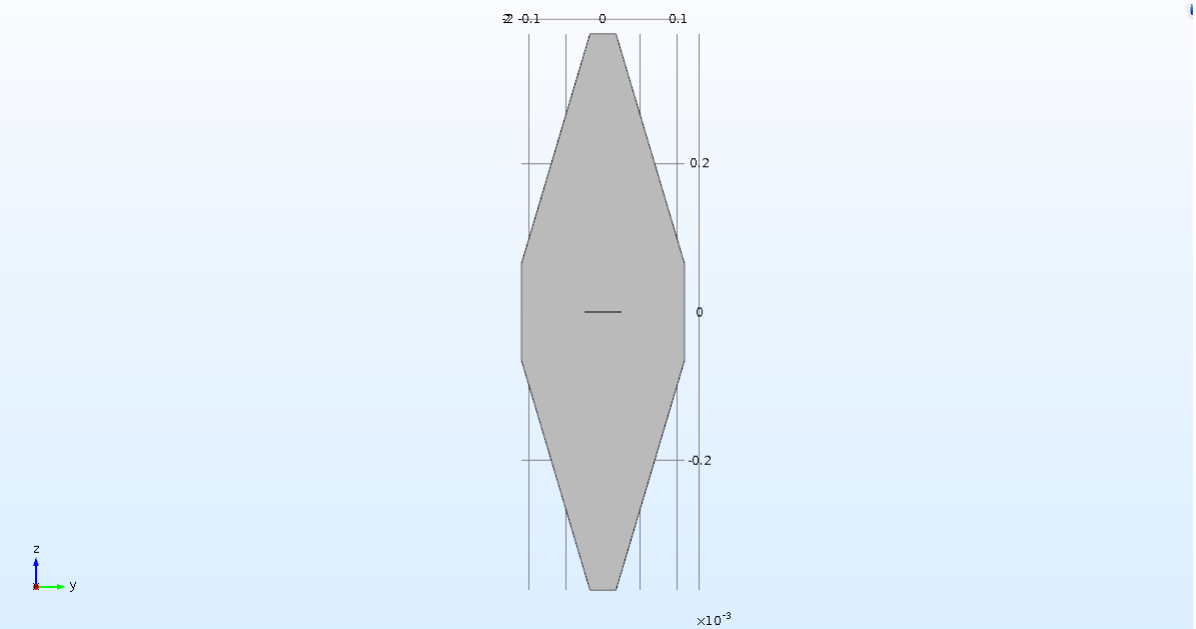

Figure 4.5: Geometry of the specimen modeled in the numerical simulation

was applied to both the air box and the structural steel specimen. The external magnetic flux density condition was used on all the external boundaries of the air box.

4.3.4. Meshing

The meshing of the model was performed using the build in meshing algorithm in COMSOL multiphysics 5.2. The meshing of both the air box and the structural steel specimen is build of second order tetrahedral elements, with the steel plate having a finer meshing structure and the air box having a more coarse meshing structure. The smallest element size used in the meshing of the structural steel specimen is $\frac{1}{3}$ of the CMOD, while the largest element size was 60 mm. The air box has a smallest element size of $\frac{1}{3}$ of the CMOD as well, while the largest elements have a length of 20 mm.

4.3.5. Results

Solving the numerical model for the previously described conditions resulted in a B-field in the structural steel specimen as seen in figure 4.6. The results of the SMFL around the crack will be analyzed by inspecting the magnetic flux density B_x in the out-of-plane direction over a linear path perpendicular to the crack center. The location of this linear path is shown in figure 4.6, with only the path in the center being of importance in this case. The path is located 1 mm above the surface of the plate, to imitated the 1 mm lift-off of the Koshava-USB magnetometer in the experiment. The resulting graphs can be found in figure 4.7. When the peak-to-peak-value over these path is plotted against the CMOD the of the different models (see 4.7), we find a linear increase in the peak-to-peak-value.

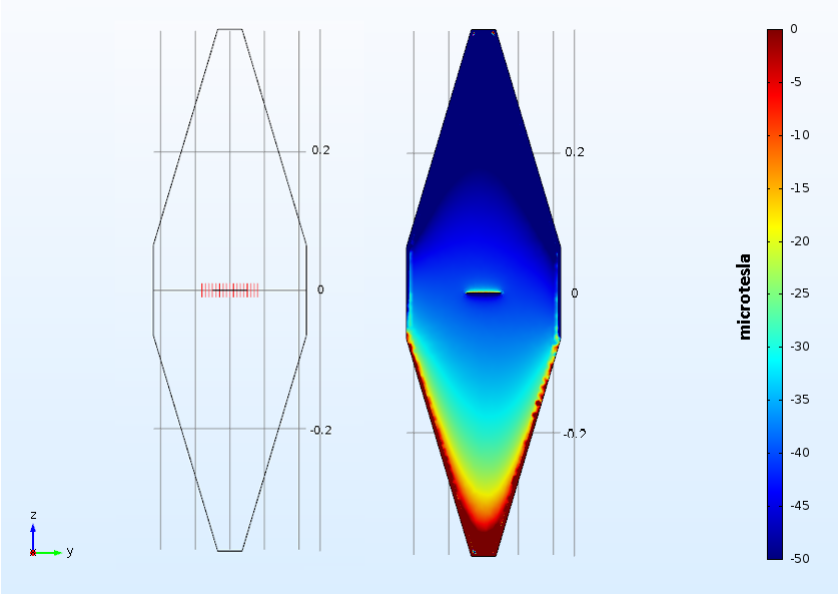

Figure 4.6: Left: Specimen with measurement lines perpendicular to crack direction depicted in red. Right: Solution of the out-of-plane component of the magnetic flux density in the structural steel specimen for a CMOD of 0.10 mm.

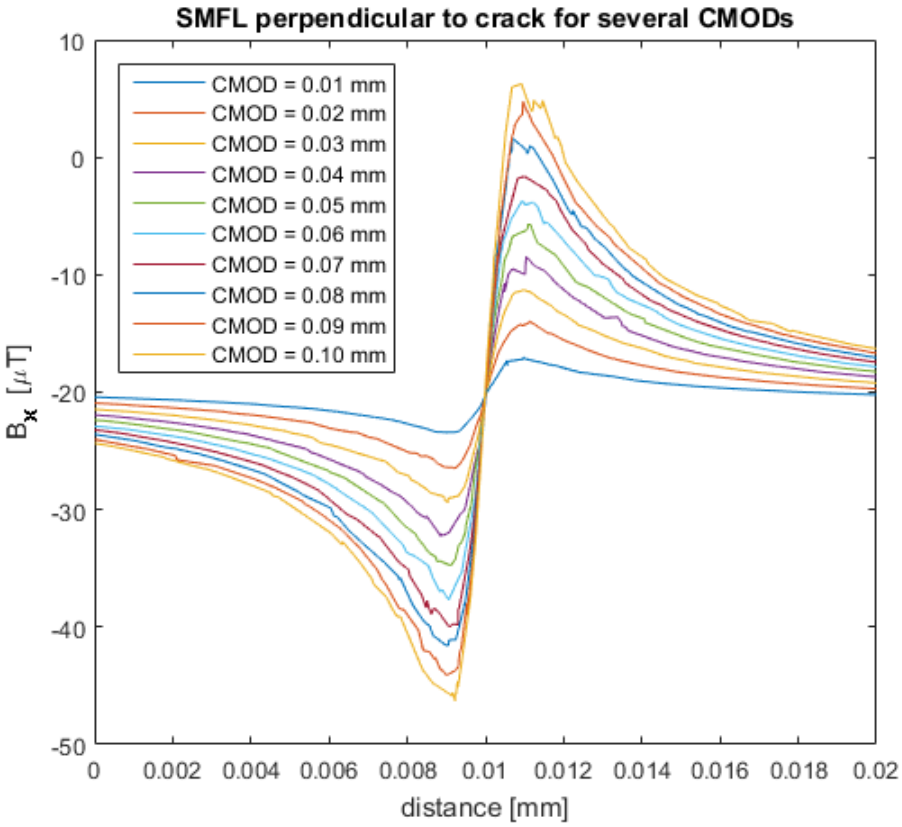

Figure 4.7: Out-of-plane flux density B_x perpendicular to the crack center for different CMODs

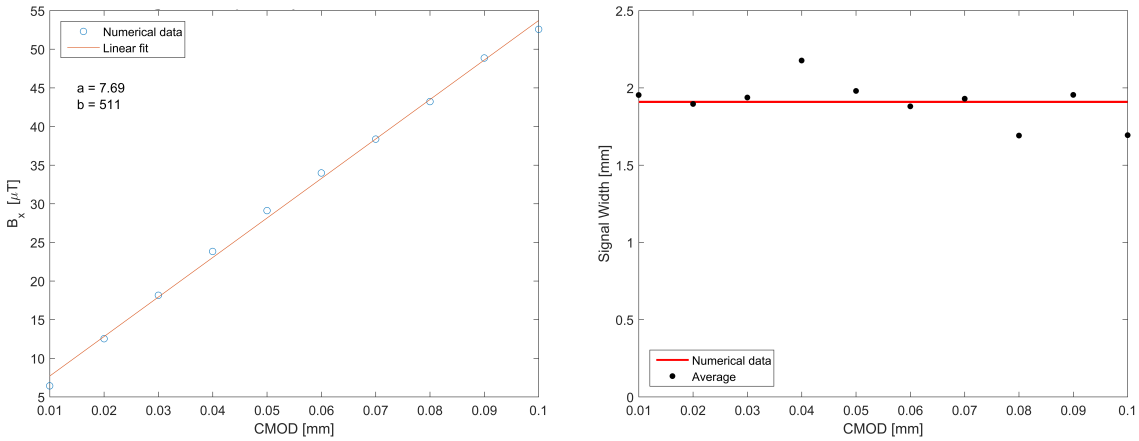

Figure 4.8: Left: Plot of the peak-to-peak value over a line perpendicular to the center of the crack with an altitude of 1 mm versus the CMOD. Right: Signal width of a line perpendicular to the center of the crack with an altitude of 1 mm versus the CMOD.

Further analysis of the results, now including the adjacent measurement paths, reaching 4 cm on both sides of the center with 5 mm spacing (see left side of figure 4.6), reveals the development the SMFL along the length of the crack. Figure 4.9 depicts the development of the SMFL parallel to the crack length for different CMODs, showing a S-curve on both sides of the crack center.

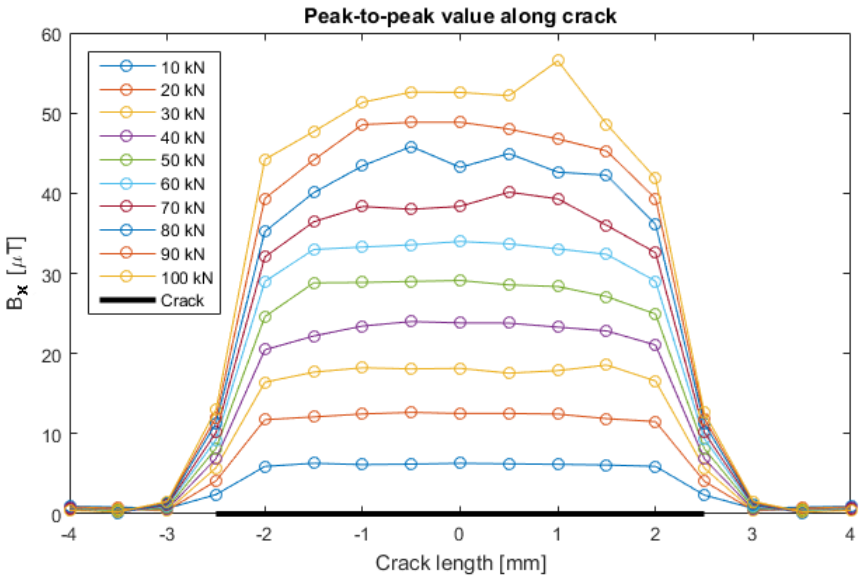

Figure 4.9: Out-of-plane flux density B_x perpendicular to the crack for different CMODs

4.3.6. Discussion

The results of the numerical simulation on the MFL over a line perpendicular to the crack direction in figure 4.7 clearly show that an increase in CMOD causes an increase in MFL amplitude. The results in figure 4.8 shows a linear relationship between the CMOD and the associated MFL amplitude, while the width of the signal remains the same. These results are in accordance with the results found in the crack opening experiment. It can be observed that the results show some numerical error as a result of a coarse meshing around the crack location. This in turn causes some deviations in the observed trends. This was however not resolved, due to computational limitations.

The results of the analysis of the signal amplitude along the crack length show a different pattern of MFL along the crack length than was observed in the crack opening experiment. The numerical results show a steep increase from crack tip towards the center of the crack, while the MFL pattern found in the crack opening experiment looked to be more gradual. This proves that the rectangular shape of the modeled crack is not realistic, as was to be expected. The rectangular crack shape has a constant crack opening along the crack length, while a more realistic crack shape is presumably characterized by a more gradual increase in crack opening from crack tip to crack center. An elliptical crack shape or a rhombus are therefore better options when modeling a fatigue crack where the MFL along the crack length is of interest.

A comparison of the numerical results and the experimental results of the crack opening experiment (see section 3.1), shows that the results are of comparable magnitude. The numerical results show a linear trend that can be extrapolated to the origin, meaning that no CMOD will result in no MFL. This is an obvious result, since a CMOD of 0 mm coincides with the absence of any flux disturbance. The experimental results however show that some SMFL can be measured when the crack is fully relaxed. it can be concluded that even a closed fatigue crack causes some disturbance in the magnetic flux. This may indicate that some CMOD is retained, even though no tensile force is applied to the specimen or as a result of plasticity around the crack mouth. Furthermore it can be concluded that the range of CMODs modeled in the numerical experiment is presumably comparable to the CMODs resulting from the tensile testing in the crack opening experiment.

4.3.7. Conclusion

A comparison between the experimental results of the crack opening experiment and a numerical simulation of the same experiment allows for a better understanding of the results of both experiments and offers an opportunity to improve the numerical modeling of the MFL around a fatigue crack. In the described numerical simulation a center cracked plate is modeled after the test specimen used in the crack opening experiment, using the exact same geometry and magnetic background field. In the simulation, a range of CMODs has been modeled, ranging from 0.01 mm to 0.1 mm, in order to simulate the tensile testing of the specimen in the crack opening experiment.

The results of the simulation show that the MFL amplitude that occurs over a line perpendicular to the center of the crack is linear with an increase in CMOD, while the signal width is unaffected by an increase in CMOD. These results are in accordance with the results found in the crack opening experiment.
An comparison between the numerical results and experimental results on the MFL that occurs along the length of the fatigue crack, shows that the modeling of the crack by a rectangular slit is not realistic. It is therefore recommended that a ellipse or a rhombus is used to model the crack if the MFL along the crack length is of interest. The comparison furthermore show that experimental results and numerical results differ in the fact that some flux leakage can be observed in the experimental results, even though the crack is in fully relaxed condition. This situation cannot be modeled numerically, as a CMOD of 0 mm would result in no MFL. Finally it is concluded that the range of CMODs modeled in the numerical simulation results in a MFL around the crack that is comparable to the SMFL results in the crack opening experiment.

4.4. T-joint numerical model

Earlier research has demonstrated that magnetic flux leakage occurs around weld, similar to the MFL pattern seen around fatigue welds. It is hypothesized that this magnetic flux leakage arises from a difference in magnetic permeability between the weld material and the base material. The weld, which is thought to have a lower magnetic permeability, will act as a disturbance to the magnetic flux in the base material and generate a leakage field, in this premise. The numerical model provides the opportunity to investigate the influence of the magnetic permeability of the weld material in more detail. How the SMFL is affected by the magnetic permeability of weld material is investigated in this simulation by varying the magnetic permeability of the weld material, while the SMFL is analyzed. With the help of this simulation the following question should be answered:

How does the magnetic permeability of a double sided fillet weld influence the magnetic flux leakage around a through thickness crack located at the weld toe?

4.4.1. Geometry

The geometry of the T-joint model can be found in figure 4.10. The numerical model includes an air box of dimensions (x,y,z) = (4, 4, 4)m, which is sufficiently large to ensure a solution that is not significantly influenced by the air box size. A through thickness fatigue crack has been modeled as a rectangular slit with a length of 50 mm and a crack opening of 0.5 mm. The fillet weld is modeled as a triangular beam between the base plate and the stiffener. Furthermore, the HAZ has been modeled as a cylinder with a diameter of 2 times the weld throat. A spacing of 1 mm between the base plate and the stiffener has been taken into account.

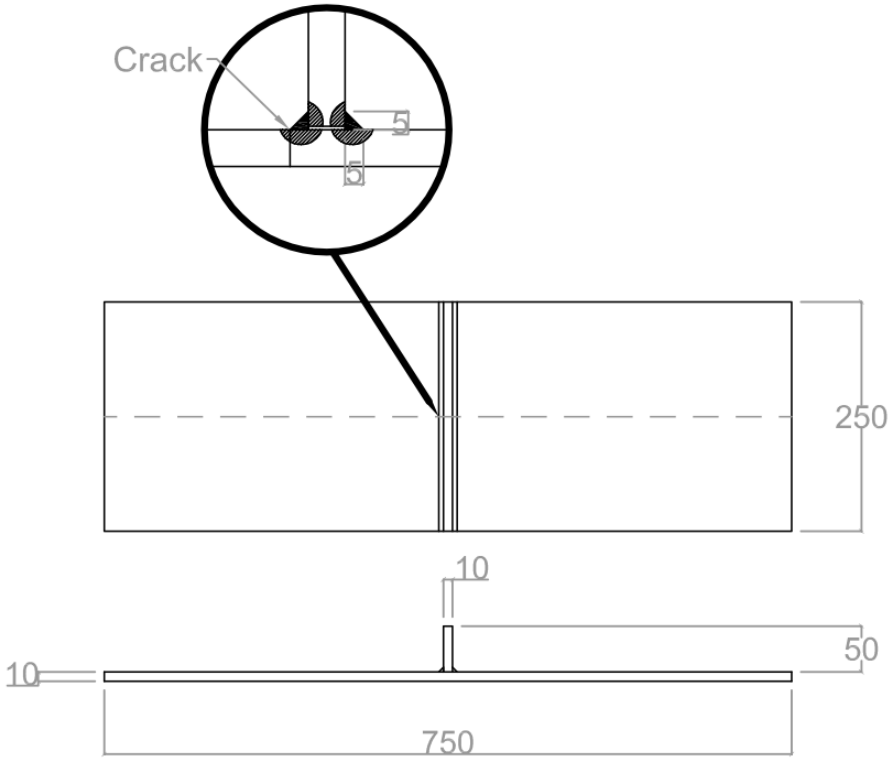

Figure 4.10: Geometry of the T-joint numerical model with double sided fillet weld

4.4.2. Material

The magnetic material parameters used in the construction of the T-joint numerical model are presented in table 4.1. A value of μ_r=225 has been adopted for the base material, which is a s235 structural grade steel and is in accordance with [10]. The values of the weld filler material is varied from 1 to 225 in five equal increments, the magnetic permeability of the HAZ is assumed to be the average of the weld filler material and the base material (see table 4.1). Finally, a relative permeability of μ_r = 1 has been adopted to model the air box.

Material description	Relative permeability
Base material (structural steel)	225
Weld filler material	1/57/113/169/225
HAZ	1/29/57/85/113
Air	1

Table 4.1: Magnetic material parameters used in the T-joint numerical model

4.4.3. Magnetic field and Boundary Conditions

The magnetic background field applied to the numerical model is of similar strength to the background field measured during the T-joint experiment $B_{background}$(x,y,z) = (40,0,0 μT). The conservation of magnetic flux was assured by applying the magnetic flux conservation condition to the air box and the T-joint geometry, while the magnetic background field was imposed by the external magnetic flux density condition.

4.4.4. Meshing

The meshing of the model was performed using the build in meshing algorithm in COMSOL multiphysics 5.2. The meshing of both the air box and the structural steel specimen is build of second order tetrahedral elements, with the steel plate having a finer meshing structure and the air box having a more coarse meshing structure. The smallest element size used in the meshing of the structural steel specimen is 0.1 mm, while the largest element size was 10 mm. The air box was meshed with elements in the range of 0.1 mm to 140 mm.

4.4.5. Results

A qualitative overview of the results of the numerical model is presented in figure 4.12. Here a section along the center of the plate is presented with a colored surface plot (background) of the z-component of the magnetic flux density, combined with a vector plot (arrows) of the flux density inside the ferromagnetic material of two situations. The first situation is the solution of the model for a relative magnetic permeability of 1 for the weld filler material, the worst case scenario. The first situation is the solution of the model for a relative magnetic permeability of 1 for the weld filler material, in which case the magnetic permeability of the weld material does not play a role.

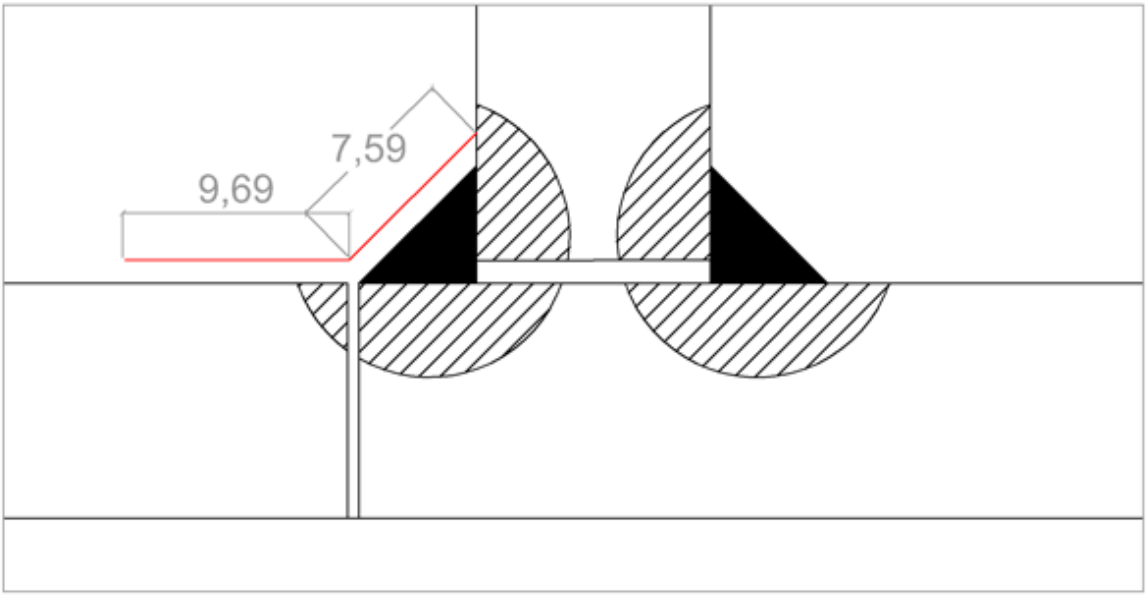

Figure 4.11: Detail drawing of the weld with the measurement path indicated in red

A drawing of the measurement path used to obtain the results in figure 4.13 and 4.14 can be found in figure 4.11. The depicted measurement path has an altitude of 1 mm with respect to the surface of the T-joint, in order to replicate the lift-off value of a magnetometer.

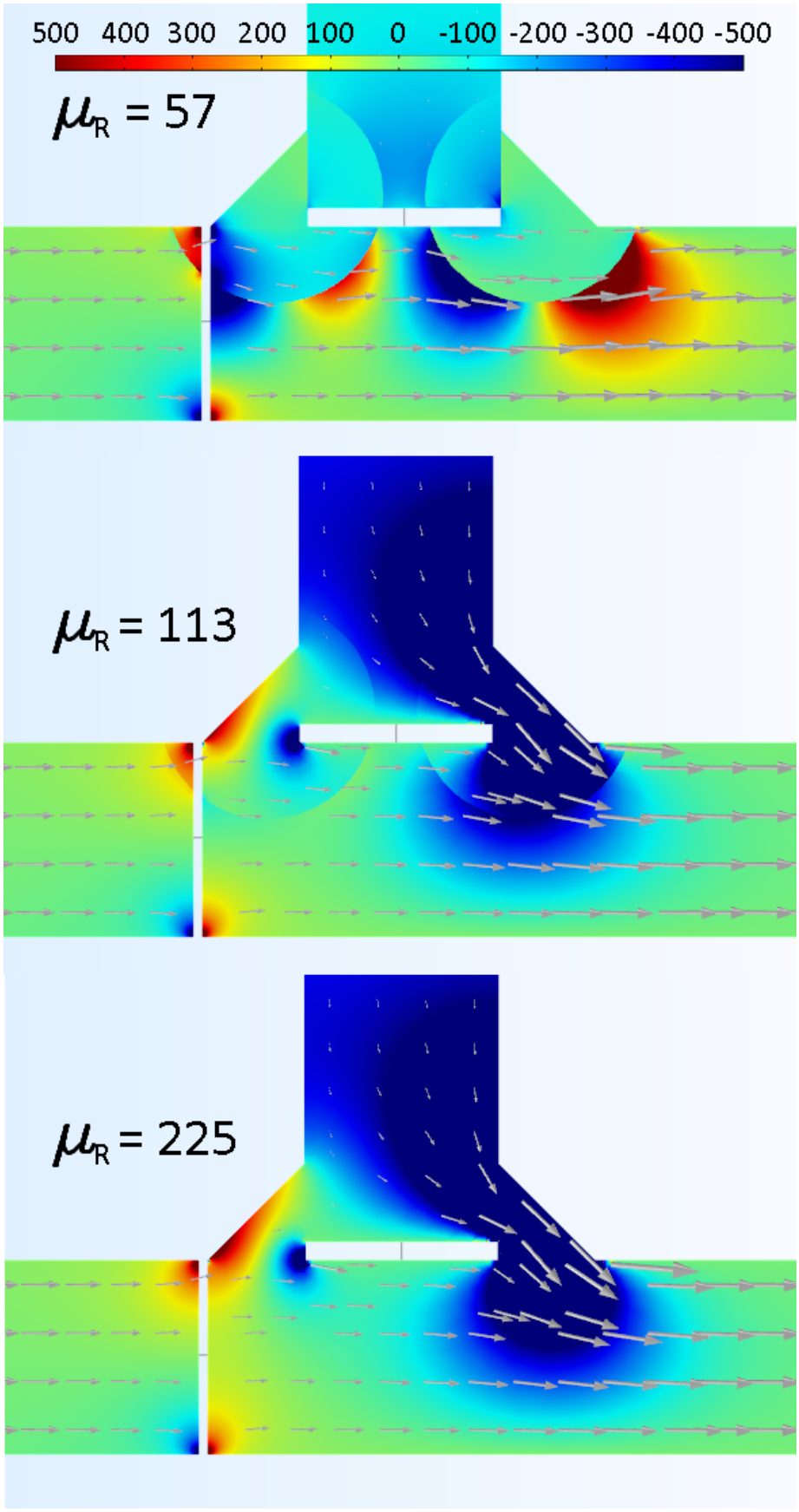

Figure 4.12: Surface plot and vector plot along a section of the center of the plate for two cases with differing relative magnetic permeabilities: Left: Model solution for a relative magnetic permeability of 1 for the weld filler material. Right: Model solution for a relative magnetic permeability of 225 for the weld filler material.

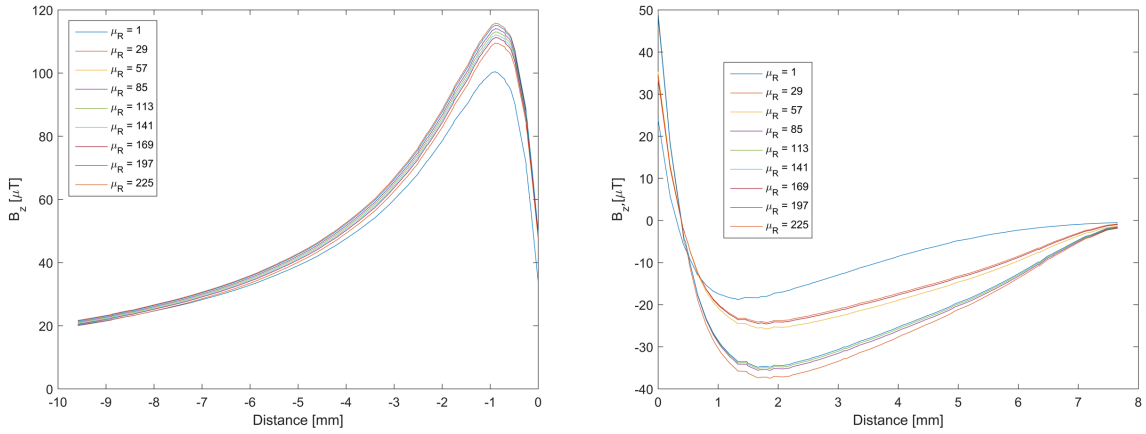

Figure 4.13: Out-of-plane magnetic flux density component plotted along the measurement path length. Left: Horizontal section of the measurement line. Right: Diagonal section of the measurement line, along the weld surface

The out-of-plane flux density component is plotted along the length of the described measurement path in figure 4.13. Notice how the curves are not continuous from the horizontal section to the diagonal section of the measurement line, since the out-of-plane magnetic flux density component changes direction.

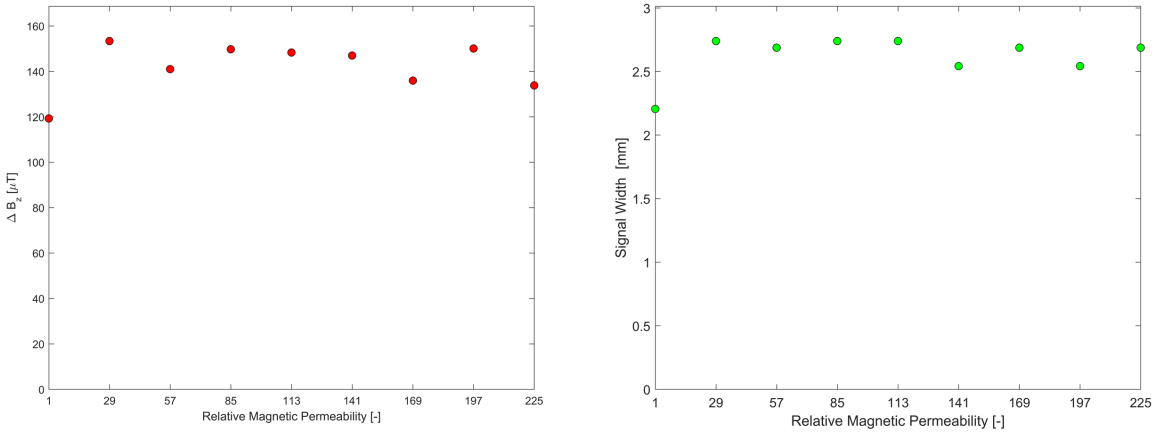

Figure 4.14: Left: Peak-to-peak value versus relative magnetic permeability of the weld filler material. Right: Signal width versus relative magnetic permeability of the weld filler material.

In figure 4.14 the results of figure 4.11 are used to analyze the influence of the relative magnetic permeability on the peak-to-peak value and the signal width.

4.4.6. Discussion

The qualitative presentation in figure 4.12 show that a reduction in relative magnetic permeability of the weld filler material and HAZ causes a disturbance in the magnetic flux around the location of the stiffener. The bigger the reduction in relative magnetic permeability, the more the flux is deflected towards the underside of the plate. The HAZ seems to be most influencial in this regard. However, leakage does still occur locally around the crack, especially at the top and bottom of the plate, where the characteristic leakage pattern can be identified. It can furthermore be observed that the magnitude of the magnetic flux, on the left side of the crack, where there is no influence of the weld, is nearly similar in all three presented cases.

The line graphs in figure 4.13 give a more detailed view on the flux leakage over the crack. The profile of the curve remains largely the same, while only the scaling can be seen to change with relative magnetic permeability. This observation is clarified by the results in figure 4.14, where it can be seen that the peak-to-peak

value is affected to some extend by a change in relative magnetic permeability. The relation between this peak-to-peak value looks to be somewhat irregular. This irregularity cannot be attributed to numerical error, since the curves in figure 4.13 show a smooth pattern. The same conclusion can be drawn for the signal width, which is affected by the relative magnetic permeability in a similar way to the peak-to-peak value.

This results of this simulation remain inconclusive on the influence of very low permeabilities of the weld filler material and HAZ on the flux leakage over the crack. It seems that very low magnetic relative permeabilities may more drastically affect the leakage pattern around the crack. However, relative magnetic permeabilities in this very low range are however not realistically to be expected.

Based on a the presented results it can be argued that the nearly similar magnitude of the magnetic flux on the left side of the crack, where there is no influence of the weld, causes the flux leakage to be relatively unaffected. The influence of the weld material does not seem to have a big influence sphere 'upstream'. The flux denisty on the left side of the crack can be said to be the driving force behind the flux leakage. On this side, the flux is 'forced' out of the material and is relatively similar, due to a similar 'driving force'., which can be observed from the left part of figure 4.13. The magnetic flux in the direction towards the material is however more dispersed, probably because of the increased influence of the relative magnetic permeability.

4.4.7. Conclusion

Earlier research has demonstrated that magnetic flux leakage occurs around weld, similar to the MFL pattern seen around fatigue welds. This flux leakage is thought to be a result of a difference in magnetic permeability, where the lower permeability of the weld would result in the characteristic leakage pattern. In this numerical simulation the effect of the magnetic permeability on the SMFL is investigated by varying the magnetic permeability of the weld filler material and the HAZ, while the SMFL is analyzed.

The results of the numerical simulation show that the magnetic flux leakage around a crack is relatively unaffected by the relative magnetic permeability of the weld material. An analysis on the peak-to-peak value over the crack and the associated signal width, shows an irregular relationship between these two values and the relative magnetic permeability.

Based on these observations it can be concluded that, if a lower relative magnetic permeability of the weld material is assumed, the magnetic flux leakage around this crack is of a similar magnitude to that of a crack not in the vicinity of a (Fillet) weld.

5

Measurement Data Post-processing

In this chapter the interpretation and post-processing of the SMFL measurement data is investigated. The possibilities to present the gathered data and utilize it as a means of monitoring fatigue crack length are explored. The following research question will be answered based on this analysis.

How can post-processing of SMFL measurement data improve fatigue crack monitoring?

5.1. Introduction

Monitoring crack length of fatigue cracks using the SMFL method relies on the characteristic MFL pattern (see figure 5.1) that occurs around cracks in ferromagnetic materials as a result of the reduced magnetic permeability at the crack location. This characteristic MFL pattern can be found around a crack when the out-of-plane magnetic flux density B_z is measured over a path perpendicular to the crack length direction. The crack location is in this case found at the location in the middle of the peak reversal, where the signal crosses the zero line. In order to monitor the fatigue crack length this characteristic pattern will have to be filtered from the SMFL measurement data and will have to be translated into a crack length in a reliable way. This requires the separation of the induced magnetization, which is responsible for the characteristic MFL pattern, and rest magnetization and precise crack localization using the obtained data. The density of the gathered SMFL measurement data is however restrained by the size of the Hall effect sensors (see A.5) responsible for the magnetic measurements and possible hardware involved, such as is the case for the PCB in the CrackGuard. This results in a measurement density with a grid spacing of 11 mm in the latest CrackGuard concept, for example. However, the desired precision of the crack monitoring method is of a higher order and will have to be in the range of 1 mm if the method is to be applied as a replacement for manual inspection. In order to improve the precision of the localization of the crack and filtering of the data, interpolation and post-processing techniques can be utilized.

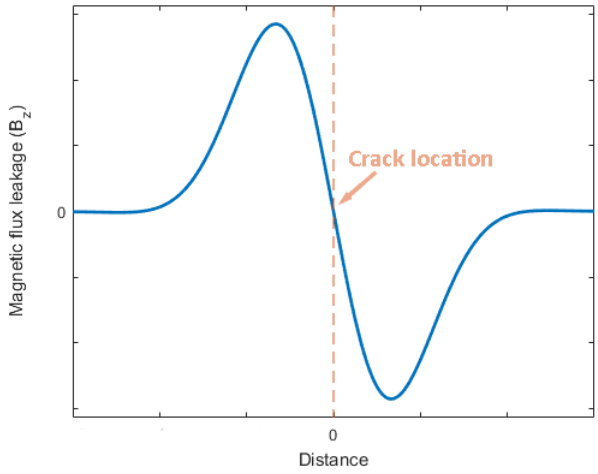

Figure 5.1: Characteristic magnetic flux leakage signal

5.2. Interpolation techniques

This section describes three interpolation techniques: linear interpolation, cubic interpolation and spline interpolation[35]. The selected interpolation techniques are of a lower order (up to second order) and are of increasing smoothness, increasing from zero to second order.

The interpolation techniques will be used to interpolated SMFL measurement data. It can be seen from the experiment in section 3.3 that these measurements consist of a component produced by the induced magnetism and a component produced by permanent and stress magnetism. The interpolation techniques can only be tested on the former, since the distribution of the latter (i.e. the rest magnetization) is unknown. Therefore, the performance of the three interpolation techniques will be tested on a MFL curve derived from a numerical simulation. In this simulation a square plate with a slit of 50 mm length and an opening of 1 mm is modeled in order to find the magnetic flux leakage at an elevation of 1 mm of the surface of the plate. The described curve can be found in figure 5.2. The length of this curve, 20 mm in total, is representative for a practically applicable grid spacing for SMFL measurements.

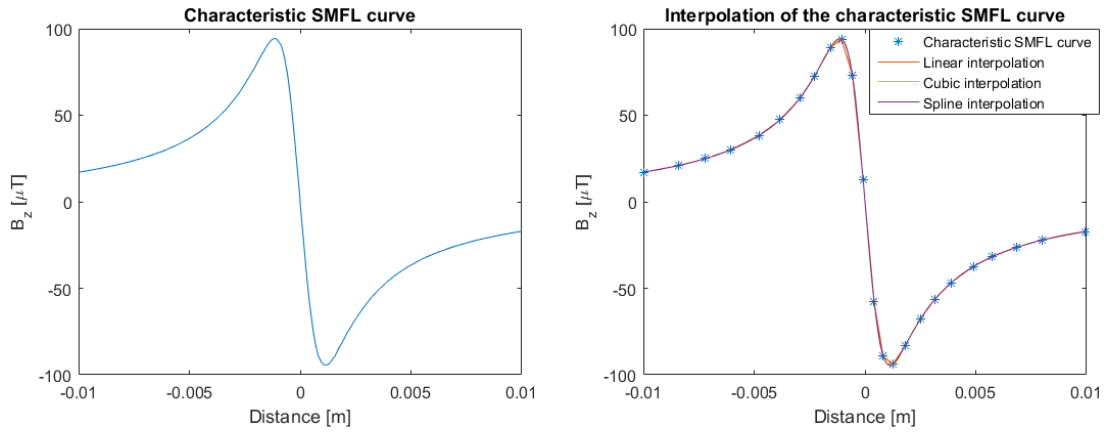

Figure 5.2: Left: The characteristic SMFL curve derived from a Numerical simulation. Right: results of the interpolation of 232 point from 24 data points along the numerically derived SMFL curve

The performance of the interpolation techniques will be evaluated based on an interpolation of 232 points along the numerically derived characteristic SMFL curve. The interpolated points are derived from 24 data points on the numerically derived SMFL curve. These data points and the interpolation results can be seen on the right side of figure 5.2. The figure shows a no big differences between the interpolation techniques at this scale. Further analysis of the results can be done by a comparison of the interpolation points and the data points of the numerically derived SMFL curve. Therefore, the error between the interpolation method and

the numerically derived SMFL curve will be calculated based on the residual sum of squares technique. The results of this analysis can be found in figure 5.3. The bar graph shows that the linear interpolation technique performs worst, while the spline interpolation technique performs best, according to the criterion. Results of the interpolation techniques applied to a SMFL measurement data set of the bridge deck experiment can be found in figure 5.4.

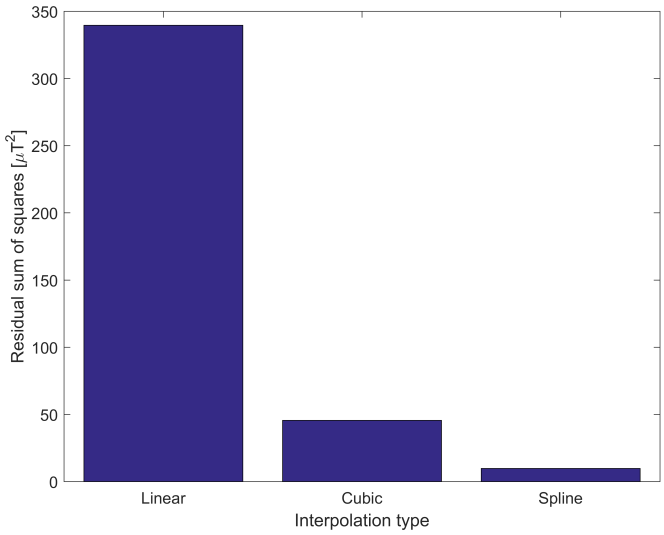

Figure 5.3: Residual sum of squares of the three interpolation methods based on interpolation of 232 points from 24 data points along the SMFL curve

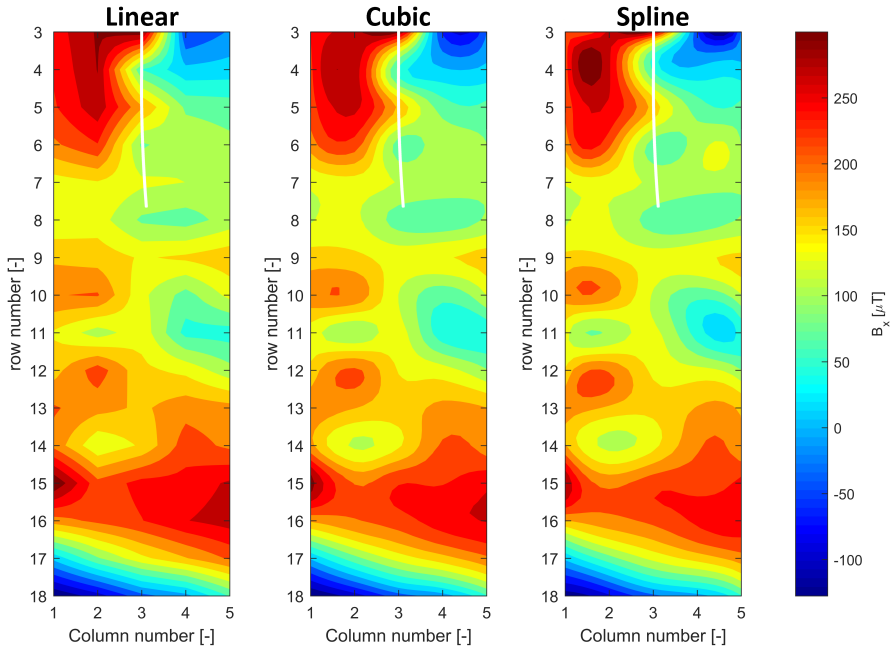

Figure 5.4: Three interpolation techniques applied to an example data set of the bridge deck experiment

5.3. Magnetic Flux Leakage data presentation

The way SMFL measurement data is presented can improve the interpretation of the measured signal and help to better understand the measurements. Two techniques are discussed in this section: the differentiated and integrated presentation technique.

5.3.1. Differentiation

The characteristic MFL pattern (see figure 5.1) can be differentiated in the direction perpendicular to the crack direction to create the the curve in figure 5.5. The location of the crack is in this presentation technique characterized by a peak in the data, surrounded by two lower peaks of the opposite sign.

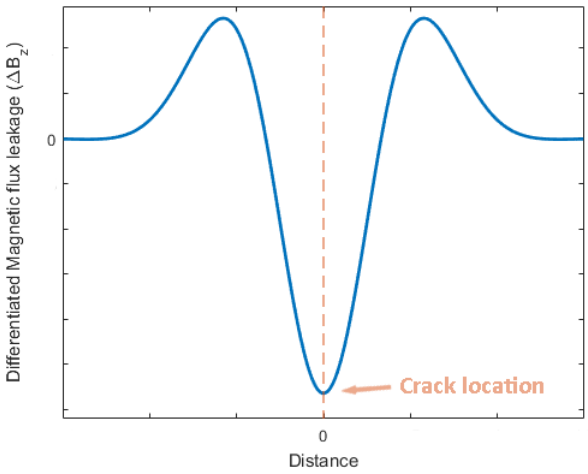

Figure 5.5: Differentiated characteristic magnetic flux leakage signal

From figure 5.6 it can be observed that the differentiated data presentation gives a clearer indication of the crack location than the unaltered presentation of the data. However, the two lesser peaks are difficult to observe. This demonstrates the influence of the permanent magnetism that appears as signal noise, since it does not produce a characteristic MFL pattern around the crack and is non-uniform [10].

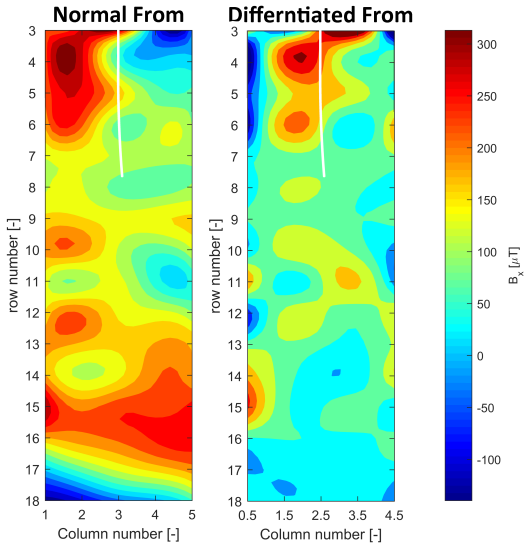

Figure 5.6: Example of presentation forms applied to a data set. Left: normal presentation form. Right: differentiated presentation form

5.3.2. Integration

A second technique for post-processing the data is the integrated presentation form. The characteristic MFL pattern is now integrated along the direction perpendicular to the crack length direction, which results in the pattern shown in figure 5.7. The crack location is in this presentation technique indicated by a peak in the data. This peak is wider compared to the peak in the differentiated presentation form.

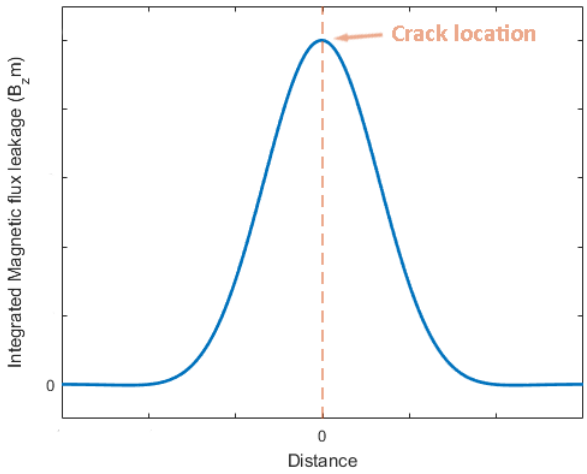

Figure 5.7: Integrated characteristic magnetic flux leakage signal

From figure 5.8.1 it can be observed that the integrated presentation form not readily leads to a clear presentation of the crack location. Furthermore, it can be observed that the resulting plot is not symmetrical, which can be attributed to the influence of rest magnetism, of which the permanent magnetization is the most important component. However, a compensation for this deviation can be done by subtracting the overall mean magnetic flux density (see figure 5.8.2) or subtracting the mean magnetic flux density per row (see figure5.8.3). This is equivalent by separating induced and rest magnetism on the basis of assuming that the rest magnetism is constant over the whole measurement grid for figure 5.8 or has a constant value per row in x-direction for figure 5.8.2.

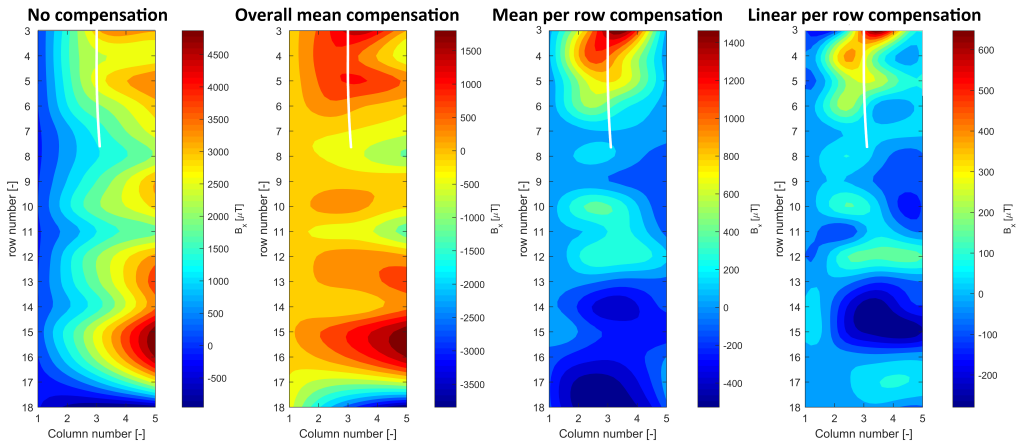

Figure 5.8: Example of the different integrated presentation forms applied to a data set. The applied compensation fields can be found in figure 5.9. From left to right: 1. Integrated presentation form, no compensation. 2. Integrated presentation form, compensation by overall mean 3. Integrated presentation form, compensation by mean per row. 4. Integrated presentation form, linear compensation

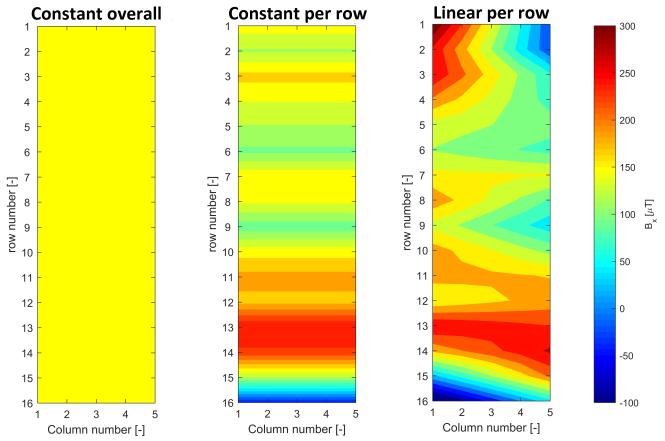

Figure 5.9: Compensation fields for the different integrated presentation forms found in figure 5.8

The described compensation can be progressed further by assuming that the rest magnetization has a linear distribution per row in x-direction. The compensation is in this case performed by a linear regression of the data along the x-direction. From figure 5.1 it can be observed that this linear regression should have no value, if no influence of rest magnetization would be present, since the curve is anti-symmetric. This procedure is performed on a example data set in figure 5.8.4. It can be observed that this separates the induced and rest magnetism in the plate even further.

5.4. Discussion

The results of the evaluation of interpolation methods show a that results for the performed interpolation are similar for the performed test. The residual sum of squares method shows that of the explored techniques, the spline interpolation technique performs best. It should be noted that other interpolation techniques are not treated in this report. However, other techniques (e.g. higher order interpolation techniques) are available and may be of interest in a later stage of research. The spline interpolation technique will suffice for now, since the current SMFL measurement results do not require a higher level of post-processing precision. In addition it should be considered that higher order interpolation techniques may suffer from overshoot at a jump discontinuity.

Further research on post-processing by interpolation of the measurement results may be of interest when more is known about the distribution of the stress magnetization and permanent magnetization. The former analysis only considers the characteristic SMFL curve, but discounts the distribution of the permanent magnetization and stress magnetization entirely. Other interpolation techniques may be shown to fit these distributions better. However, this remains to be seen for now.

The results of the exploration of the different presentation forms demonstrate that post-processing can improve the localization of the crack location. Of the two presentation forms that require processing of the data, i.e. the differentiated and integrated presentation form, the differentiated presentation form requires the least processing of the data and is therefore the most straight forward. Besides, the differentiated characteristic SMFL curve has a more pronounced peak and the crack location is therefore more emphasized and easier to locate. However, an important factors are inherent to this presentation form: information is lost in the process. Only changes in the MFL measurement data are presented in this form, including the changes not generated by the induced magnetic field. However, the amount of rest magnetization that is relatively constant is lost.

The differentiated presentation form is more sophisticated and requires more processing. It can be seen from 5.8 that more precise filtering of the rest magnetization results in a clearer crack localization. The same figure shows the best results when the assumption of a linear distribution of the rest magnetization per row is adopted. This rest magnetization may consist of permanent magnetization and stress induced magnetization to a lesser extend, since these factors are known to influence SMFL measurements (see 2.2.3). It is to be

expected that the linear distribution of the rest magnetization per row is the better approximation, since it is known that the permanent magnetization has a non-uniform distribution and the described assumption of the distribution of the permanent magnetization is expressed with more parameters, when compared to the other compensation techniques. It should be noted that this linear compensation is still not sufficient to fully compensate for the rest magnetization, as can be seen from the irregularities of the background field in figure 5.8.4. Furthermore, the integrated presentation form is more reliable when it comes to crack localization, since the peaks in the integrated data are a result of accumulated changes in the x-direction, while the differentiated presentation from may show a peak due to a single sudden change in the slope in x-direction. Finally, it should be noted that the analysis of both the interpolation and presentation of the SMFL data assumes that the crack is parallel with the y-axis. The example data is derived from the bridge deck experiment and it is known that the crack direction is approximately parallel to the y-axis of the measurement grid. This is however not always the case and it is therefore recommended that the characteristic SMFL curve is orientated parallel to the x-axis of the measurement grid. Further research is recommended that focuses on first determining the crack orientation and subsequently applying post-processing techniques consistent with this direction, since results of the analyses in this report will be prone to errors when the crack direction altered.

5.5. Conclusion

Post-processing of the SMFL measurement data can be helpful to improve interpretation of the measurements and improve the localization of the crack using the SMFL measurement data. This chapter discusses three presentation forms: the normal presentation form, the differentiated presentation form and the integrated presentation form. These forms are based on displaying the data with the help of the characteristic SMFL curves.

A test of three techniques for interpolation of SMFL measurement data shows that the spline interpolation technique is better suited to interpolate measurement data of the characteristic SMFL curve then cubic interpolation and linear interpolation. Spline interpolation is therefore applied as the preferred interpolation technique for SMFL data in this report.

The exploration shows that the differentiated and integrated presentation forms are superior to the normal presentation form, when it comes to presentation of the data and indicating the crack location. Between these forms, the differentiated presentation form is the most straight forward, requires the least amount of processing, but is the most crude as well. The integrated presentation form requires more filtering of the data, in order to be effective, but offers a completer and more reliable characterization of the data. It is furthermore shown that filtering of the data is best done by assuming that the distribution of the permanent magnetization changes linearly perpendicular to the crack, while no particular distribution of the permanent magnetization along the crack length is assumed.

In order to improve the presentation of the data even further a more precise compensation of the permanent magnetization should be explored, for example by approximating the permanent magnetization with the help of higher order polynomials. Information about the distribution of the stress magnetization and permanent magnetization is advantageous in this regard.

6

Conclusion

Operating ship and offshore structures are continuously subjected to the action of waves, that, due to their cyclic nature, cause fatigue cracks to develop. Regular inspections, which are currently performed manually, are therefore required in order to guarantee the structural integrity of the structure. Cracks of critical length have to be repaired, while cracks of sub-critical length have to be monitored. The CrackGuard JIP has the goal of developing an affordable system for reliably monitoring detected fatigue cracks based on the characteristic magnetic pattern that occurs around a fatigue crack as a result of magnetization by the Earth magnetic field. The method used for the monitoring of cracks is called the Self Magnetic Flux Leakage (SMFL) method and makes use of the disturbance caused by a fatigue crack on the magnetic flux inside the material and can be detected by a leakage pattern of the magnetic flux around the fatigue crack. In order to develop this system three knowledge gaps have been identified: The effect of the crack opening on magnetic flux leakage, the effect of complex geometries and welded joints and the application of this methods to full-scale structures.

It is known that fatigue cracks develop in steel structures as a result of cyclic opening and closing, it is important to know the effect of the crack opening on the SMFL measurements. In the crack opening experiment the Crack Mouth Opening Displacement (CMOD) of a fatigue crack is increased by means of applying a tensile load on a center cracked plate, while the SMFL around the crack is monitored. This is action is performed to replicate the opening portion of a fatigue cycle and discover how the SMFL is influenced. Based on the results of the experiment it can be concluded that the SMFL signal increases with an increase in CMOD, whereas the signal width is unaffected by CMOD. These results are confirmed with the help of numerical model of the same situation. The results furthermore show that some SMFL can even be detected, when the fatigue crack is fully relaxed. This means for the application of the SMFL for monitoring on operating ship structures that the measured SMFL signal strength may change significantly over time, as a result of cyclic opening of the fatigue crack.

The Finite Element Method (FEM) can be a useful tool to analyze and understand SMFL measurements around fatigue cracks in welded joint. Numerical models require reliable material models to produce reliable results. Based on previous experiments and differences in material properties, that may impact the magnetic permeability, between base material and weld material it is expected that a difference between the magnetic permeabilities of base material and weld material may exist. In order to construct numerical models that involve welded joints it is essential to know the magnetic permeability of weld material. One of the experiments in this thesis is designed to determine the magnetic permeabilities of s235 structural steel and weld filler material and HAZ of a fully penetrated weld manufactured using MIG welding. The results of the experiments show a relative magnetic permeability of 173.41 for base material, 175.09 for weld filler material and 171.84 for the HAZ. The difference between the magnetic permeabilities is however not statistically significant. These results implicate that SMFL around welds do not occur as a result of a change in magnetic permeability. A numerical simulation of a T-joint with a double-sided fillet weld furthermore shows furthermore that, even when a reduction in magnetic permeability between the base material and weld material is present, the amplitude and signal width of the magnetic flux leakage will still remain of a similar magnitude as a crack not influenced by a fillet weld. Further research to better understand the mechanisms that cause flux leakage around welds is however recommended. It is suggested that residual stresses and electrical cur-

rents may play a role.

The SMFL method used for monitoring fatigue cracks in ship and offshore structures will find its application on operating ship and offshore structures. The method has already proven to be an effective technique for monitor fatigue cracks in test specimens under laboratory conditions, but will have to be be tested on full-scale structures to demonstrate its effectiveness in larger structures. The bridge deck experiment consists of a series of measurements of the SMFL field with the help of a handheld magnetometer on 3 different fatigue cracks in a full-scale replica of a bridge deck that has been subjected to fatigue loading. The results of the measurements show that it is possible to detect and monitor fatigue cracks in the described structure using a hand-held magnetometer by taking measurements on a 20x100 mm grid with 5 mm grid spacing. The measurements furthermore show that it is even possible to follow the development of a propagating fatigue crack to some extend. The measured SMFL pattern is of a significantly greater magnitude than the SMFL pattern observed in small-scale experiments. Exact prediction of the crack location and length based on the measurement results is however not possible. It is recommended that in further research SMFL measurement data is combined with detailed information about the crack shape (obtained with e.g. ultrasonic inspection), in order to determine if the crack tip, which is still a surface defect, can be identified using the obtained data.

One of the first steps towards a system for crack monitoring in steel structures based on the SMFL method is the CrackGuard LT. This prototype has already shown to produce measurement results that enable the detection of fatigue cracks in the later stages of crack propagation in full-scale replica of a bridge deck. During the experiment the SMFL around one of the fatigue cracks was tracked during sailing and unloading of the ship, while the heading of the ship was recorded. The experimental results show that the CrackGuard is able to detect SMFL with an amplitude of 220 μT, although the sensitivity should be improved in order to obtain measurements suitable for reliable crack monitoring. It is recommended that further research on the application of the CrackGuard on steel structures focuses on long duration fatigue crack monitoring. The described experiment demonstrates that measurements are influenced by external factors, which may interfere with precise crack length prediction. Further research that focuses on longer duration testing on full-scale structures is recommended to see if the measurement data is affected by long term influences, such as changes in the magnetization of the ship. With regards to the CrackGuard LT it is recommended that the precision of the SMFL measurements is improved, in order to allow for reliable crack monitoring. The backplane and the altitude and sensitivity of the hall sensors can play a role in achieving this.

Post-processing of the SMFL measurement data can be helpful to improve interpretation of the measurements and improve the localization of the crack using the SMFL measurement data. An exploration into techniques to post-process the data focus on the interpolation of the data and the interpretation of the characteristic flux leakage pattern. A comparison of interpolation shows that interpolation with a spline function produces the best results, when compared to linear and cubic interpolation. The exploration furthermore shows that differentiation or integration of the data perpendicular to the crack direction is superior to unprocessed presentation of the data, when it comes to indicating the crack location. It is furthermore shown that filtering of the data is best done by assuming that the distribution of the permanent magnetization changes linearly perpendicular to the crack, while no particular distribution of the permanent magnetization along the crack length is assumed. This post-processing technique allows for partial separation of the flux leakage pattern and the permanent magnetization. The post-processing of the data will play an important role in order to develop the SMFL method towards improved monitoring of fatigue cracks. The separation of the induced and permanent magnetization is especially of interest in this regard. Better understanding of the distribution of the permanent magnetization will be necessary to improve post-processing of the data and thereby improve crack localization.

Bibliography

[1] J. Schijve, *Fatigue of structures and materials* (Springer, Dordrecht, 2009).

[2] M. Janssen, J. Zuidema, and R. Wanhill, *Fracture mechanics, 2nd,* (2004).

[3] D. Jiles, *Introduction to Magnetism and Magnetic Materials*, third edition ed. (CRC Press Company, 2015).

[4] M. P. van der Horst, M. L. Kaminski, E. Puik, *et al.*, *Methods for sensing and monitoring fatigue cracks and their applicability for marine structures,* in *The Twenty-third International Offshore and Polar Engineering Conference* (International Society of Offshore and Polar Engineers, 2013).

[5] S. Park, J.-W. Kim, C. Lee, and J.-J. Lee, *Magnetic flux leakage sensing-based steel cable nde technique,* Shock and Vibration **2014** (2014).

[6] M. Creager and P. C. Paris, *Elastic field equations for blunt cracks with reference to stress corrosion cracking,* International Journal of Fracture Mechanics **3**, 247 (1967).

[7] J. Schijve, *Four lectures on fatigue crack growth,* Engineering Fracture Mechanics **11**, 167 (1979).

[8] W. Elber, *The significance of fatigue crack closure,* in *Damage tolerance in aircraft structures* (ASTM International, 1971).

[9] C. A. Wert and R. M. Thomson, *Physics of solids,* (1970).

[10] van der Horst M.P. and K. M.L., *Magnetic properties of structural steels for simulation of crack monitoring by finite element method,* (2018).

[11] M. P. van der Horst and M. L. Kaminski, *Slit induced self magnetic flux leakage in a square steel plate,* (2013).

[12] S. M. Krol, M. Middelburg, K. A. T. J. Franken, and A. Botterma, *The Effect of Welding and Cracks on the Magnetic Field in a S235JR Steel Plate*, Bachelor thesis, Delft University of Technology, Delft University of Technology (2012).

[13] S. Thompson and B. Tanner, *The magnetic properties of pearlitic steels as a function of carbon content,* Journal of magnetism and magnetic materials **123**, 283 (1993).

[14] B. Tanner, J. Szpunar, S. Willcock, L. Morgan, and P. Mundell, *Magnetic and metallurgical properties of high-tensile steels,* Journal of materials science **23**, 4534 (1988).

[15] E. Du Tremolet de Lacheisserie, D. Gignoux, and M. Schlenker, *Magnetism. vol. 2, materials and applications,* (2005).

[16] M. Lovejoy, *Magnetic particle inspection: a practical guide* (Springer Science & Business Media, 2012).

[17] A. Sophian, G. Y. Tian, and S. Zairi, *Pulsed magnetic flux leakage techniques for crack detection and characterisation,* Sensors and Actuators A: Physical **125**, 186 (2006).

[18] A. Dubov, *Diagnostics of boiler tubes with usage of metal magnetic memory,* Moscow: Energoatomizdat , 6 (1995).

[19] A. Dubov, *Principle features of metal magnetic memory method and inspection tools as compared to known magnetic ndt methods,* Cinde Journal **27**, 16 (2006).

[20] R. Suárez-Ántola and D. Suárez-Bagnasco, *The physical foundations of magnetic memory method for ndt,* las "Segundas Jornadas Técnicas de la Asociación Uruguaya de Ensayos No Destructivos", Montevideo Uruguay (2004).

[21] S. Bao, M. Fu, S. Hu, Y. Gu, and H. Lou, *A review of the metal magnetic memory technique,* in *ASME 2016 35th International Conference on Ocean, Offshore and Arctic Engineering* (American Society of Mechanical Engineers, 2016) pp. V004T03A006–V004T03A006.

[22] E. L. M.P. van der Horst, M.L. Kaminski, *Testing and numerical simulation of magnetic fields affected by presence of fatigue cracks,* (International Ocean and Polar Engineering Conference, 2014).

[23] M. Sablik, *Modeling the effect of grain size and dislocation density on hysteretic magnetic properties in steels,* Journal of Applied Physics **89**, 5610 (2001).

[24] L. Dong, X. Binshi, D. Shiyun, C. Qunzhi, and W. Dan, *Monitoring fatigue crack propagation of ferromagnetic materials with spontaneous abnormal magnetic signals,* International Journal of Fatigue 30 **294–295**, 1599 (2008).

[25] K. M. Van der Horst MP, Van Kreveld SL, *Effect of stress-induced magnetization on crack monitoring by self magnetic flux leakage method,* (2018).

[26] V. der Horst M.P. and K. M.L., *Simulation and analysis of earth-induced magnetic flux leakage for monitoring cracks in ship and offshore structures,* (2018).

[27] W. GmbH, *Magnetometer KOSVAHA-USB User Manual.*

[28] A. S. for Testing and Materials, eds., *Annual Book of ASTM Standards*, ASTM-A342-A342M-14 (ASTM, West Conshohocken, PA, 2014).

[29] E. Pardo, D.-X. Chen, and A. Sanchez, *Demagnetizing factors for square bars,* IEEE transactions on magnetics **40**, 1491 (2004).

[30] L. Luming, H. Songling, W. Xiaofeng, S. Keren, and W. Su, *Magnetic field abnormality caused by welding residual stress,* Journal of Magnetism and Magnetic Materials **261**, 385 (2003).

[31] *AC/DC Module User's Guide*, COMSOL, comsol 5.2 ed. (2015).

[32] *World magnetic model,* Internet site (2017).

[33] M. van der Horst, *Passive Monitoring of Fatigue Cracks in Steel Ship- and Offshore Structures*, Master thesis, Delft University of Technology (2013).

[34] B. D. Cullity and C. D. Graham, *Introduction to magnetic materials* (John Wiley & Sons, 2011).

[35] G. H. Behforooz, *A comparison of thee(3) and not-a-knot cubic splines,* Applied Mathematics and Computation **72**, 219 (1995).

[36] E. Ramsden, *Hall-effect sensors: theory and application* (Elsevier, 2011).

A

CrackGuard sensor technology

This section describes the development of the CrackGuard, the working principles behind the CrackGuard and the sensors used to measure the magnetic field. Furthermore, a short introduction into its application, communication and installation is provided.

A.1. Development of the CrackGuard

The CrackGuard JIP has resulted in multiple prototypes of the CrackGuard: the CrackGuard I, the CrackGuard II, the CrackGuard 2D and the CrackGuard LT. This section discusses the different prototypes the CrackGuard has seen through its development.

The CrackGuard I

The CrackGuard I is the first prototype produced by the CrackGuard JIP and functioned as a proof of concept model. The CrackGuard I exists of a single Hall sensor inside a cylindrical hull. Using a set of wheels, the prototype is able to make scanning movements along the surface of a plate with help of a rotational spring and a motor. This prototype is unable to measure the length of a crack, but is however able to detect a crack in the hull of a ship section. Thereby confirming the working of the concept.

Figure A.1: Hall sensor inside the CrackGuard I

The CrackGuard II

The next step in the development of the CrackGuard is the CrackGuard II. This prototype consists an array of five sensors, in which sensors can be placed on either side of the crack. This prototype has been developed to research the hypothesized sign change in flux density perpendicular to the crack length. Experiment carried out with this prototype indeed confirmed this hypothesis. This prototype is the first prototype to incorporate a backplane (see A.4).

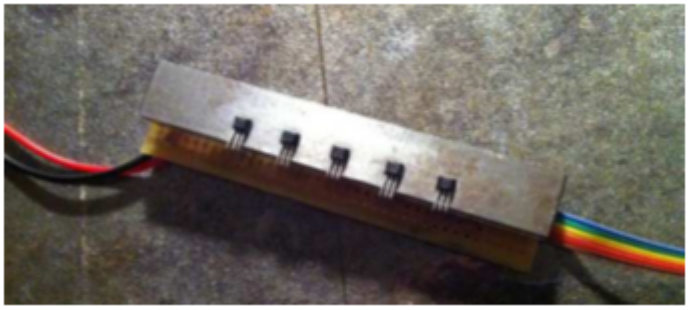

Figure A.2: the CrackGuard II

The CrackGuard 2D

With the hypothesis of a sign change over the crack confirmed, this prototype has been developed to be able to measure crack length. A grid of 8x8 Hall sensors has been created to be able to monitor the length of the crack, adding a dimension to the measurements. The sensors are again attached to a PCB with a backplane on top of it, intended to magnify the detected signal. The prototype makes use of more sensitive sensors that can be calibrated for improved crack monitoring. This prototype allows for connection with a PC by a USB connection.

Figure A.3: the CrackGuard 2D

The CrackGuard LT

The CrackGuard Lateral Transmission is the latest prototype. This prototype is developed to be more suitable for application under more demanding environmental conditions and installation on curved surfaces. The CrackGuard LT is hexagonally shaped with a backplane consisting of triangular shapes, although the newest version features a backplane of hexagonal elements, for improved alignment with the sensor PCB (see figure A.4). This design of the backplane is more flexible and can be bend around multiple axes. The electronic components of the unit are cast in a PMR (Polyurethane Moulding Rubber) material, where the layer between the sensors and the crack is kept to 1 mm thickness, in order to maximize the SMFL signal. The cover is flexible as well and makes sure that the electronics are protected against water and dirt. This prototype is powered by a 3-volt Lithium Manganese Dioxide battery, which, together with the receiver, is moved to the outside of the sensor grid to make it more compact. The latest version has a equilateral hexagonal shape, allowing multiple CrackGuards to be 'stacked' to cover a bigger surface.

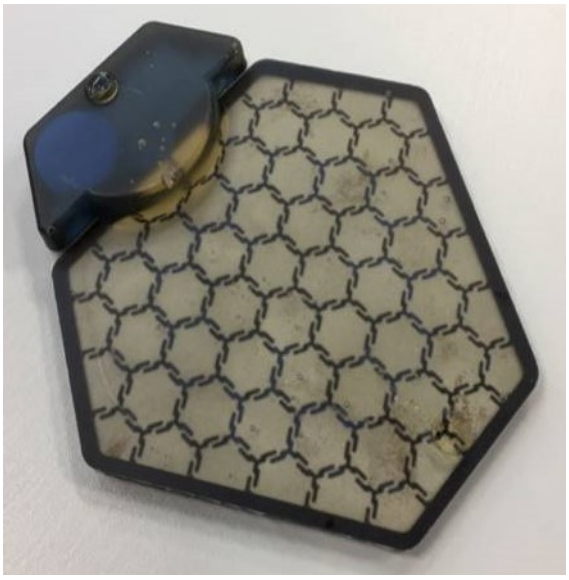

Figure A.4: the CrackGuard LT

A.2. Hall effect sensors

In essence, the CrackGuard can be seen as a collection of Hall effect sensors, placed in a matrix. The Hall effect sensors (described in subsection A.2) are able to detect the local magnetic flux density in a designated direction. Hall effect sensors in the CrackGuard are positioned so as to measure the magnetic flux density in the out-of-plane direction. It is in this plane, that the most pronounced deviations in the magnetic field of a plate as a result of a crack can be expected. Cracks and other defects are characterized by a sign change that occurs suddenly in the out-of-plane flux density at the location of the crack (see 2.2.3).

A.3. Sensor output

The signal is read sequentially from the sensor array and is organized in the CPU on the transceiver board. Before use a zero measurement is performed, by holding the device away from any ferromagnetic influences. This zero measurement will later be used to calculate the offset and calibrate the recorded signal. This calibrating procedure is not done on the sensor hardware, but is performed during post-processing. Data communication is performed by a Zigbee protocol at a frequency of 868 MHz. This frequency is able to penetrated the surrounding material relatively well, which is needed in order to communicate with the receiver.

A.4. The Backplane

Using a collection of Hall sensors placed in a 2D matrix makes it possible to track the crack tip and monitor the length of the crack. In order to amplify the signal and spread the local sign change over a bigger area with the aim of improving the detection of the signal by the sensors, a magnetically conductive back plane is added to the CrackGuard (see figure A.5). This backplane enables more accurate localization of the crack. The backplane is designed to attract flux lines, increasing the magnetic flux through the Hall sensors to emphasize the flux leakage effect. The material used to construct the backplane is s235 structural steel.

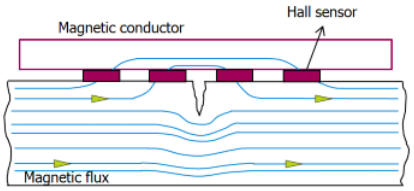

Figure A.5: Attraction of the magnetic flux lines by the magnetically conductive back plane

The backplane used in the CrackGuard LT is made of a single sheet of perforated steel with hexagonal tiles (see figure A.6), to ensure that the backplane is flexibility around multiple axes. furthermore, this backplane design has the added advantage of better alignment with the sensor array. An earlier concept of the backplane with triangular tiles was abandoned in the development because of difficulties with the alignment of the tiles and the sensors.

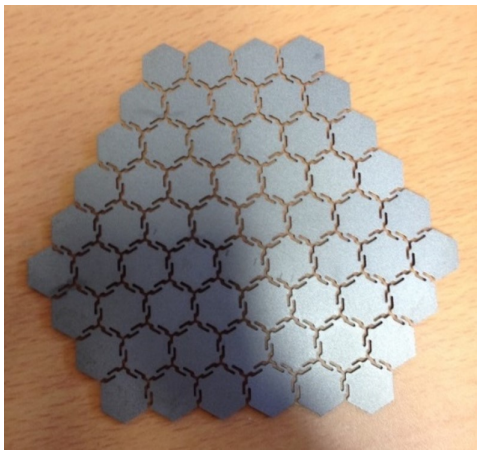

Figure A.6: Photo of the backplane of the CrackGuard LT and its hexagonal elements

A.5. The Hall effect sensor

Fundamentally a Hall effect sensor is a device that converts magnetic flux density into an electrical signal. It consists of a rectangular semiconductor material with a continuous current passing through it. When the device is placed within a magnetic field, the magnetic flux lines exert a force on the semiconductor material which deflects electrons to either side of the semiconductor slab. This sideways movement of the electrons is a result of the Lorentz force they experience passing through the semiconductor material [36]. The imbalance of electrons produces a measurable potential over the slab in the direction perpendicular to the flow of electrons, see figure A.7. This effect is called the Hall effect, named after Edwin Hall who discovered it in 1870's. The effect provides information regarding the type of magnetic pole and magnitude of the magnetic field. The output voltage, called the Hall voltage V_H, of the basic Hall element is directly proportional to the strength of the magnetic field passing through the semiconductor material. This output voltage can be quite small (only a few micro volts) even when subjected to strong magnetic fields, so most commercially available Hall effect devices are manufactured with built-in DC amplifiers , logic switching circuits and voltage regulators to improve the sensors sensitivity, hysteresis and output voltage [36]. This also allows the Hall effect sensor to operate over a wider range of power supplies and magnetic field conditions.

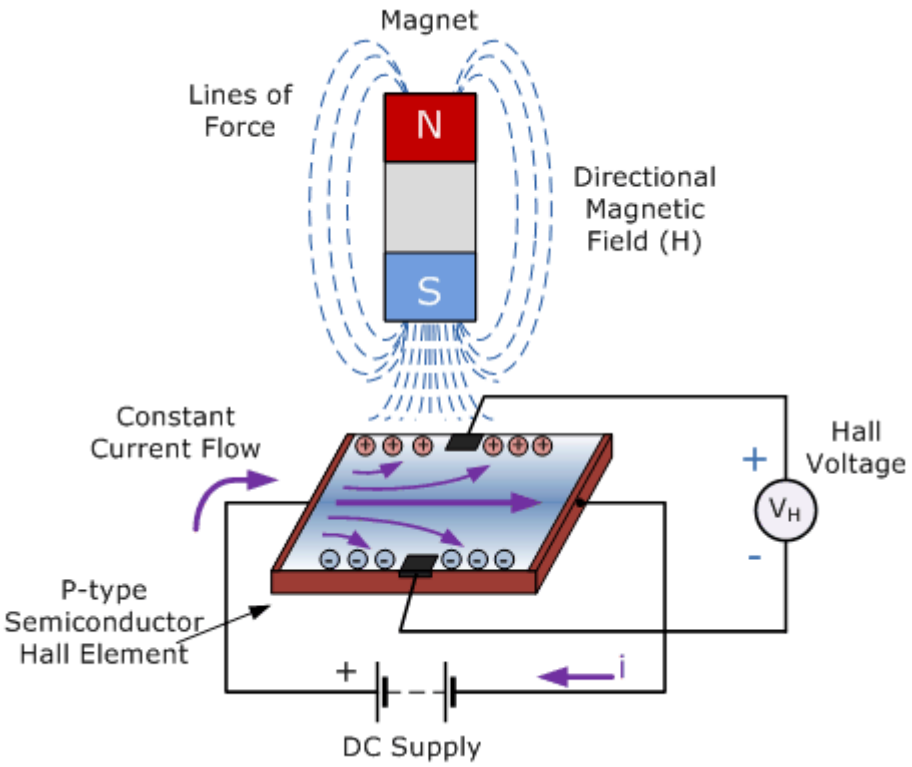

Figure A.7: Representation of the working principle behind the Hall effect sensor

A.6. Application of the CrackGuard

The foregoing sections have focused on the technical aspects of the CrackGuard that facilitate the monitoring of fatigue cracks. The CrackGuard is however intended to be part of an overarching structural health monitoring system of the structure, in which multiple sensors, of which possibly multiple CrackGuards, work together to monitor the status of the structures structural state. The system should allow operators to monitor the status of multiple fatigue cracks from an onshore location. This means that the individual sensors will have to communicate the gathered data to a device that is capable of collecting and transmitting the data toward the operator.

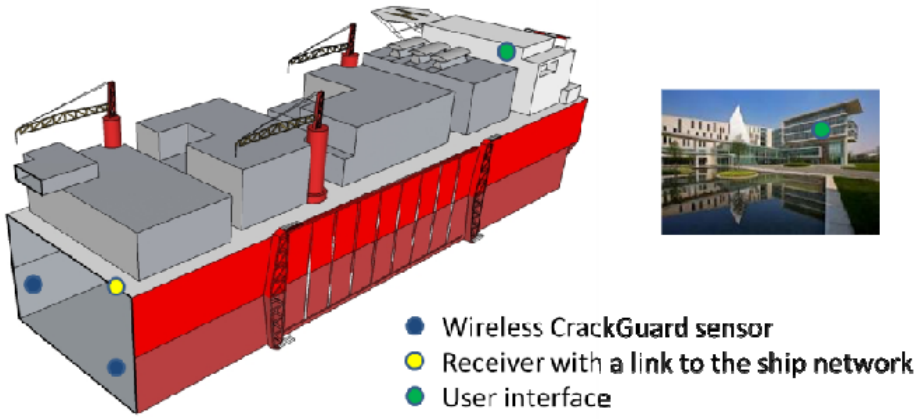

Figure A.8: Envisaged system architecture

As can be seen from figure A.8, the CrackGuard(s) will communicate wirelessly with a locally installed receiver. Currently the sensor is capable of transmitting the signal over a distance of approximately 100 meter. The reach of the sensor outside storage tanks is however limited, due to the storage tank preventing the escape of electromagnetic fields. This necessitates the use of an antenna inside the storage tank and further transmission of the signal through a wire, carrying the signal through the tank wall. Reflection of the signal against the steel walls of the tank may aid in improving the communication between the sensor and the antenna. A pressure sensor will make sure that the signal is only transmitted when the device is not submerged in water or oil, otherwise storing the data for later transmission. The sensors communicate with each other using a ZigBit network with a coordinator. The coordinator in turn uses a UART connection to connect to a installation gateway, which acts as a database and supports a webserver. This allows the information to be accessible to the operator from an onshore location as well as a location on board the ship.

A.7. Installation of the CrackGuard

As part of compulsory rules for ship and offshore structures, operators are obliged to carry out a full inspection of the structure every five years. During this inspection a fatigue detection test is carried out by the surveyor. Detected cracks may be categorized as having differing levels of risk, ranging from low to unacceptable. Cracks posing an unacceptable risk will have to be repaired, while cracks of a lower risk classification may be candidates for crack monitoring using the CrackGuard [22]. The CrackGuard may also be installed on locations with a higher risk of developing cracks of locations which are expected to develop cracks and have limited accessibility, such as locations with high stress concentration factors in the outer hull of a ship.

Prior to installation the sensitivity of the sensor is determined by the mechanic installing the device. In this stage the settings can be adjusted using a designated installation gateway. The CrackGuard is subsequently installed by simply gluing the device onto the crack. The device is switched on by a magnetically activated reed switch, in order to prevent power consumption during transportation and installation. Upon activation the CrackGuard establishes connection with a transmission gateway, to ensure communication between the CrackGuard and the database. Following activation the CrackGuard will remain active for at least 5 years, which is in accordance with the class survey interval for FPSO's . During operation the CrackGuard will take measurements on a predefined measurement interval. A more frequent heartbeat interval ensures proper function of the sensor and communication with the receiver. Inspection during the next mandatory survey will present the opportunity to replaced the battery and possibly prepare the device for another 5 years of crack monitoring.

B

Determination of magnetic permeability

The permeability μ of a material is used to determine the relationship between the flux density B in the material and the applied magnetic field strength.

$$\mu = B / H \tag{B.1}$$

For certain types of material the ratio is constant, not depending upon the degree of magnetization, while for other materials the ratio depends upon the flux density inside the material. The permeability as defined in equation B.1 can be easily determined from plot of the flux density B inside the material against the applied field strength H, as can be seen from figure B.1.

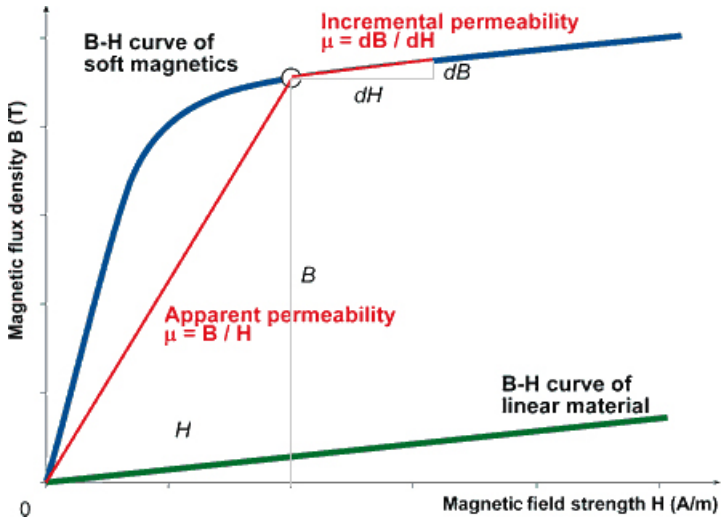

Figure B.1: Relation between the flux density B and the permeability μ of an unknown material

The permeability determined using this procedure will be applied in a numerical simulation using COMSOL multiphysics 5.2. Two important simplifications will therefore be applied, as described in section 4.1: A linear relation between B and H is assumed and no permanent magnetism is present in the material. The first assumption can be safely made, when the magnetization in the material is low, as can be seen from the blue curve in figure B.1. Although the permeability curve in this figure is not derived from s235 structural steel, a similar curve may be expected from this material. Because the Earth magnetic field is relatively weak, a low magnetization of the material will result and a linear permeability curve may be assumed. The apparent and incremental permeability will therefore be of the same value. Equation B.1 can therefore be applied in order to find the permeability of the material.

Relation B.1 is valid when the applied magnetic field strength is equal to the effective magnetic field strength inside the material. This is whoever often not the case, as the geometry of the object placed inside the field has an influence on the magnetic field inside the object itself. When a specimen of device component of open shape, such as a cylinder, made of a ferromagnetic material is magnetized by an applied field, magnetic poles are formed at the opposite ends of the specimen. These poles cause within the specimen a magnetic field opposite in direction to the applied field. The demagnetizing field H_s of the poles of the specimen is proportional to the specimen's magnetization M [34].

$$M = -N * M \tag{B.2}$$

The coefficient N in this formula is called the demagnetizing factor and represents the ratio of the strength of the specimen's demagnetizing field and magnetization of the specimen [34]. A specimen located in an applied magnetic field H_a has an internal field strength equal to:

$$H_{eff} = H_a - N * M \tag{B.3}$$

The demagnetizing factor can be calculated precisely only for ellipsoids, which have a uniform magnetization throughout. For some specimens of simple geometry, the demagnetizing factor is calculated by empirical formulas, but in most cases is determined experimentally. The value of N depends mainly on the shape of the body, but is also dependent on the permeability itself. The sum of the demagnetizing factors along the three orthogonal axes of an ellipsoid is constant.

$$N_x + N_y + N_z = 1 \tag{B.4}$$

Specimens often encountered in practice are cylindrical rods magnetized along the axis and in-plane magnetized disks. Since these are not ellipsoids, the demagnetizing factors calculated according to the previous formulas will be erroneous to some degree. Rods and disks are never uniformly magnetized except when completely saturated. The demagnetizing field varies from one point to another in the specimen and so has no single value. Two specific effective demagnetizing factors may be used in this case, depending on the way the magnetization is defined [34]. The fluxmetric N_f and the magnetometric demagnetizing factor N_m can be determined for this type of specimen. The fluxmetric demagnetizing factor N_f is defined as the ratio of the average demagnetizing field to the average magnetization in the mid plane of the sample. The magnetometric demagnetizing factor N_m, which is defined as the ratio of the average demagnetizing field to the average magnetization of the entire sample, is to be used when the magnetization is measured with help of a vibrating sample, an alternating-gradient or a SQUID magnetometer. For this reason, the magnetometric demagnetizing factor N_m will be used in the determination of the permeability.